Meteorite aerodynamics during dark flight

An experimental investigation using a subsonic wind tunnel

S.G.V.S. Aduru

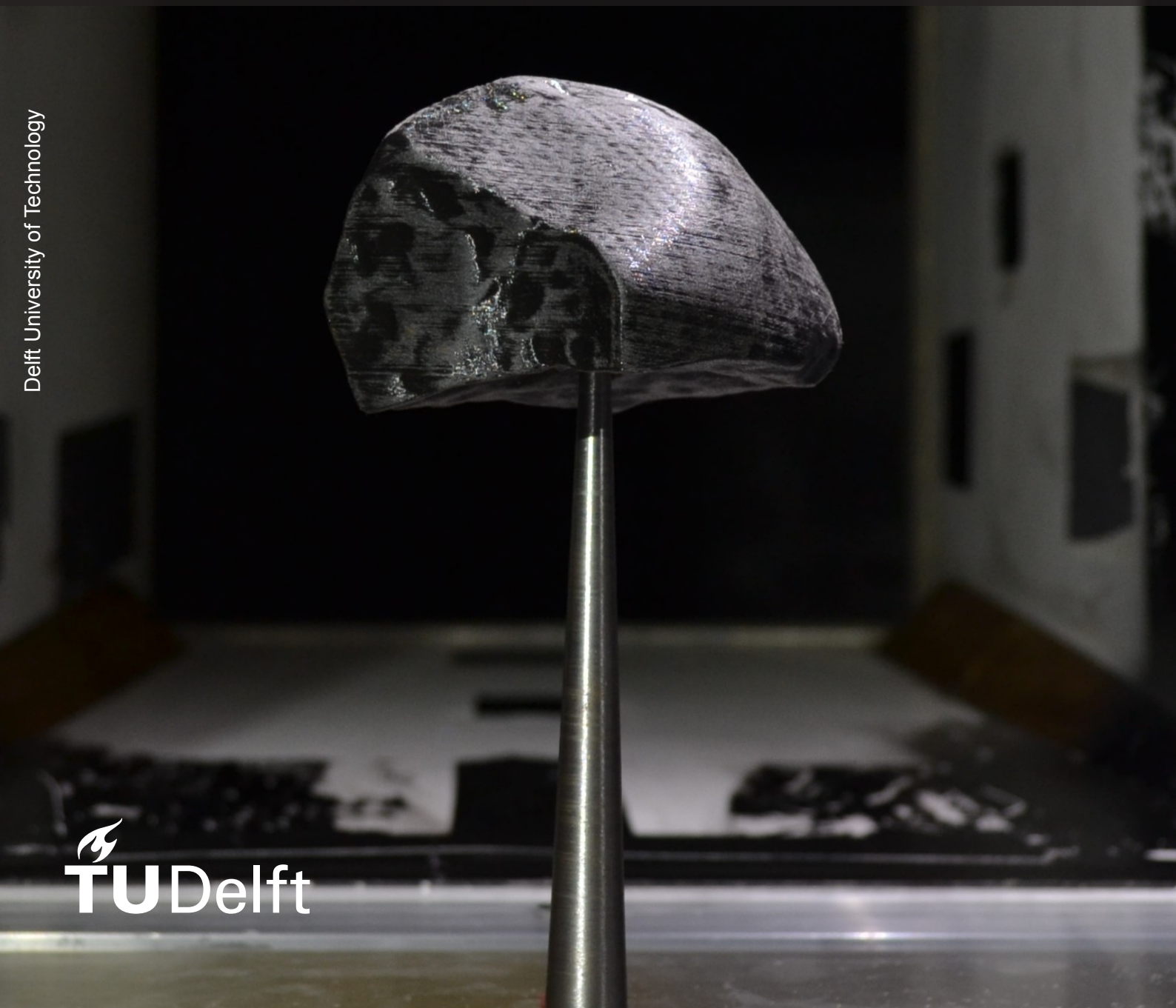

Delft University of Technology

TU Delft

Meteorite aerodynamics during dark flight

An experimental investigation using a subsonic wind tunnel

by

S.G.V.S. Aduru
5024730

to obtain the degree of Master of Science
at the Delft University of Technology,
to be defended publicly on Friday January 28,2022.

Supervisor:	Dr. S.J. de Vet
Institution:	Delft University of Technology
Place:	Faculty of Aerospace Engineering, Delft
Project Duration:	April, 2021 - January, 2022

TU Delft

Preface

The objective of this graduation thesis is to experimentally investigate the aerodynamics of a meteorite. This thesis topic marks the completion of my master's study in Space flight track at the faculty of Aerospace engineering of Delft University of Technology. After the completion of my internship at SRON, I was searching for a thesis topic. That is when this thesis topic found me. As a person who has an innate love for the aerodynamics, a strong passion for space, and intrinsic fervour for unexplored territories, I found this thesis topic to be very unique and extremely intriguing to work upon. In my opinion, this thesis topic is a small step towards a completely unfathomed domain in the field of meteoritics.

First of all, I want to thank my supervisor, Dr. Sebastiaan de Vet, for the inception of such a brilliant thesis topic and for providing me the opportunity to work on this topic. And I am forever grateful for giving me the independence to work on this topic, yet guiding me with constant support and critical feedback during this period. The informal discussions over coffee will be remembered for a long time, and thanks for being a wonderful guide. I would place my deepest gratitude to Dr. Andrea Sciacchitano, whose insights and suggestions have been extremely crucial for the experimental investigations and being a part of this thesis project. I would like to thank Felix Bettonvil for your immense interest in this work and taking time to answer my questions patiently. Finally, yet importantly, I would like to thank the technicians of the High-Speed Laboratory for their help during the experiments. Especially, I would like to thank Peter Duyndam, for materialising my design ideas even in busiest times.

Most importantly and obviously, I am always grateful for my family for their unconditional love, belief, and support in my life. I am forever indebted to Chinnu, for being there for me and supporting me even in my hardest times. Without you, I could not imagine this journey. Next, I always loathe Chanda, Wasee, Peepa & Buji back at home for not including me in their trips and movies, and for all the stickers. I would like to thank 'Aravind LOL' for the assignments, F1, *stuff* from home, lame jokes and for your incessant "fun" facts. To *Dr.* Raghavendran, I am forever indebted for you for your *help* and for your ginger tea!

"అనుభవాల క్రమమే జీవితం, అనుభవమే గురువు!"

I strongly believe in this philosophy told to me by my maternal grandfather, which translates to "*Life is the order of experiences, experience is the teacher!*". Until now, my life has been a roller coaster ride of experiences and emotions. My decisions, be it good or bad, brought me here at this point of life and I am excited where this journey will lead me further. Nevertheless, this master's programme at Delft University of Technology, which once used to be a dream, is now a milestone in my life! Ultimately, I want to thank everyone who has been part of my life and teaching me the nuances of good and bad in life.

S.G.V.S. Aduru
Delft, January 2022

Abstract

Meteor is a luminous phenomenon that occurs when a solid object travelling through the interplanetary space enters the Earth's atmosphere and ablates during its entry. These extra-terrestrial solid objects, which are smaller than asteroids, are called meteorites, and they carry crucial elements that were part of the planetary formation few billions years ago. Dark flight is one of the phases of the atmospheric flight of a meteorite which happens after the ablation of the meteoroid in the atmosphere. During the dark flight the meteorite flies without emitting any light, thus making it hard to estimate its impact point on the surface of the Earth. The laborious task of meteorite recovery is always complicated by the effects of aerodynamic forces acting on the meteorite during this dark flight, as well as the meteorite shape. In multiple meteorite recoveries, the effect of aerodynamic forces acting on the meteorite during its dark flight is speculated as the reason for this deviation from the predicted trajectory. Hence, limited knowledge of the aerodynamic properties of meteorite can be attributed as one of the major reasons for partial recovery of the meteorite. With the advancement in the current 3D printing techniques, experimental studies can be conducted to for a better understanding of the meteorite aerodynamics. Hence, the current project is a study of experimental investigation of the aerodynamic behaviour of a meteorite. In this study, the effect of the irregular meteorite shape on its dark flight will be analysed. To evaluate these effects, experiments were conducted in a low-speed wind tunnel. A 3D printed meteorite model was used to study various aerodynamic forces acting on the meteorite. Broek in Waterland meteorite was considered for the current study as the test model. Firstly, the drag coefficient of the model was measured accurately. Based on literature, it was identified that, from an altitude of 10 km, meteorite travels at subsonic velocities in denser atmosphere for a considerable time. This can offer an important insight into the aerodynamic effects. Hence, this study investigates the free fall of the meteorite from an altitude of 10 km until Mean Sea Level. Firstly, an accurate drag coefficient of the meteorite model was estimated to calculate the terminal velocities at these altitudes. On the basis of calculated terminal velocities, a scaled model was used to create similar flows conditions for the free fall over the meteorite model. The required scaling factor of the test model was estimated using flow similarity analysis. With the scaled meteorite model the variation of the aerodynamic forces during the free fall of the meteorite descent was studied. Using an additional setup, the rotational aspects of the meteorite were also investigated in this study. Finally, the estimated drag coefficient and shape factor were implemented in a dark flight code to study the influence of these parameters on the impact points of a meteorite fall. Based on the results, it was identified that a range of drag coefficient values exists for a single meteorite and for the Broek in Waterland meteorite, the range lies between 0.36 to 0.88. The results of the experiment have proved that there is a finite amount of lift and side forces are experienced by the meteorite during its atmospheric flight. Furthermore, the experiments showed that for a non-rotating oriented flight of the meteorite, side and lift forces exists and strongly influence the impact points. The impact points for a single body gets separated by 24 km when the orientation of the meteorite is changed, assuming an oriented flight. In summary, this experimental study has proved that aerodynamic forces are very crucial in the meteorite dark flight and strongly affect the trajectory of dark flight, thereby influencing the impact points of the meteorite. Therefore, better parametrisation of meteorite aerodynamic parameters in the dark flight model is needed for better strewn field estimation.

Contents

Preface iii

Abstract v

Nomenclature ix

List of Figures xi

List of Tables xv

1 Introduction 1
- 1.1 Shedding light on the dark flight . . . 3
- 1.2 Problem statement . . . 7
- 1.3 Research objective & questions . . . 7
- 1.4 A Novel Approach . . . 8
- 1.5 Thesis Outline . . . 8

2 Journal Article 11
- 2.1 Introduction . . . 14
- 2.2 Experimental Setup . . . 16
  - 2.2.1 Wind tunnel & Instrumentation . . . 16
  - 2.2.2 Test Model . . . 16
  - 2.2.3 Test Setup in the wind tunnel . . . 18
- 2.3 Methodology . . . 19
  - 2.3.1 Determination of drag coefficient for the meteorite model . . . 19
  - 2.3.2 Free fall analysis of the meteorite during the dark flight . . . 21
  - 2.3.3 Study of rotation of the meteorite . . . 22
- 2.4 Results & Discussion . . . 22
  - 2.4.1 Estimation of C_D . . . 22
  - 2.4.2 Free fall analysis . . . 28
  - 2.4.3 Rotation of meteorite . . . 32
  - 2.4.4 Implementation . . . 35
- 2.5 Conclusions . . . 39

3 Supplemental Material 41
- 3.1 Experimental data acquisition . . . 41
- 3.2 Flow similarity analysis . . . 42
- 3.3 Implementation of the Dark flight model . . . 44

4 Conclusions 47

5 Recommendations 51

References 57

A Conversion of STL file into SLDPRT format 59

Nomenclature

Abbreviations

Abbreviation	Full Form
3D	Three Dimensional
COP	Center Of Pressure
DFN	Desert Fireball Network
EOM	Equations of Motion
FRIPON	Fireball Recovery and InterPlanetary Observation Network
MSL	Mean Sea Level
PIV	Particle Image Velocimetry
PLA	Polylactic Acid
PRISMA	Prima Rete Italiana per lo Studio sistematico delle Meteore e dell'Atmosfera
SLDPRT	SOLIDWORKS Part
STL	STereoLithography
UT	Universal Time

Symbols

Symbol	Definition	Units
μ	Coefficient of dynamic viscosity	Pa.s
ν	Coefficient of kinematic viscosity	m^2s^{-1}
ω	Rotational velocity of Earth	$rads^{-1}$
ϕ	Geographic latitude	Deg
ρ	density	kgm^{-3}
Γ	Drag Coefficient	-
a	acceleration	ms^{-2}
a	Lapse rate	Km^{-1}
g	Acceleration due to gravity of Earth	ms^{-2}
h	Altitude	m
m	Mass	kg
v	Velocity	ms^{-1}
A	Shape coefficient	-
A_C	Corrected area	m^2
A_{Proj}	Projected area	m^2
A_{TS}	Test section area	m^2
C_D	Coefficient of drag force	-
C_F	Coefficient of force	-
C_L	Coefficient of lift force	-
C_S	Coefficient of side force	-
D	characteristic length	cm

Symbol	Definition	Units
F	Force	N
M	Mach number	-
Re	Reynolds number	-
R_E	Radius of Earth	m
S	Cross sectional area	m^2
S	Ratio of meteoroid mass to its cross section	kgm^{-2}
T	Temperature	K
V	Velocity	ms^{-1}

List of Figures

1.1 Atmospheric flight of a meteoroid and its phases (Ceplecha et al., 1998). . . . 2
1.2 Generic strewn field of a meteorite fall (Lissauer and De Pater, 2013). 3
1.3 Results of variation of airborne fragment velocity with the altitude (Vinnikov et al., 2016). 5
1.4 Wind profiles measured by radiosonde at White Lake, Michigan. Top plot is for 0 UT and bottom one at 12 UT (Brown et al., 2019). 6

2.1 Broek in Waterland meteorite and its 3D model created using SOLIDWORKS. . 17
2.2 Threaded holes created using SOLIDWORKS to mount the test model vertically and horizontally on the support strut. 17
2.3 3D printed meteorite test model with cubic infill using Prusa i3 MK3S+ printer. . 18
2.4 Experimental setup for the determination of drag coefficient and the free fall analysis. The meteorite is fitted on a vertical strut which is mounted on the six-component balance using a base plate. 18
2.5 Experimental setup for the study of rotation of meteorite. The meteorite is fitted with the spindle which is inserted in the additional support attachment mounted on the vertical strut. With this mounting, the rotation of the meteorite can be studied with a rotational axis parallel to the flow direction. 19
2.6 Six faces of meteorite that face the flow in the wind tunnel. The direction of the flow is into the paper. 20
2.7 Orientation of the meteorite model with faces 1 and 6 facing the flow in the wind tunnel test section. 20
2.8 Radar plot of the variation of C_D, C_L & C_S for each face of the meteorite model orientation. The force coefficients are averaged over the Reynolds number range of $1.29 \times 10^4 - 1.94 \times 10^4$. The dotted hexagon represents the zero value of the force coefficients. 23
2.9 Variation of the force coefficients and ΓA for each face of the meteorite model orientation. The force coefficients are averaged over the Reynolds number range of $1.29 \times 10^4 - 1.94 \times 10^4$. 24
2.10 Variation of the aerodynamic parameters for six faces of the meteorite model with Reynolds number of the flow. (a) Variation of C_D; (b) Variation of C_L; (c) Variation of C_S; (d) Variation of ΓA. 26
2.11 Pair 1 of the six meteorite faces facing the air flow in the wind tunnel. The ellipse represents the dimple shaped regmaglypt on the meteorite model and the rectangle represents the flat shape in face 2. 26
2.12 Pair 2 of the six meteorite faces facing the air flow in the wind tunnel. The dotted line represents the dominant surface with higher curvature present behind the model. 27
2.13 Pair 3 of the six meteorite faces facing the air flow in the wind tunnel. The ellipse on face 5 represents the dimple shaped regmaglypt on the meteorite model and the top and bottom rectangles on face 6 represents the top and bottom slant surfaces present on the meteorite body. 27

2.14 Variation of the mean coefficient of drag force with the altitude and corresponding flow Reynolds number. 29
2.15 Variation of the mean coefficient of lift force with the altitude and corresponding flow Reynolds number. 29
2.16 Variation of the mean coefficient of side force with the altitude and corresponding flow Reynolds number. 30
2.17 Variation of the mean value of ΓA of the meteorite with the altitude and corresponding flow Reynolds number. 30
2.18 Variation of the aerodynamic parameters for six faces of the meteorite model with Reynolds number of the flow measured during the free fall analysis. (a) Variation of C_D; (b) Variation of C_S; (c) Variation of C_L; (d) Variation of ΓA. . . . 32
2.19 Flow over two orientations of the meteorite model mounted on a shaft. It can be observed that for the horizontal and vertical orientations, Faces 1 and 5 will be against the incoming flow. 33
2.20 Variation of the drag force with Reynolds number of incoming flow for a rotating model. (a) Horizontal orientation with **face 1** facing the incoming flow. (b) Vertical orientation with **face 5** facing the incoming flow. 33
2.21 Variation of the lift force with Reynolds number of incoming flow for a rotating model. (a) Horizontal orientation with **face 1** facing the incoming flow. (b) Vertical orientation with **face 5** facing the incoming flow. 34
2.22 Variation of the side force with Reynolds number of incoming flow for a rotating model. (a) Horizontal orientation with **face 1** facing the incoming flow. (b) Vertical orientation with **face 5** facing the incoming flow. 34
2.23 Illustration of dark flight simulation implemented as a part of study to verify the influence of the aerodynamics on the atmospheric flight. Yellow line illustrates the fictitious luminous trajectory of the meteorite which was assumed to enter the atmosphere at 50° near Broek in Waterland region. The dark flight was assumed to start at Delft University of Technology. The green marker with star label points the beginning point of luminous trajectory at $(52.50, 5.00)$ at an altitude of 85,000 m. The red marker labelled as 'D' denotes the beginning point of dark flight at $(51.99, 4.376)$ at an altitude of 25,000 m. The group of multi-coloured markers at the bottom represent the group of impact points estimated from the simulation. 36
2.24 Impact points calculated using a dark flight calculator for each face of the meteorite model. Fig. 2.23 is presented as Panel 'A' at the upper left corner of the image. Panel A illustrates the fictitious luminous trajectory of the meteorite which was assumed to enter the atmosphere at 50°, close to the Broek in Waterland region. The dark flight was assumed to start at Delft University of Technology. The dark yellow rectangular box in Panel A is zoomed in as Panel 'B' which consists of the fall points with the same legend from Fig. 2.23. The red markers denote the impact points for each face of the Broek in Waterland meteorite with the number denoting the meteorite face. The yellow marker denotes the impact point estimated using the mean value of all six faces ($\overline{\Gamma} = 0.563$ and $\overline{A} = 1.343$). The cyan markers represent the fall points that are estimated using the assumed values from the literature. The broad yellow line in Panel 'B' illustrates the separation of 24 km between the impact points of face 1 and 6 of the meteorite. . . 37

A.1 STEP 1: Click Add-ins in the 'Options' to check the existing Add-ins. 59
A.2 STEP 2: Select ScanTo3D in the add-ins window 60
A.3 STEP 3: Change the file format to ScanTo3D Mesh Files in the 'Open file' window. 60

A.4 STEP 4: Select 'Options' in the 'Open file' window before opening the required STL file, to import the 3D mesh data as a Solid Body. 61
A.5 STEP 5: View of the high-quality mesh imported into SOLIDWORKS as 'Mesh1'. 61
A.6 STEP 6: After launching Mesh Prep Wizard, select the 'Orientation Method' based on the requirement, The red dots present in the mesh, represents the manually selected points for Y and Z axes. 62
A.7 STEP 7: Simplification of the mesh size based on feeding the required 'Reduction amount' of the surface quality. 62
A.8 STEP 8: Choose the quality of smoothness and then create the body using either automatic or guided creation. 63
A.9 STEP 9: Choose the required 'Surface Detail' to see the preview of the model with the resultant surface errors. 63
A.10 3D model of the Broek in Waterland meteorite. (a) Preview of the surface details with the resultant surface errors. (b) Final solid model created from the imported mesh data. 64

List of Tables

2.1 The variation of mean values of the coefficient of side, drag and lift forces and ΓA for different meteorite faces. 25

3.1 Flow Reynolds number and corresponding wind tunnel velocities to create similar flows at five altitudes for the free fall analysis of a 1.75x scaled model of Broek in Waterland meteorite. 43
3.2 Value of input variables for different test cases for the dark flight implementation using dark flight calculator. 45
3.3 Values for the remaining input parameters to the simulator common for all test cases 45

1

Introduction

The atmospheric phenomenon that is observed when a streak of light appears in the sky is commonly referred as a '*Meteor*' (IMO, 2021). It is caused when the interplanetary solid objects, called '*Meteoroids*', pass through the Earth's atmosphere (IAU, 2021). These interstellar passengers, which looks akin to the rocks on the Earth, find their origin usually from the Asteroid belt and the neighbouring planetary debris (Spurny, 1997). When the orbits of these bodies intersect with the Earth's orbit, they make their descent through the Earth's atmosphere. Due to the unfamiliarity in the arrival and the fall locations if these meteors, these are referred as *Sporadic meteors* (Campbell-Brown, 2007). However, the similar occurrence of meteors in form of showers can be observed annually at a known location in the sky, called as *Shower meteors* (Lissauer and De Pater, 2013). Unlike the former phenomenon, the bodies of these showers originate from the debris from cometary flight and have known location of inception in the sky (Bronshten, 2012).

Nevertheless, in both the cases, when the body enters the Earth, a continuous interaction in the form of collisions occurs in the rarefied atmosphere. Due to this interaction, the surface of the body starts to heat up and results in *pre-heating* of the meteoroid (Opik, 2004; Rogers et al., 2005). A part of this heat will be transferred to the body and the rest will be radiated outside in the atmosphere. When these meteoroids continue their descent through the atmosphere, the temperature increase incessantly due to increase in the collision rate with the molecules and the body starts to burn away (McKinley, 1961). During this *ablation* phase, the temperatures reach around 2500K making the surface of the meteoroid to melt away in form of liquid droplets (Ceplecha et al., 1998). These liquid droplets vaporise and instantly radiates large amount of heat and light around the meteoroid. Very bright light is created due to the vaporization and ionization of the plasma surrounding the body (Öpik and Singer, 1959). If the brightness of this meteor exceeds a magnitude of -4 or higher, it is referred as '*Fireball*' or '*Bolide*' and sometimes '*Superbolide*', which can be seen from the ground with naked eye (Ceplecha et al., 1999; Konovalova et al., 2011). And, sometimes when the dynamic pressure exerted by the atmosphere exceeds the internal structural strength of the meteoroid, the meteoroid breaks down and *fragments* into several smaller pieces. With its further descent, the meteoroid starts to experience a denser atmosphere, which in turn results in higher atmospheric drag and deceleration of the meteoroid. After the conversion of the kinetic energy into thermal energy, at certain point, the meteoroid starts *Dark flight*, without emitting any light from then and rapidly reaches lower velocities less than 3 kms^{-1} (Carter et al., 2011). During this phase, the meteoroid starts to cool down very quickly, thereby solidifying its molten crust. The meteoroid trajectory will be affected due to the complex shape created during the ablation

and the presence of turbulent wind gusts. And, finally, the meteoroid reaches the surface of the Earth, often creating a small pit in the surface around its impact point at velocities 100 ms^{-1} to 10 ms^{-1} (Ceplecha et al., 1998). In such case, when the meteoroid survives its atmospheric flight, it is called '*Meteorite*'. Thus, once the meteoroid enters from space follows a complex trajectory in the atmosphere and finally reaches the surface as a meteorite, which is presented in Fig. 1.1. Due to the effects of the shape of meteoroid, fragmentation, and wind gusts, the meteoroid fragments generally disperse on the Earth's surface (Jenniskens et al., 2009; Lissauer and De Pater, 2013; Moilanen et al., 2021). This geographical area with the probability of the meteorite presence is referred as *Strewn field* and will be elliptical in shape as presented in Fig. 1.2. This strewn field serves as the most probable search area for the meteorite recovery. Depending on the mass of the fragments and the aforementioned influential factors the size and shape of the strewn field varies.

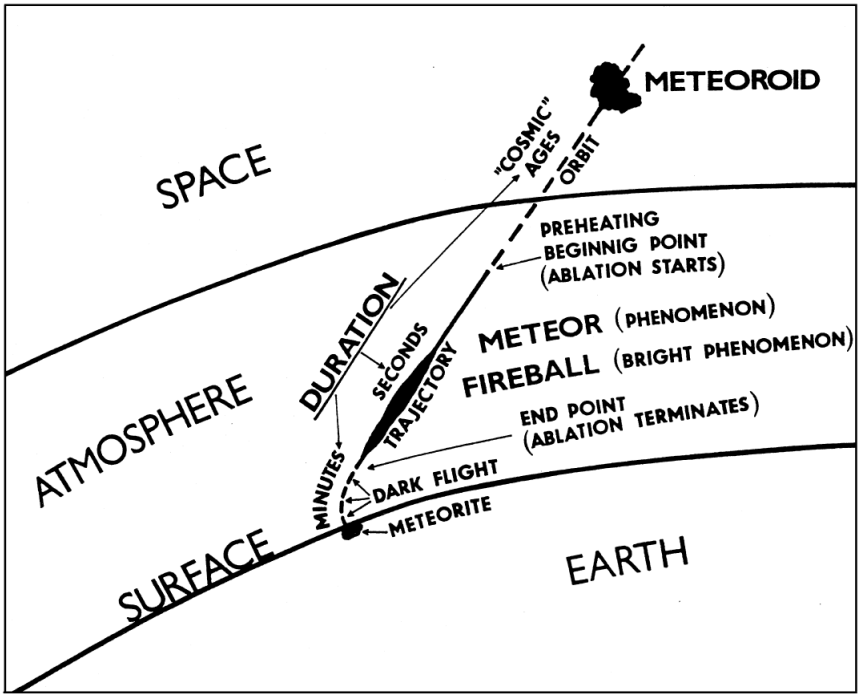

Figure 1.1: Atmospheric flight of a meteoroid and its phases (Ceplecha et al., 1998).

The meteorites that arrive on the surface of the Earth can be considered as the messengers of the cosmic history as they carry the most crucial and indigenous elements that were part of the planetary formation few billions years ago (Jenniskens and Jenniskens, 2006; Spurny, 1997). With these materials, scientists can get an opportunity to investigate the origin of the solar system and asteroids (Spurný et al., 2012), not just limited to the telescopic observations of the planets from Earth. Not only this, but meteorites have also been an impetus to the scientific research during the space race for studying the dynamics of re-entry vehicles (Hansen et al., 1957; Riddell and Winkler, 1962; Silber et al., 2018). The dynamics and the heat transfer phenomenon experienced by a meteoroid during its fall quite similar to the flight of re-entry vehicles. This research provided a plethora of data to thrust the study of high-speed vehicles. In summary, these small fragments of rocks that visit the Earth sporadically, carries indispensable information and myriad opportunities to the mankind.

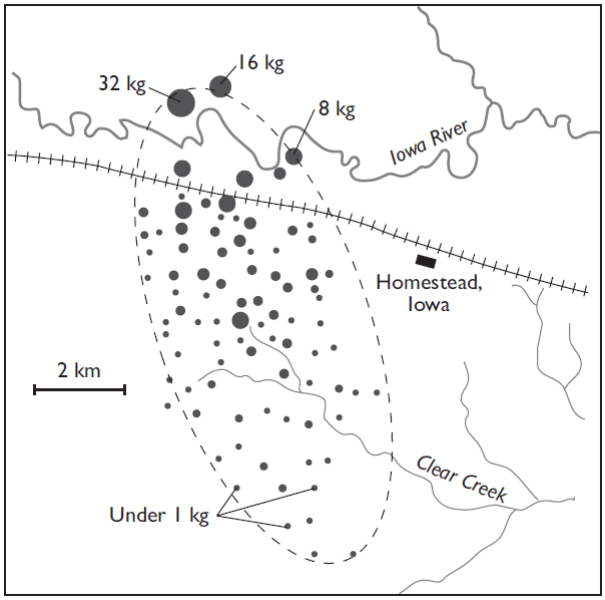

Figure 1.2: Generic strewn field of a meteorite fall (Lissauer and De Pater, 2013).

These meteorite falls are photographically observed and recorded from the surface of the Earth using multi-station camera networks spread worldwide such as Global Meteor Network (Vida et al., 2021), including Prairie meteor network (Artemieva and Pierazzo, 2009; Brown et al., 1996; Ceplecha and McCrosky, 1997) and Desert Fireball Networks (Bland et al., 2004; Devillepoix et al., 2018) in USA and Australia respectively. and in Australia. Such networks are spread across Europe such as AllSky7, FRIPON, Spanish Fireball Network, PRISMA, Swedish Allsky meteor network, Prairie meteor network etc., and associations such as The Meteor Section[1] in the Netherlands (Anderson et al., 2020; Brown et al., 2011; Brown et al., 2019; Colas et al., 2020; Devillepoix et al., 2018; Gardiol et al., 2016; Hankey et al., 2020; Oberst et al., 1998; Olech et al., 2017; Sansom et al., 2019; Sansom et al., 2015; Spurný et al., 2012; Stempels and Kero, 2016; Trigo-Rodríguez et al., 2006; Vida et al., 2021). These cameras record the meteorite fall from different locations on the surface at various angles. With this data, the data regarding various properties of the meteoroid such as its position, mass, interplanetary orbit as well as radiation, fragmentation can be extracted (Ceplecha et al., 1998). However, these instruments record the data of the luminous trajectory of meteorite flight only. Once the meteoroid enters dark flight, it will be difficult to follow the trail of its path. The complex shape and the wind effects considerably influence the dark flight trajectory. For this, certain mathematical models based on the equations of motions (EOM) will be used by the scientists to predict the strewn field and to estimate the most probable locations of impact points of the meteorite fall. A detailed discussion about these dark flight models, their shortcomings and their application in numerous meteorite falls will be presented in the following section.

1.1. Shedding light on the dark flight

Significant progress has been made in the meteoritics field in terms of fireball trajectory estimation from the photometric data analysis with the help of enhanced observation techniques and powerful computational techniques (Borovička et al., 2019; Olech et al., 2017; Rodríguez et al., 2009a; Spurný et al., 2020; Vida, Brown, et al., 2019; Vida, Gural, et al., 2019; Zurita et al., 2020). However, the aerodynamics aspect of the meteorite falls is overlooked (Haack

[1] https://werkgroepmeteoren.nl/english/

et al., 2019; McCrosky et al., 1971; Sansom et al., 2019). Consequently, this resulted in abundant scientific literature that deals more with the trajectory analysis rather than the dynamics of a meteorite fall (Gritsevich, 2009; Sansom et al., 2015; Spurný et al., 2014). Hence, there is sparse literature that encompasses the dynamics of meteorite falls, in particular that deals with the dark flight (Andreic, 2011; Borovĭcka and Kalenda, 2003; Borovička et al., 2021; Carter et al., 2011; Vinnikov et al., 2017; Vinnikov et al., 2016; Vlasek, 1963). So, a detailed discussion about the relevant literature is presented below.

The work of Ceplecha (1987) presents the fundamental theoretical framework for the dark flight modelling. This model is employed in most of the meteorite fall analyses until today. In this model, the properties such as the position (h_T), velocity (v_T) and deceleration (a_T) of the meteorite at the terminal point (point at which the luminous trajectory ends) as well as the direction of flight will be used to estimate the 'dark flight trajectory' of the meteorite as well as the impact point of the meteorite on the surface. In this model, the Equations of Motion (EOM) of the non-ablating body as shown in equations (2.1),(2.2),(2.3) will be used.

$$\frac{dv_l}{dh} = \frac{-1}{v_h}\left[\Gamma S\rho v(V_1 + v_1) + 2\omega(v_x\ sin\ \phi + v_h\ cos\ \phi\ sin\ a_R)\right] \tag{1.1}$$

$$\frac{dv_h}{dh} = \frac{-1}{v_h}\left[\Gamma S\rho v v_h + g - 2\omega\ cos\ \phi(v_l\ sin\ a_R + v_x\ cos\ a_R)\right] \tag{1.2}$$

$$\frac{dv_x}{dh} = \frac{1}{v_h}\left[\Gamma S\rho v(V_x + v_x) + 2\omega(v_l\ sin\ \phi - v_h\ cos\ \phi\ cos\ a_R)\right] \tag{1.3}$$

where 'v' and 'V' are the meteoroid and the wind respectively. Subscripts l, h, x represent the meteoroid velocity in three perpendicular directions. 'Γ' is the drag coefficient of the meteoroid, which is a function of the Mach number, and 'S' is the ratio of the mass to the cross-sectional area of the meteoroid. The other parameters $\rho,\ \omega,\ \phi$ & a_R are the air density, the angular velocity of Earth's rotation, geographic latitude, and the astronomical azimuth of the flight direction respectively.

The differential equations (2.1),(2.2) and (2.3) are solved using Runge-Kutta integration technique with a usual step size of 0.01 km. However, the step size varies according to the altitudes, larger at higher altitudes and smaller at lower altitudes. And at each step the velocity of the meteoroid is calculated from the integration from the terminal point to the impact point.

Although this model can be applied to any atmospheric model, the main complexities in this model are the little-known wind field as well as the unknown shape of the meteoroid. With the latest meteorological models, precise wind models solve the first complication. However, to resolve the second complexity, a symmetrical shape such as sphere is assumed. This has been adopted in most of the dark flight simulations, without any sound argument for the assumption. The initial value of 'ΓS' parameter in the EOM is dependent on the mass, shape, density and drag coefficient, which are unknown to the observer at the terminal point. Thus, to solve the EOM, it is assumed that Γ changes as the function of Mach number (M) and S is assumed to be constant during the dark flight. This implies that the orientation of the meteoroid remains same throughout the dark flight.

This mathematical model is extensively used in the contemporary dark flight studies. However, this model does not consider the lift and side forces and other aerodynamic effects caused by the shape, orientation, and rotation of the meteoroid. Based on the few case studies of

meteorite falls discussed below, it was observed that these effects influence the dark flight trajectory. Therefore, in this study, various forces acting on an irregular shaped meteorite will be studied experimentally to investigate the effects of shape and rotation on the aerodynamics of the meteoroid. From the work of Vinnikov et al. (2016), it can be observed that the substantial part of the dark flight falls rapidly to subsonic velocities around the altitude of 10,000 m as shown in Fig. 1.3 and, covers considerable portion of time of flight. At these altitudes, the variation in the wind effects is also noticeable, as shown in Fig. 1.4 for one of the meteorite falls. At these altitudes, the atmosphere becomes denser enough to influence the airflow around the meteorite body.

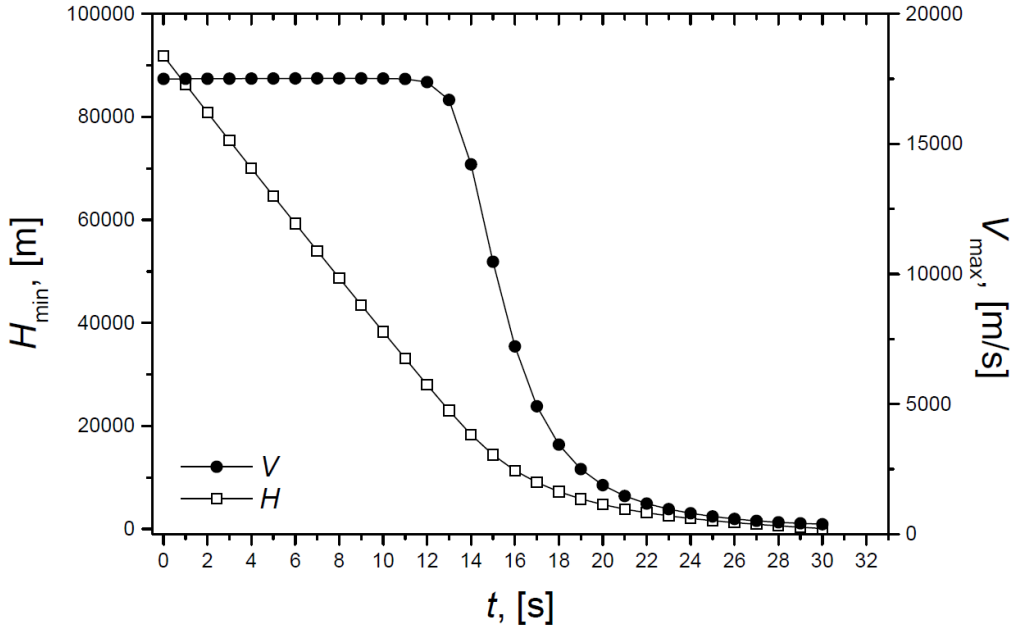

Figure 1.3: Results of variation of airborne fragment velocity with the altitude (Vinnikov et al., 2016).

Also, most of the dark flight analysis is performed using a dimensionless factor known as 'Shape Coefficient' (A) of the meteorite will be used to solve the EOM, which is defined by McCrosky et al. (1971) as follows.

$$A = S\left(\frac{\rho}{M}\right)^{2/3} \tag{1.4}$$

where, M, ρ and S is the mass, bulk density, and projected frontal area of the meteorite cross section respectively.

The necessity for the analysis of meteorite aerodynamics can be clearly seen in the Ejby meteorite recovery, where Haack et al. (2019) attributes the deviation of its heaviest fragment - '*Herlev*' fragment, primarily to the aerodynamic effects and concludes that only aerodynamics can explain its recovery. In addition to this, Haack further contemplates the effects such as Magnus force or the oriented fall might have influenced its trajectory during the dark flight phase. In addition to this, regarding the Flensburg fall, Borovička et al. (2021) argues that changing the product of drag coefficient (Γ) and Shape coefficient (A) from 0.8 to 0.65, results in better estimate in the predicted mass of meteorite. However, no argument was presented for the initial value assumption. On the contrary, in the other work that deals with the Morávka fall (Borovĭcka and Kalenda, 2003), this inconsistency is clearly observed when Borovička and Kalenda argues that reduction of 'ΓA' from an assumed value of 1.0 resulted in the un-

derestimation of the initial fireball mass and overestimation predicted meteorite mass. For this purpose, it is stated that reduction from 1.0 to 0.8 would result in better but not complete agreement with recovered meteorites. Hence, this inconsistency in the 'ΓA' was observed in the dark flight modelling part of meteorite fall.

Furthermore, it was seen that large jumps that are made in the trajectory assumptions in terms of assumptions, resulted in strange results in the meteorite recovery, which was not delineated by authors themselves. The fall of Grimsby meteorite (Brown et al., 2011) can be considered as one such case, where the variation of shape and drag coefficient were not considered in modelling. Interestingly, a small fragment with unusual wafer shape of mass 17g was found directly under fireball trajectory. To explain this, it was assumed that odd drag behaviour must be exhibited by this fragment during its dark flight. Although, this cannot be stated as a causal relationship, it sure explains the need to consider the aerodynamic effects during modelling of the meteorite fall. Particularly, in case of the oriented fall for irregular shaped meteorites, projected area can vary during their flight if the meteorite orientation changes due to any perturbation. Hence, aerodynamic effects do play a crucial role in the flight of irregular shaped fragments.

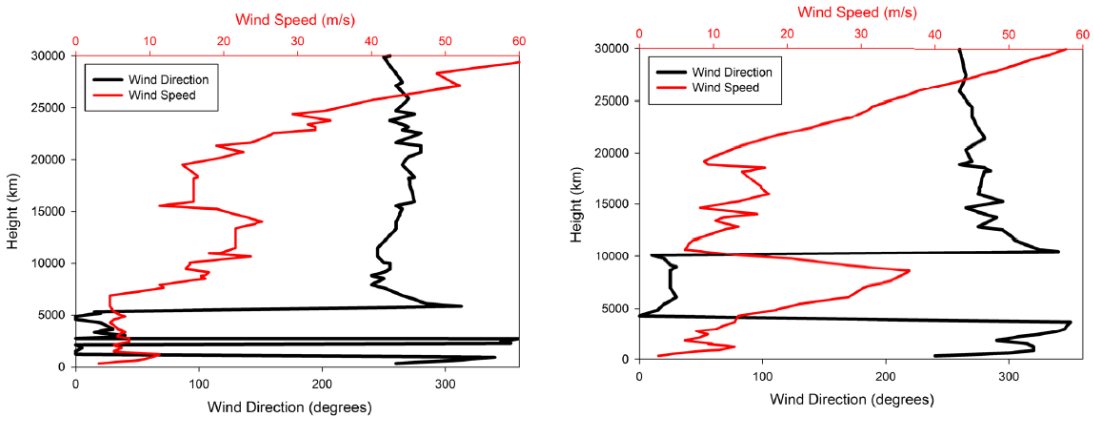

(a) Wind profile at 0 UT.

(b) Wind profile at 12 UT.

Figure 1.4: Wind profiles measured by radiosonde at White Lake, Michigan. Top plot is for 0 UT and bottom one at 12 UT (Brown et al., 2019).

Likewise, the numerical and other mathematical models (Vinnikov et al., 2017) does not consider the lift forces created by the flow around the fragments. In particular, Vinnikov et al. (2016) states that fragments are not symmetric, but still uses the spherical assumption for the dark flight calculation. Also, Vinnikov admits that the effects of the lift force created by the irregular fragments as well as the Magnus force were not considered in his model and further adds that Magnus force influences the fragment dispersion. Moreover, most of the dark flight models still utilise the mathematical model put forth by Ceplecha (1966) and Ceplecha (1987), with few modifications accounting the variation in wind profiles and other minor modifications. However, this model does not account for the aforementioned effects. In addition to this, few research works (Andreic, 2011; Brown et al., 2011; Haack et al., 2019) consider the drag coefficient for the sphere based on the work of Carter et al. (2009), which is only applicable for the spherical shapes. Even though, Zhdan et al. (2007) proposed the drag coefficients for the meteorite shape fragments in their work, it was only limited to the supersonic flow regime. Besides, Nguyen et al. (2019) study concluded that for an ellipsoid, the drag force will be doubled due to roughening the surface. Given that, an irregular fragment can be approximated as an ellipsoid (Kljuno and Catovic, 2019), similar affect might be observed in case of the meteorite.

The last experimental study on the aerodynamics of a meteorite was conducted on the Pribram meteorite (Vlasek, 1963). This study focused on the estimation of drag coefficient and did not study on the other aerodynamic forces. Moreover, the flow Mach number for this experiment lies between 0.5 to 3.5. Thus, the entire subsonic flow regime is not covered.

Thus, the need for the analysis of aerodynamic effects acting on the meteorite during its dark flight, for a better estimation of the impact points, was observed from various meteorite falls, numerical and experimental studies. The knowledge gaps identified from the literature is presented in detail in the following section.

1.2. Problem statement

From the literature review presented above, it is observed that the dark flight models that are extensively employed in the meteorite recovery studies makes assumptions regarding the shape of the meteorite and aerodynamic forces acting on it. Moreover, based on the case studies, it was evident that there is a need for the comprehensive analysis of the aerodynamics of the meteorite. It is not only for an improved estimation of the strewn field of a meteorite fall, but also to improve existing models with better insights of aerodynamic effects acting on the meteorite. Thus, from the above literature review, following fundamental research gap was identified in the meteorite aerodynamics, which was subdivided further.

- Lift and drag forces acting on irregular shaped meteorites in the subsonic regime is required for a better strewn field prediction.
  - Effects of the shape of the meteorite on the aerodynamic forces.
  - Lateral forces acting on the meteorite during the free fall is a requisite for better estimation of orientation and width of strewn field.
  - The key question on the rotational effects such as Magnus forces on a meteorite during the atmospheric descent still remains uninvestigated and is crucial in understanding the free fall dynamics of the meteorite.
  - Effect of bow shock on the trajectory of a meteorite in dark flight on the lift and drag forces needs to be addressed.
  - Effect of the atmospheric winds and gusts on the stability of the oriented meteorites has not yet been clarified.

No dedicated study was made to fill in these gaps in terms of the irregular shaped meteorites. This can be understood from the complexity involved in each of the subdivided research idea. Therefore, the aerodynamic analysis of meteorites is something that remained as a dark corner in the meteoritics field and has a potential to open door for numerous research opportunities.

1.3. Research objective & questions

With the advancement in the experimental facilities, measurement techniques as well as fabrication techniques, experimental studies can be carried out for a better comprehension of aerodynamics effects acting on a meteorite. Till date, no exclusive experimental study was carried out for the aerodynamic analysis of meteorites in the subsonic flow regime. From the work of Vinnikov et al. (2016), it can be noticed that subsonic flow regime is significant amount of meteorite dark flight lies in the subsonic regime and this occurs approximately around an altitude of 10 km. At these altitudes, the flow over the meteorite body will be more noticeable and crucial due to its travel in denser atmosphere. Hence, an experimental investigation

encompassing the analysis of the meteorite dark flight from an altitude of 10 km can provide interesting insights regarding meteorite aerodynamics. Thus, using a recovered meteorite model, the aerodynamic characteristics of a meteorite during dark flight can be studied using a subsonic wind tunnel. This experimental study can serve as a potential benchmark for the prospective studies in the meteorite aerodynamics. This can also be used to validate the assumptions used in existing dark flight models. Hence, for the scope of the current thesis project, on the basis of aforementioned knowledge gaps from the literature study, the following research question was formulated:

What are the aerodynamic characteristics of an irregularly shaped meteorite during the subsonic regime of its dark flight?

This research question can be further subdivided as follows:

1. What is the variation of the aerodynamic forces acting on a meteorite with respect to the altitude?
2. How does the shape of a meteorite affects the aerodynamic forces?
3. How does the shape factor (A) and 'ΓA' vary for a single meteorite?
4. What is the effect of the rotation in the variation of the aerodynamic forces on the meteorite?

1.4. A Novel Approach

With the advancement of the 3D printing technologies, such as the high-quality 3D scanning of the surface details, better precision and accuracy on the printing and range of materials, meteorite models with fine surface details can be printed using 3D printers. Since meteorite's shape is highly irregular, 3D printing can be considered as the most appropriate technique for the fabrication of meteorite model. Using computer aided modelling software such as SOLIDWORKS and CATIA, the meteorite model can be modified, such that it can be used as a test model in the wind tunnel. With these software, necessary modifications such as scaling of the model for creation of similar flows and any design additions can be done. This offers a great flexibility to print the meteorites for various test conditions with great quality and precision. Therefore, this offers a possibility for a better and accurate study of meteorite aerodynamics, compared to other studies till date.

Hence, with the amalgamation of these techniques, a 3D printed model of Broek in Waterland meteorite will be used as the test model in the subsonic wind tunnel in the current thesis project. Thus, the approach used for the current thesis project is completely novel and can be considered as the state of the art in the field of meteoritics.

1.5. Thesis Outline

In this thesis report, the fundamental backdrop required for the basic understanding of the thesis work is presented in Chapter 1, including the research questions. Chapter 2 contains the entire thesis work presented as a journal article for professional audience of the meteoritics community. In this journal article, a brief introduction about the thesis project and a condensed review of relevant literature is presented in the section 2.1. The detailed description regarding the experimental setup including the instrumentation will be presented in Section 2.2. The methodology of the experimental procedure will be discussed in Section 2.3. Based on the results presented and discussed in Section 2.4. Finally, current study is concluded in Section

2.5 which also contains the recommendations for the future work. The supplementary material that discusses the underlying work of the thesis project is presented in Chapter 3. Section 3.1 deals with the experimental data acquisition, followed by the flow similarity analysis in Section 3.2. Detailed discussion regarding the dark flight calculator implemented in the current thesis study is presented in Section 3.3. Again, in Chapter 4, the overarching conclusion for the thesis work is presented, followed with detailed recommendations for future work in Chapter 5. Finally, Appendix A presents a detailed procedure for the conversion of 3D mesh data into a solid model for interested audience.

2

Journal Article

Meteorite aerodynamics during dark flight using subsonic wind tunnel experiments

S.G.V.S. Aduru *et al.*[1]

[1] *Department of Astrodynamics and Space Missions, Delft University of Technology, the Netherlands*

Abstract

The laborious task of meteorite recovery is always complicated by the effects of aerodynamic forces acting on the meteorite during the dark flight, as well as its shape. In multiple meteorite recoveries, the effect of aerodynamic forces acting on the meteorite during its dark flight is speculated as the reason for this deviation from the predicted trajectory. Hence, limited knowledge of the aerodynamic properties of meteorite can be attributed as one of the major reasons for partial recovery of the meteorite. Therefore, in the current study, we investigate the various aerodynamic forces acting on the meteorite during its free fall in the dark flight phase and the effect of meteorite shape on the aerodynamic forces. To evaluate these effects, experiments were conducted in a low-speed wind tunnel. A 3D printed meteorite model was used to analyse various aerodynamic forces acting on the meteorite. Broek in Waterland meteorite was considered for the current study as the test model. Firstly, the drag coefficient of the model was measured accurately. From an altitude of 10 km, meteorite travels at subsonic velocities in denser atmosphere for a considerable time. This can offer an important insight into the aerodynamic effects. Hence, the free fall analysis of the meteorite during its dark flight was considered from 10 km until Mean Sea Level. Firstly, an accurate drag coefficient of the meteorite model was estimated to calculate the terminal velocities at the required altitudes. On the basis of calculated terminal velocities, a scaled model was used to create similar flows conditions for the free fall over the meteorite model. The required scaling factor of the test model was estimated using flow similarity analysis. With the scaled meteorite model the variation of the aerodynamic forces during the free fall of the meteorite descent was studied. Using an additional setup, the rotational aspects of the meteorite were also investigated in this study. Finally, the estimated drag coefficient and shape factor were implemented in a dark flight code to study the influence of these parameters on the impact points of a meteorite fall. Based on the results, it was identified that a range of drag coefficient values exists for a single meteorite and for the Broek in Waterland meteorite, the range lies between 0.36 to 0.88. The results of the experiment have proved that there is a finite amount of lift and side forces are experienced by the meteorite during its atmospheric flight. the experiments showed that for a non-rotating oriented flight of the meteorite, side and lift forces exists and strongly influence the impact points. And the impact points for a single body gets separated by 24 km when the orientation of the meteorite is changed. We show that aerodynamic forces are very crucial in the meteorite dark flight and strongly affect the trajectory of dark flight, thereby influencing the impact points of the meteorite. We propose that better parametrisation of meteorite aerodynamic parameters in the dark flight model is needed for better strewn field estimation.

Keywords: Broek in Waterland, Strewn field, Oriented flight, Rotation, Shape factor.

2.1. Introduction

The meteoritics domain has witnessed tremendous progress during the last decades due to the evolution of robust observation techniques coupled with efficient as well as powerful computational methods of data analysis (Gritsevich, 2009; Sansom et al., 2015; Spurný et al., 2014). This allowed for abundant research to be carried out in terms of fireball trajectory analysis as well as reconstruction of the interplanetary trajectory of the meteoroid to trace back its genesis (Borovička et al., 2003; Borovička et al., 2021; Brown et al., 2011; Devillepoix et al., 2018; Spurny et al., 2002; Spurný et al., 2012). In contrast, very little light was shed on the meteorite's dark flight, making this dimension of meteoritics still obscure. Moreover, the available literature usually discusses individual meteorite fall and focuses more on the trajectory analysis (Borovička et al., 2019; Olech et al., 2017; Rodríguez et al., 2009a; Spurný et al., 2020; Vida, Brown, et al., 2019; Vida, Gural, et al., 2019; Zurita et al., 2020), and the aerodynamics aspect is overlooked (Haack et al., 2019; McCrosky et al., 1971; Sansom et al., 2019). As a consequence, the volume of literature concerning meteoroid dynamics, particularly during the dark flight can be considered minuscule (Andreic, 2011; Borovĭcka and Kalenda, 2003; Borovička et al., 2021; Carter et al., 2011; Vinnikov et al., 2017; Vinnikov et al., 2016; Vlasek, 1963).

Over the decades, the dark flight model presented by Ceplecha (Ceplecha, 1987; Pecina and Ceplecha, 1983) remained ubiquitous and unvaried in several meteorite fall recoveries. The foundational framework for Ceplecha's analytical model is based on the equations of motion (EOM) of a non-ablating meteorite as follows.

$$\frac{dv_l}{dh} = \frac{-1}{v_h}\left[\Gamma S\rho v(V_1 + v_1) + 2\omega(v_x\ sin\ \phi + v_h\ cos\ \phi\ sin\ a_R)\right] \tag{2.1}$$

$$\frac{dv_h}{dh} = \frac{-1}{v_h}\left[\Gamma S\rho v v_h + g - 2\omega\ cos\ \phi(v_l\ sin\ a_R + v_x\ cos\ a_R)\right] \tag{2.2}$$

$$\frac{dv_x}{dh} = \frac{1}{v_h}\left[\Gamma S\rho v(V_x + v_x) + 2\omega(v_l\ sin\ \phi - v_h\ cos\ \phi\ cos\ a_R)\right] \tag{2.3}$$

where 'v' and 'V' are the meteoroid and the wind respectively. Subscripts l, h, x represent the meteoroid velocity in three perpendicular directions. 'Γ' is the drag coefficient of the meteoroid, which is a function of the Mach number, and 'S' is the ratio of the mass to the cross-sectional area of the meteoroid. The other parameters $\rho,\ \omega,\ \phi$ & a_R are the air density, the angular velocity of Earth's rotation, geographic latitude, and the astronomical azimuth of the flight direction respectively.

This analytical model is considered advantageous because it supports wide range of atmospheric models to derive the properties of wind at various altitudes. However, the unknown shape of the meteoroid remains as a complexity of this model, for which Ceplecha assumes a symmetrical spherical shape for the meteorite. Numerous meteorite fall studies have used the Ceplecha's model for the dark flight analysis (Borovĭcka and Kalenda, 2003; Borovička et al., 2013; Brown et al., 2011; Brown et al., 2019; Haack et al., 2019; Rodríguez et al., 2009b; Spurný et al., 2014; Trigo-RodrÍguez et al., 2010). Most of these studies adopted Ceplecha's model with the same assumptions regarding the shape of the meteorite and the aerodynamic forces involved.

Also, most of the dark flight analysis is performed using a dimensionless factor known as 'Shape Coefficient' or 'Shape Factor' (A) of the meteorite will be used to solve the EOM, which

is defined by McCrosky et al. (1971) as follows.

$$A = S\left(\frac{\rho}{M}\right)^{2/3} \tag{2.4}$$

where, S,ρ and M is the projected frontal area, bulk density, and mass of the meteorite respectively.

Although Ceplecha's model (Ceplecha, 1987; Pecina and Ceplecha, 1983) was considered the standard dark flight model in the meteoritics field, it did not encompass the effects of shape and aerodynamics of a meteorite. On the other hand, Vinnikov et al. (2016) proposed a mathematical model for the dark flight dynamics. This model covers other dark flight features such as the possibility of fragmentation and presents a discussion on the aerodynamic interaction of a meteorite in hypersonic and supersonic flow regimes. But both the models fall on the same line in terms of the meteorite shape assumption. Based on the results, it was identified that the meteorite attains subsonic terminal velocities rapidly after the fragmentation event. It was stated that the wind effects become more prominent near an altitude of 12 km due to the strongest winds at those altitudes. While it may be true that the simulation of this model performed well, Vinnikov et al. (2016) states that the even though the real fragments will not be symmetrical, the model did not cover the important factors such as lift forces and the Magnus effect acting on the meteorite.

Therefore, the strewn field estimation of existing dark flight models is susceptible to the values of aerodynamic parameters assumed for the meteorite (Brown et al., 2019). Furthermore, the assumptions made by the researchers do not appear rational every time and mostly oversimplifies the dark flight models. In addition to this, an inconsistency in the assumption of the drag coefficient and shape factor for the meteorite during the dark flight or ablation studies was observed in the literature (Borovĭcka and Kalenda, 2003; Borovička et al., 2021; Borovička et al., 2013; Brown et al., 1996; McCrosky et al., 1971). Each study considers different value for the drag coefficient (Γ) and shape factor (A) for a spherical shape of the meteorite. These values range between 0.5 (Borovička et al., 2019) to 1.6 (Andreic, 2011) for the drag coefficient, and between 1.21 (Gritsevich, 2008) and 1.8 (Haack et al., 2019). The aftermath of this inconsistency of assumptions can be observed in the deviation of the strewn field estimation (Borovička et al., 2019; Brown et al., 2011; Haack et al., 2019; McCrosky et al., 1971; Oberst et al., 2004; Trigo-RodrÍguez et al., 2010) as well as the discrepancy in the terminal mass estimation (Borovĭcka and Kalenda, 2003; Borovička et al., 2021). As there has been limited understanding regarding the meteorite aerodynamics during the dark flight, few fundamental characteristics need to be investigated for a better comprehension of the dynamics of a meteorite. To start with, these include (1) variation of aerodynamic forces acting on a meteorite with altitude and (2) effects of meteorite shape and its rotation on these forces. As mentioned earlier, the atmospheric flight covers a considerable amount of time in the subsonic regime (Brown et al., 1996; Vinnikov et al., 2016) and travels in a denser atmosphere from 10 km altitude, due to which airflow around the meteorite is more pronounced. Hence, this study focuses on the experimental study of the aerodynamics of a meteorite during dark flight.

The objective is to study the variation of the aerodynamic forces acting on the meteorite in the subsonic flow regime from 10 km altitude. To achieve this, the following aspects were examined. Firstly, the drag coefficient of the meteorite is determined. Secondly, the variation of the aerodynamic forces during its free fall in the dark flight will be analysed for the non-rotating model. Finally, the possibility of rotation of the meteorite will be explored. The experimental setup is explained in detail in section 2.2, followed by the methodology in section 2.3. The

results of the experimental analysis are presented and discussed in section 2.4, based on which the conclusions are drawn in section 2.5 including the recommendations for the future work in this path.

2.2. Experimental Setup

2.2.1. Wind tunnel & Instrumentation

The experiments were performed in a subsonic wind tunnel called 'W-Tunnel' at the Delft University of Technology. W-Tunnel is an open jet wind tunnel with a square test section. For the current experimental study, the test section of 40×40 cm^2 cross-section was used. With the contraction of this test section, a maximum speed of 35 ms^{-1} can be achieved in the wind tunnel. The minimum level of attainable turbulence level can be of order 0.5% depending upon the flow velocity. The forces and moments acting on the meteorite model were measured in three perpendicular directions (X, Y & Z axes) using a six-component balance (Alons, 2008). The acquisition of the data of forces and moments is carried out continuously using six load cells connected to the balance. Using this balance, the lift, drag, and side forces along with pitching rolling and yawing moments can be measured. Further information regarding the data acquisition during the experiment is presented in Section 3.1.

2.2.2. Test Model

For this experimental study, Broek in Waterland meteorite[1] was considered as the test model. On 11th January 2017, it fell in the Noord-Holland province of the Netherlands, making it one of the recent meteorites falls in the Netherlands. Older Dutch meteorites were sampled for the scientific studies and the present-day shape does not represent the state of the meteorite when it was recovered after the fall. In contrast, the three-dimensional shape of the Broek in Waterland meteorite was documented shortly after the recovery using photogrammetry before scientific sampling and its shape was altered. And a 3D model of this meteorite can be viewed in the Delft Meteorite Lab[2]. The irregular shape observed from Fig. 2.1a, makes is an interesting case study due to its contrasting shape parameters. Therefore, Broek in Waterland was chosen as the meteorite model.

Using SOLIDWORKS, the 3D model was converted into an SLDPRT (3D solid part) file as presented in Fig. 2.1b. Consequently, allowing to design threaded holes in the meteorite surface as shown in Fig. 2.2. With this, the model can be fitted on top of the model mount, both in horizontal and vertical orientations. Again, this design is converted into an STL file (stereolithography file), supportive of 3D printing. This conversion was carried out without losing the quality of surface detail. Detailed procedure of this conversion of 3D mesh data into a solid body was presented in Appendix A.

Finally, the model was 3D printed with Polylactic Acid (PLA) filament using a Prusa i3 MK3S+ printer. PLA is a widely used filament material in the 3D printing industry. The characteristics such as lower melting temperature, lower thermal expansion, and ease of printing aid PLA in capturing small and detailed surface features. Since meteorites usually have very high surface details that have a strong influence on the flow around them, PLA can be considered as the most appropriate filament material to print the meteorite model. For the experiments,

[1] https://www.lpi.usra.edu/meteor/metbull.php?code=65715
[2] https://sketchfab.com/3d-models/broek-in-waterland-l6-37b21c91ec5142008c72c743c8f10ab6

the meteorite was printed with PLA filament with a layer height of 0.1 mm and with a 30% cubic infill as presented in Fig. 2.3. Thus, the surface detail including the threaded hole was printed with very high surface detail and precision. Finally, the smooth surface of the meteorite is roughed using sandpaper to roughen the surface.

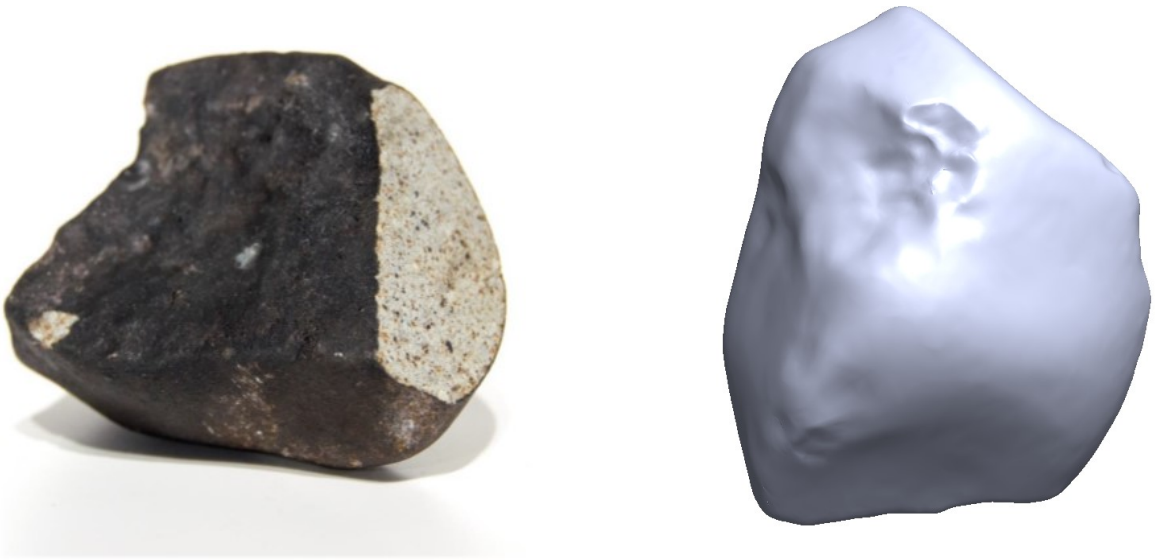

(a) Part of meteorite is sliced off for scientific study.

(b) 3D model of the original (uncut) meteorite.

Figure 2.1: Broek in Waterland meteorite and its 3D model created using SOLIDWORKS.

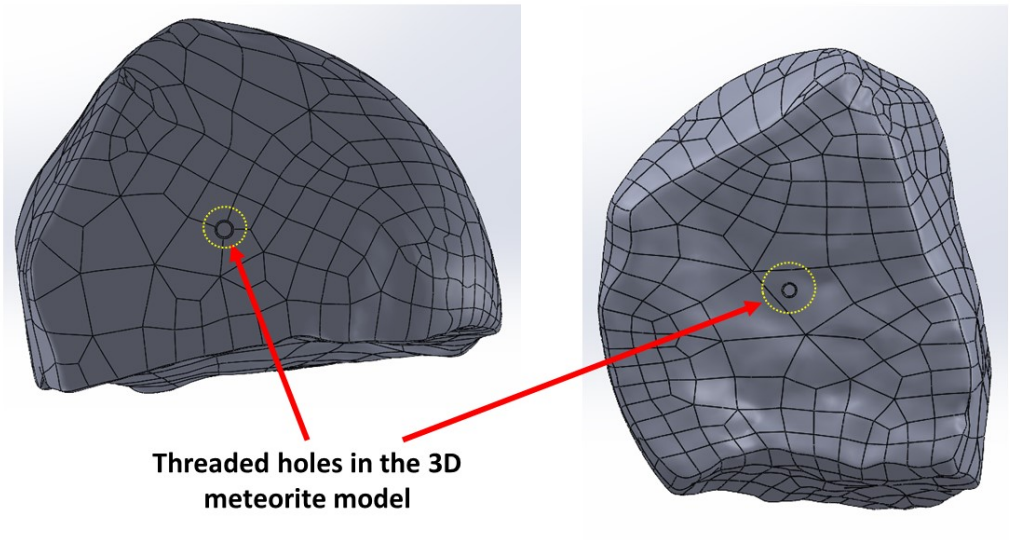

Figure 2.2: Threaded holes created using SOLIDWORKS to mount the test model vertically and horizontally on the support strut.

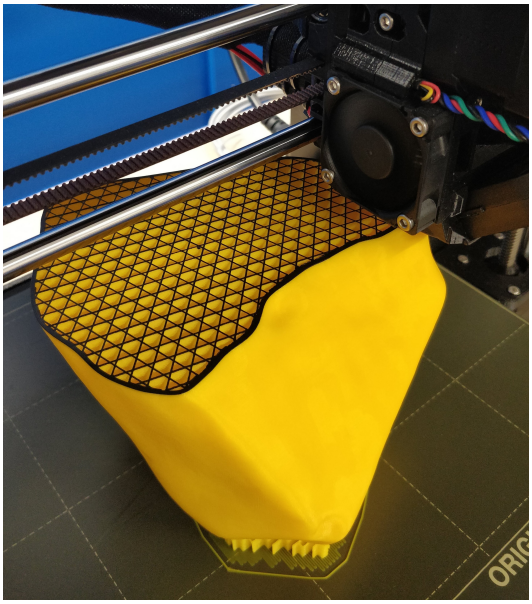

Figure 2.3: 3D printed meteorite test model with cubic infill using Prusa i3 MK3S+ printer.

2.2.3. Test Setup in the wind tunnel

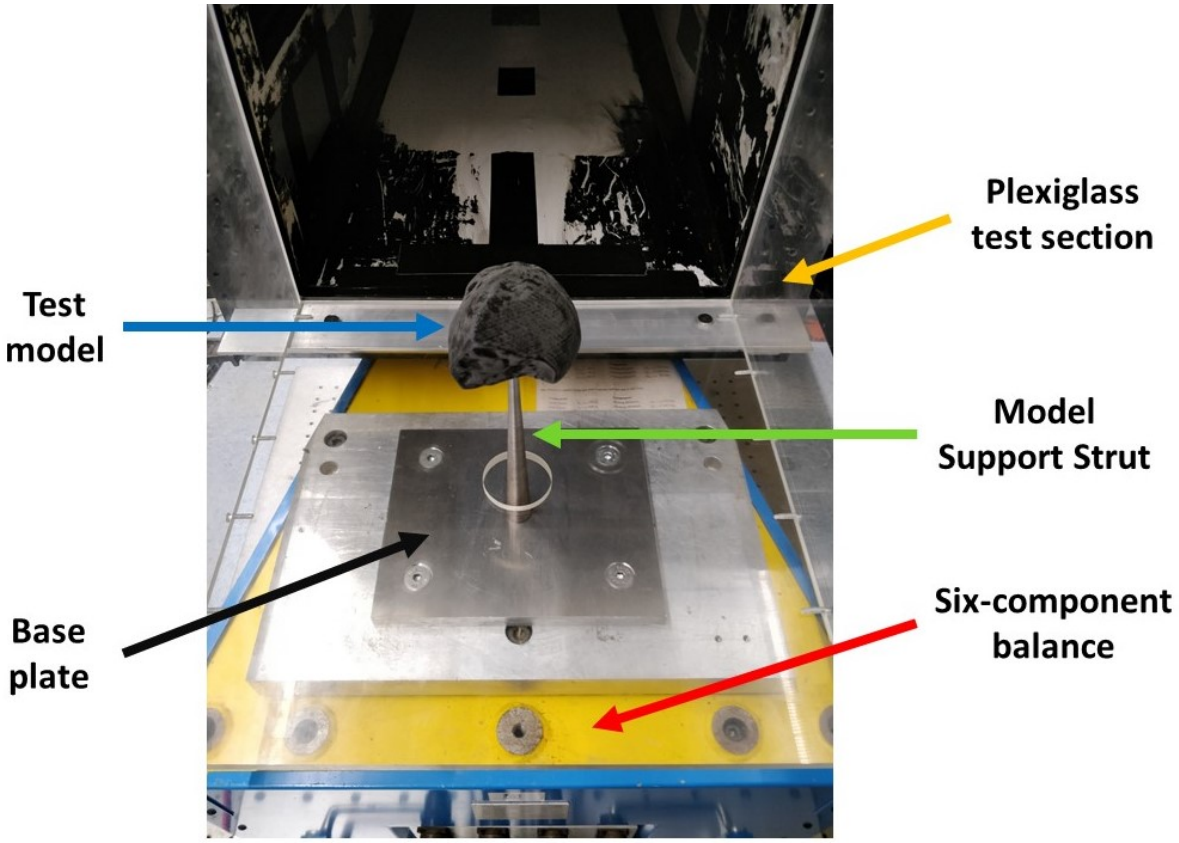

Figure 2.4: Experimental setup for the determination of drag coefficient and the free fall analysis. The meteorite is fitted on a vertical strut which is mounted on the six-component balance using a base plate.

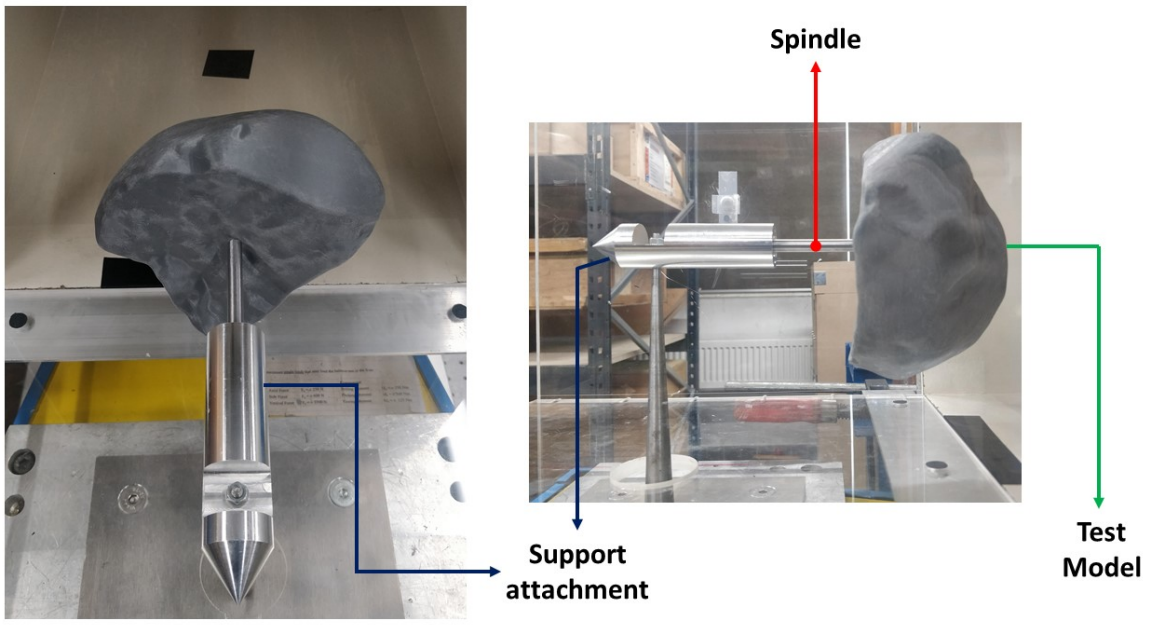

Figure 2.5: Experimental setup for the study of rotation of meteorite. The meteorite is fitted with the spindle which is inserted in the additional support attachment mounted on the vertical strut. With this mounting, the rotation of the meteorite can be studied with a rotational axis parallel to the flow direction.

For the experiments, initially, a 198 mm long cylindrical rod with 5 mm diameter was chosen as the vertical strut. However, at the wind velocities above 25 ms^{-1}, the strut started to vibrate continuously, which can be observed with a naked eye. Hence, it was replaced by a 180 mm long conical rod with 5 mm and 20 mm as top and base diameters. The rod had a threaded top that could be used to fit the meteorite model on the top of it. Finally, this vertical strut was mounted on the surface of the aforementioned six-component balance by using a base plate. A plexiglass test section is fitted over this setup to create a uniform control volume around the flow of meteorite. Since the meteorite stands on the top of the force balance, a small hole of 50 mm is created on the bottom wall of the test section. The setup is presented in Fig. 2.4. For the study of the rotation of meteorite with a rotational axis parallel to the flow direction, an additional attachment is designed which can be fitted on the top of the vertical strut as shown in Fig. 2.5. A shaft is inserted into this attachment and the meteorite model is then fitted on the top of the shaft to face the flow.

2.3. Methodology

2.3.1. Determination of drag coefficient for the meteorite model

The drag coefficient of an object is dependent on its shape. Particularly, in the case of meteorites, as the shape varies, consequently, the drag coefficient differs for each meteorite. Thus, firstly, in this study the accurate drag coefficient of the Broek in Waterland meteorite model is determined. The Broek in Waterland meteorite resembles an irregular shape which can be enclosed by rectangular cuboid, due to its two flat surfaces perpendicular to each other and its overall geometry. Therefore, for the wind tunnel investigations a 1:1 test model is studied with six faces facing the flow as shown in Fig. 2.6.

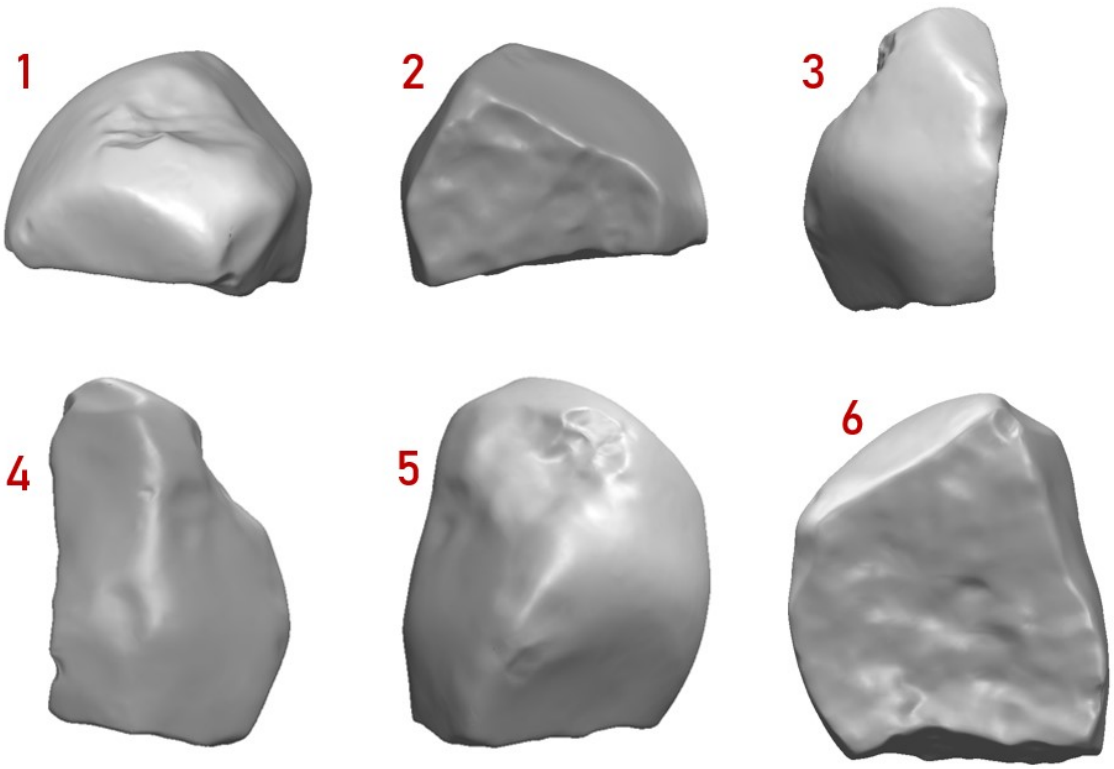

Figure 2.6: Six faces of meteorite that face the flow in the wind tunnel. The direction of the flow is into the paper.

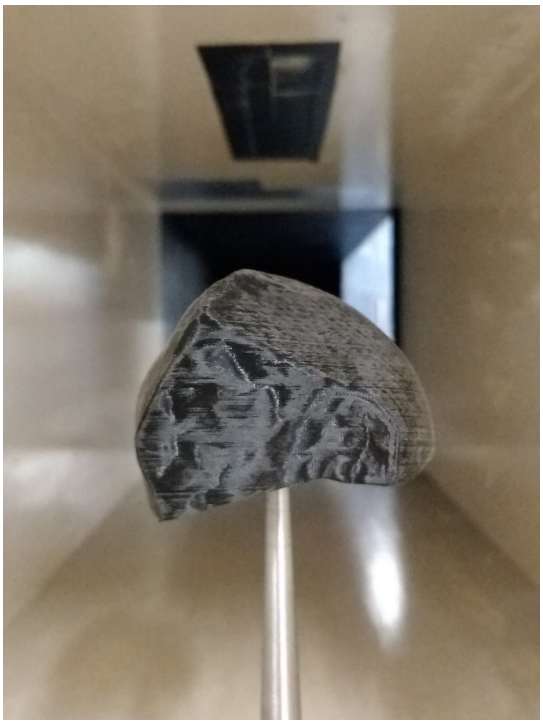

(a) Horizontal Orientation (face 1 facing the flow).

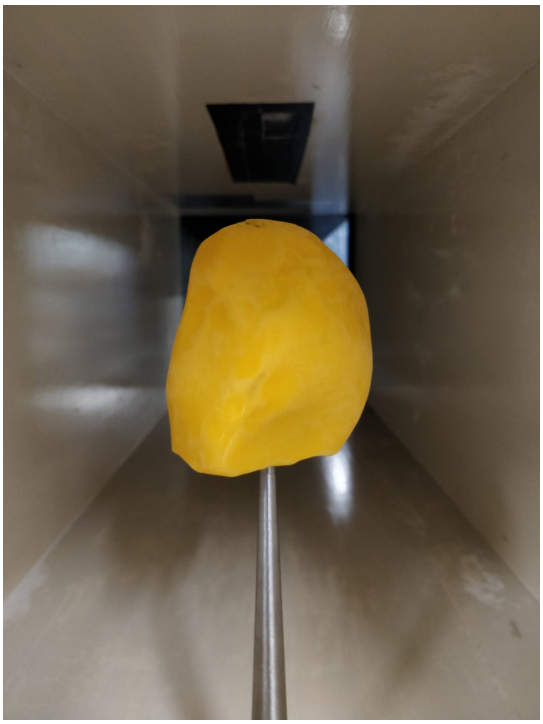

(b) Vertical Orientation (face 6 facing the flow).

Figure 2.7: Orientation of the meteorite model with faces 1 and 6 facing the flow in the wind tunnel test section.

Experiments on the face 1 and 2 are performed by mounting the model horizontally as shown

in Fig. 2.7a. Similarly, faces 3,4,5 and 6 are mounted vertically as shown in 2.7b. The drag force for each of these six meteorite faces is measured between the wind tunnel velocities of 20^{-1} to 30 ms^{-1}. Considering the vertical length of the meteorite (as in faces:3,4,5 & 6), these velocities correspond to the flow Reynolds number (Re) between $\mathbf{1.29 \times 10^4}$ and $\mathbf{1.94 \times 10^4}$. Since the forces are measured using the six-component balance, along with the drag force, the side force as well as lift forces can also be measured. With the projected area for each of these faces (S), the coefficient of each force is calculated as follows

$$C_F = \frac{2F}{\rho V^2 S} \tag{2.5}$$

where F: lift, drag and side forces and ρ and V are the flow density and velocity respectively.

2.3.2. Free fall analysis of the meteorite during the dark flight

The variation of the aerodynamic forces such as the lift, drag, and side forces acting on the meteorite during its free fall from an altitude of 10 km in the dark flight will be measured. However, there will be a considerable variation in the atmospheric parameters such as density and viscosity of air between the Mean Sea Level (MSL) and at an altitude of 10 km. Also, the terminal velocity of the meteorite varies with the altitude. As a result, these atmospheric conditions cannot be exactly created in the wind tunnel. Nevertheless, using the 'Flow Similarity', dynamically similar flows can be created as long as (1) the flow similarity parameters such as M and Re stay the same and (2) the geometric shape remains geometrically similar for both flows (Anderson, 2017).

The variation of the aerodynamic forces will be measured from 10 km altitude until the MSL at steps of 2500 m using the flow similarity. However, at MSL, the velocity will be zero as the meteorite will touch down the surface of the Earth. So, 100 m will be considered as the endpoint of the current study. Therefore, the experiments will be performed for the dynamically similar flows at altitudes 100 m, 2500 m, 5000 m, 7500 m, and 10,000 m for a stationary model. The flow similarity can be attained in two ways. Firstly, for a constant wind tunnel velocity, different geometrically similar models can be used to recreate similar flows. Conversely, a single geometrically scaled model can be used to create similar flows at different operating velocities in the wind tunnel. Since the second approach is very less logistical complexity, in this study, the second method is used to create similar flows.

Therefore, based on the accurate drag coefficient measured for the meteorite, terminal velocity of the meteorite at each altitude will be calculated. Based on this, the scaling factor of the meteorite model to be used for the free fall analysis can be determined based on the trade-off study between the maximum wind tunnel velocity and the blockage ratio. Detailed discussion regarding the trade-off study and the free fall analysis is presented in sections 3.1 and 3.2. If the test model mounted in the test section blocks more than 5% of the test section area, then the velocity measured during the experiments will be corrected accordingly to account the blockage. The corrected velocity (V_C) can be calculated by applying the mass conservation principle as follows

$$V_\infty A_{\mathsf{TS}} = V_C A_C \qquad \text{with} \qquad A_C = A_{\mathsf{TS}} - A_{\mathsf{Proj}}$$

$$\therefore V_C = V_\infty \left[\frac{A_{\mathsf{TS}}}{A_C} \right] \tag{2.6}$$

where V_∞, V_C are the free stream and corrected flow velocities respectively, and A_{TS}, A_{Proj} & A_C are the test section area, projected area of the meteorite model and corrected test section area respectively.
Subsequently, using the corrected velocity, the force coefficients (C_F) are estimated using equation (2.5). The corrected force coefficient is calculated as follows:

$$C_F = \frac{2F}{\rho V_C^2 S} \tag{2.7}$$

where F: lift, drag and side forces and ρ and V are the flow density and velocity respectively.

2.3.3. Study of rotation of the meteorite

Finally, in this set of experiments, the free fall during the dark flight of the meteorite will be analysed for a rotating model with a rotational axis parallel to the flow direction. The test model used in the previous set of free fall analysis will be used in this set of experiments. This is carried out to explore the rotational characteristics of the meteorite, such as the variation of drag, lift, and side forces acting on the rotating body. The possibility of the free rotation of the meteorite will be verified in this set of experiments. It is carried out by attaching the model to a spindle which is inserted inside an additional attachment as shown in Fig. 2.5. The spindle is rotated by means of two ball bearings fitted inside the attachment. The axis of spindle is set parallel to the flow direction, thus making the meteorite model face the incoming flow. The experimental investigation of free rotation will be formed for the rotation of the model in horizontal and vertical orientations.

2.4. Results & Discussion

As mentioned in section 2.3, the wind tunnel experiments are conducted in three stages. Firstly, the drag coefficient of the meteorite model is measured accurately. Secondly, based on the estimated C_D, a free fall analysis from an altitude of 10 km was conducted. Finally, the possibility of rotational and associated aspects is studied. The results obtained from these stages of experiments are discussed in detail in sections 2.4.1, 2.4.2 and 2.4.3 respectively. Then, the effect of variation of drag and shape factor for each face is implemented using a dark flight calculator and the corresponding results were presented in section 2.4.4.

2.4.1. Estimation of C_D

Wind tunnel tests were carried out to accurately measure the Drag coefficient (Γ or C_D) for the Broek in Waterland meteorite model. In addition to this, the lift and the side forces acting on the meteorite model were measured and analysed, and the results are tabulated in Table 2.1. The variation of the aerodynamic parameters of the meteorite model such as Coefficients of drag, lift, and side forces (C_D, C_L&C_S) for each face is presented in Fig. 2.8 & 2.9.

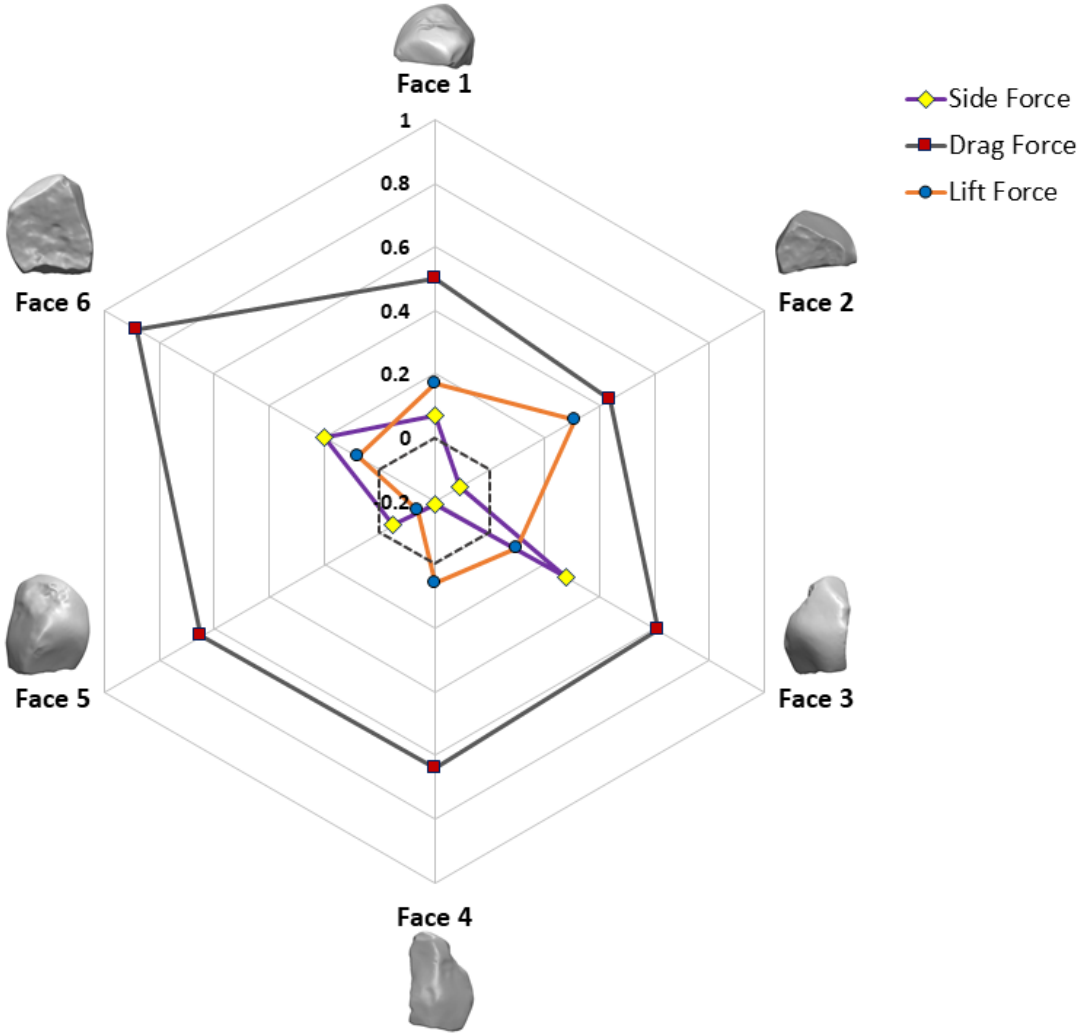

Figure 2.8: Radar plot of the variation of C_D, C_L & C_S for each face of the meteorite model orientation. The force coefficients are averaged over the Reynolds number range of $1.29 \times 10^4 - 1.94 \times 10^4$. The dotted hexagon represents the zero value of the force coefficients.

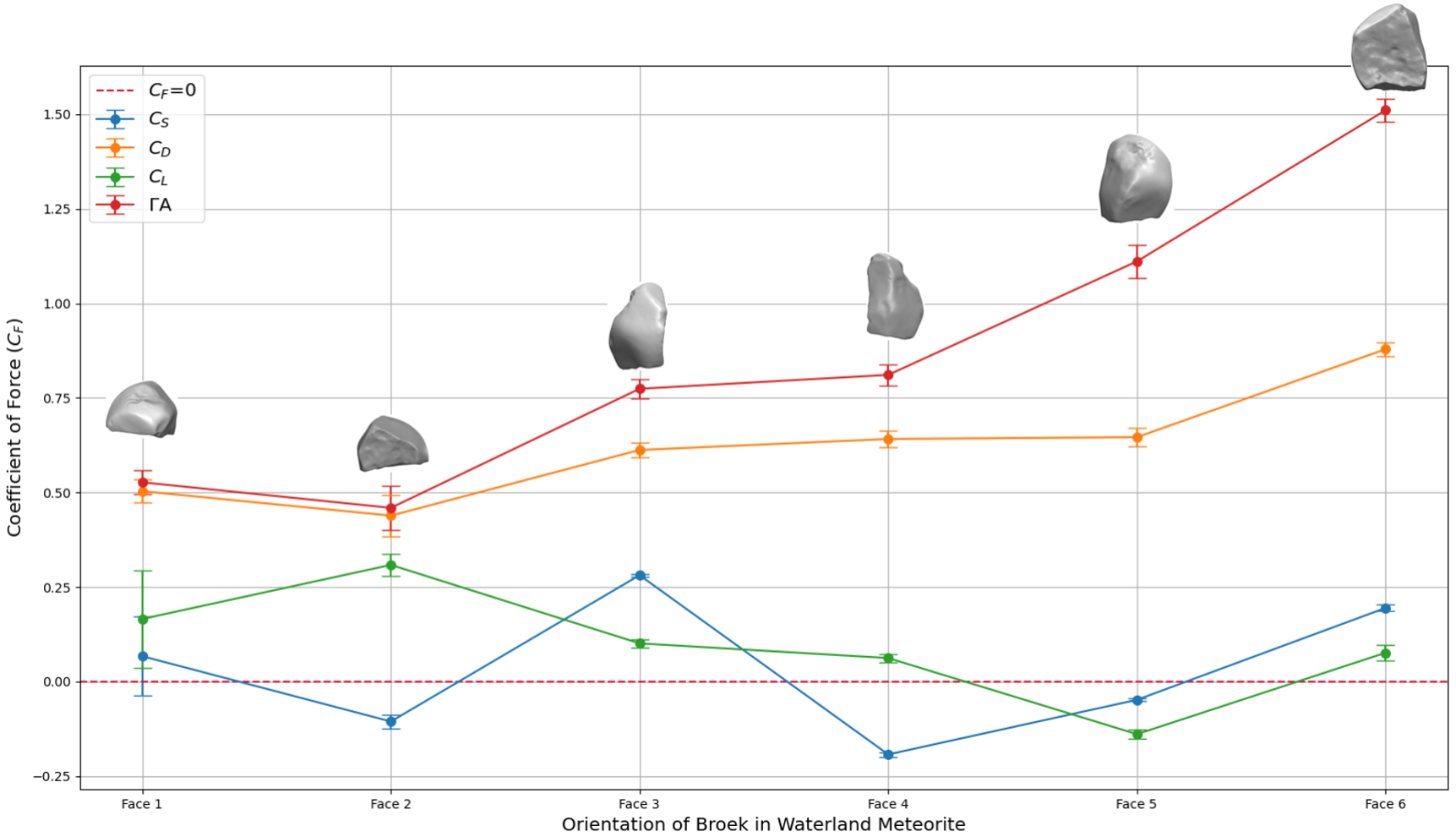

Figure 2.9: Variation of the force coefficients and ΓA for each face of the meteorite model orientation. The force coefficients are averaged over the Reynolds number range of $1.29 \times 10^4 - 1.94 \times 10^4$.

Fig. 2.8 presents the holistic radar plot of the variation of the of lift, drag and side force coefficients for each of the six faces of the meteorite orientation. For each face, the mean value of the magnitude of force coefficients averaged over the Reynolds number range of 1.29×10^4 and 1.94×10^4 is presented in the radar plot. It can be observed that unlike the assumptions held in the usual dark flight studies, there is a finite amount of the lift and side forces acting on the meteorite. On the other hand, Fig. 2.9 presents a delineated picture of this variation including the ΓA value of six faces. It can be observed that each of the meteorite model has a unique C_D value that ranges from 0.44 to 0.88 with a mean value of 0.62. However, a single value is assumed for the drag coefficient for a meteorite in the dark flight studies that lies between 0.5 to 1.6 (Andreic, 2011; Borovĭcka and Kalenda, 2003; Borovička et al., 2021; Borovička et al., 2019; Ceplecha, 1987). Therefore, the mean value of the current study falls within the range of literature. Hence, if the orientation of the meteorite facing the flow during the free fall of its dark flight changes, the drag value can change considerably, approximately by 100% in the current study. Consequently, the impact points for each of the face changes accordingly. Therefore, considering a single value for the drag coefficient can be inefficient for the strewn field estimation for a meteorite fall. Because considering a single value for drag coefficient can exclude other possible impact points of the meteorite fall.

The variation of the aerodynamic parameters for each face of meteorite model with flow Reynolds number is presented in Fig 2.10 .The six faces of the meteorite model that were analysed in the current study are grouped into three pairs to provide better insight into the interesting aerodynamic traits observed from the analysis. Each pair consists of two faces that are turned apart by 180°, thus exactly opposite to each other.

Table 2.1: The variation of mean values of the coefficient of side, drag and lift forces and ΓA for different meteorite faces.

Face	Coefficient of Side force (C_S)	Coefficient of Drag force (C_D)	Coefficient of Lift force (C_L)	ΓA
1	0.06713	0.503389	0.165511	0.526943
2	-0.10557	0.438842	0.308587	0.459376
3	0.281332	0.612442	0.101049	0.774254
4	-0.19269	0.641534	0.062173	0.811032
5	-0.04826	0.646271	-0.13911	1.11111
6	0.194725	0.878835	0.076187	1.510949

Pair 1 (Face 1 & 2):

Face 2 was expected to experience higher drag force due to the flat surface facing the flow. But the opposite was observed from the results as shown in Table 2.1 and Fig. 2.10a. On the other hand, the lift force acting on the face 2 is higher than face 1. Therefore, face 2 has twice the lift to drag ratio than face 1. This can be accounted to the fact that orientation of model with face 1 facing the flow is similar to an automobile shape and the presence of dimple shaped regmaglypt as shown in Fig. 2.11 may have attributed to further down force acting on the model producing lesser lift. Similarly, the flat surface at the bottom of the face 2 might have created an airflow similar to aerofoil which have resulted in the higher lift and lesser drag forces. Similarly, the surface with higher curvature as shown in Fig. 2.11 is noticed to have higher pressure. This differential pressure force has created a side force towards right.

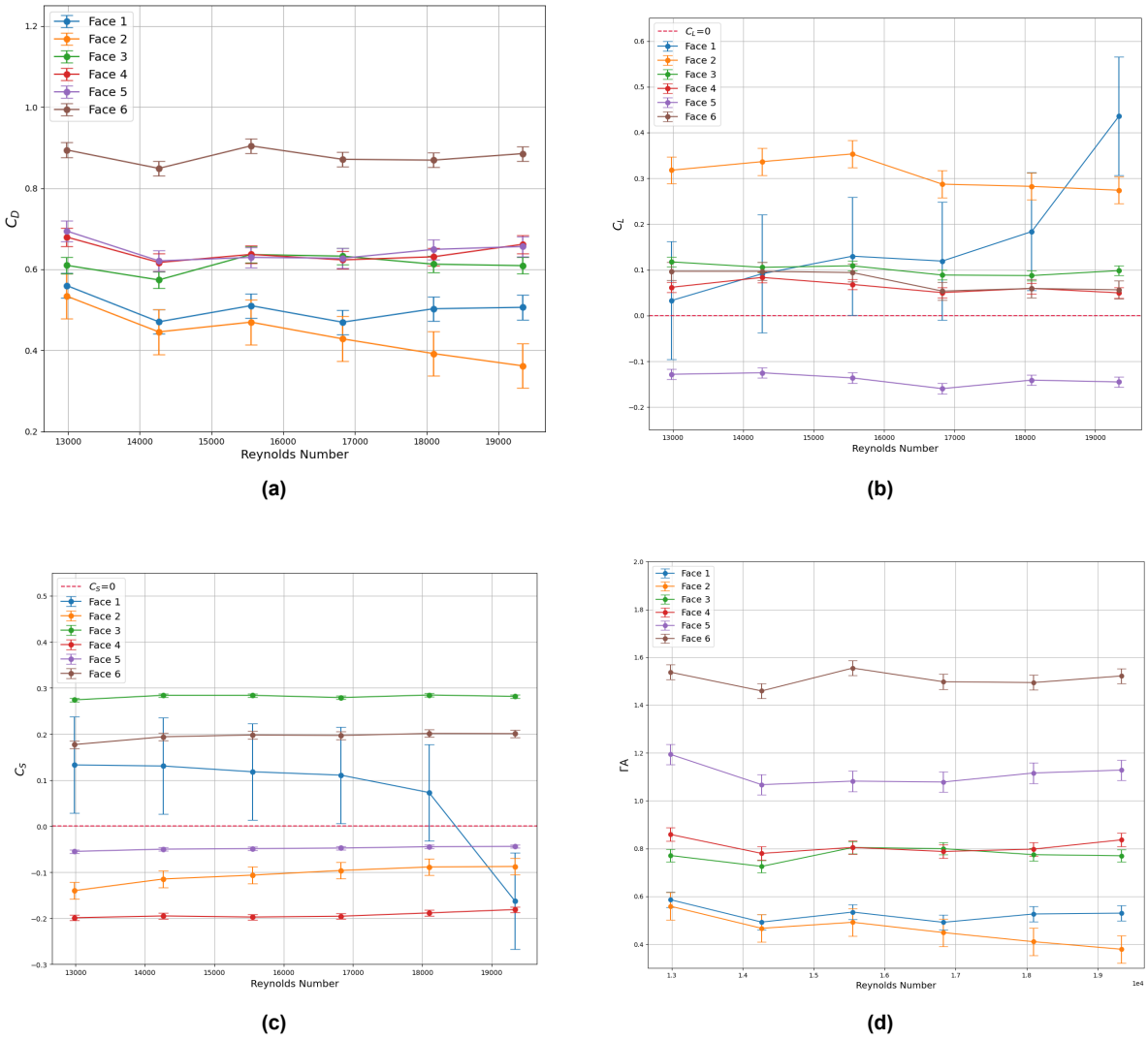

Figure 2.10: Variation of the aerodynamic parameters for six faces of the meteorite model with Reynolds number of the flow. (a) Variation of C_D; (b) Variation of C_L; (c) Variation of C_S; (d) Variation of ΓA.

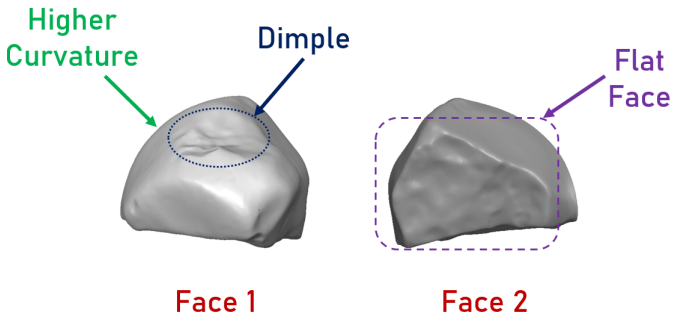

Figure 2.11: Pair 1 of the six meteorite faces facing the air flow in the wind tunnel. The ellipse represents the dimple shaped regmaglypt on the meteorite model and the rectangle represents the flat shape in face 2.

Once the orientation of model is changed from face 1 to face 2, the side force experienced by the model was reversed in direction, but similar in magnitude. Thus, the surface with higher surface curvature influences the direction of the side force. As a result, it can be inferred that

shape of the meteorite facing the flow can have a substantial impact on the lift force acting on the meteorite. In case of meteorites with flat plate shape, the effect of lift force can be even higher based on its orientation. Therefore, this pair of orientation highlights the importance of lift force as an important factor in the meteorite dark flight and cannot be neglected during strewn field estimation.

Pair 2 (Face 3 & 4):

Similar to Pair 1, the presence of the surface with the higher curvature forces dominates the side force acting on the body. When the meteorite is placed with face 3 facing the flow, the meteorite experiences the side force towards right, similar to face 1. Once the direction is reversed, the dominant side goes behind the body as shown in Fig. 2.12. Nevertheless, both Faces 3 and 4 experience lift and drag forces of similar magnitude and same direction. Hence, the pair 2 emphasises the importance of the side force during a flight.

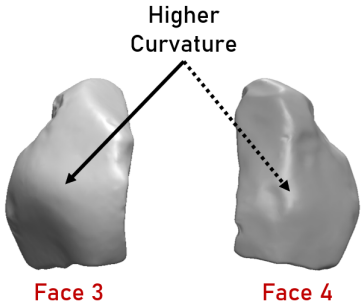

Figure 2.12: Pair 2 of the six meteorite faces facing the air flow in the wind tunnel. The dotted line represents the dominant surface with higher curvature present behind the model.

Pair 3 (Face 5 & 6):

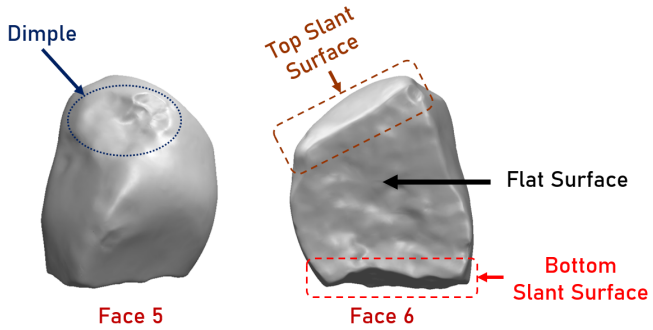

Figure 2.13: Pair 3 of the six meteorite faces facing the air flow in the wind tunnel. The ellipse on face 5 represents the dimple shaped regmaglypt on the meteorite model and the top and bottom rectangles on face 6 represents the top and bottom slant surfaces present on the meteorite body.

As expected, face 6 experiences more drag force due to the slant surface present on the top of meteorite along with its flat surface as seen in Fig. 2.13 and has highest C_D. However, face 5 has a bit lower magnitude of C_D which can be due to its curved surface. The presence of the dominant side can also be observed here as both face 5 and 6 experience side forces in opposite direction. However, of all faces, only face 5 experience negative lift, thus creating a down force. This can be attributed to the dimple on the top of the meteorite model as shown

in Fig. 2.13. The slant surface present at the bottom surface of face 6 may have contributed to the lift force. Additionally, face 5 also experiences lowest side force. Therefore, face 5 can be considered as a stable orientation of meteorite from the perspective of aerodynamic forces and the well-rounded edges might even support this hypothesis that Broek in Waterland might have experienced an oriented fall with face 5 facing the flow and resulting in a well-rounded surface due to ablation. However, the aspect of the meteorite stability in flight needs to be investigated further. This can be achieved by untethered flights in a vertical wind tunnel. Also, by estimating accurate Center of Pressure (COP), the axis of rotation can be predicted. With this, the model can be mounted on a spindle in the axis of rotation to study the rotational aspects of the meteorite when placed in a flow.

Therefore, from the above discussion, it is evident that a single meteorite model has a range of C_D and there is a finite amount of lift and side forces which are heavily influenced by the shape and orientation of the meteorite. Thus, for a real meteorite, in addition to the drag force, there is a strong chance that it experiences additional lift and side forces during its dark flight in the atmosphere. Interestingly, this additional lift force, that was observed in the wind tunnel experiments, will be translated to another side force in a direction perpendicular to other drag and side forces. This is because, in the wind tunnel experiments, the lift force act perpendicular to the incoming flow. When this motion is converted into the free fall through atmosphere, the lift direction pushes the body further in the direction of motion. Therefore, higher lift force implies the body travels farther in the direction of motion. Hence, both lift and drag forces must be considered during the dark flight simulations to maps accurate strewn fields.

2.4.2. Free fall analysis

The free fall analysis involves the estimation of terminal velocity as mentioned in section 2.3.2, which is a functioned of the drag coefficient. Since, considering each of the drag value of all six faces complicates the experiments, the average value of the drag coefficients was considered to study the free fall characteristics of the meteorite. Therefore, based on the results obtained for the 1:1 Broek in Waterland model, the mean drag coefficient of 0.62 is considered. With this value, the scaling factor to simulate the similar flows over the meteorite was calculated to be 1.75 considering the trade-off between the wind tunnel velocities and its blockage. Using the 1.75x model, the similar flows at altitudes 100 m, 2500 m, 5000 m, 7500m and 10,000 m were studied in the wind tunnel. The Reynolds numbers corresponding to flow from 10,000 m and 100 m lie in between $\mathbf{2.14 \times 10^5}$ and $\mathbf{3 \times 10^5}$ respectively. The flow velocities were corrected as per equation (2.6) accounting the blockage created in the test section of wind tunnel by the 1.75x mode for each orientation. The aerodynamic parameters at each Reynolds number are averaged for all faces to obtain the mean value for the entire meteorite model. The variation of these mean values of aerodynamics parameters for the meteorite model with aforementioned altitudes and corresponding flow Reynolds number is presented in Fig. 2.14, 2.15, 2.16 and 2.17.

Since the shape factor of the entire six faces is averaged, the influence of shape factor 'A' cannot be noticed in Fig. 2.17 and the trend is identical to the variation of C_D as in Fig. 2.14. It can be noticed that all the aerodynamic parameters decrease with decreasing altitude, therefore, decrease with increasing Reynolds number. On the other hand, the side force first increases with decreasing altitude and then plummets sharply as shown inf Fig. 2.16. Highest variation can be observed in the lift force, where C_L drops 10% with the meteorite descent as shown in Fig. 2.15. Similarly, smaller variations of 5.82%, 5.35% and 5.24% was observed for the variation of C_S, C_D and ΓA respectively.

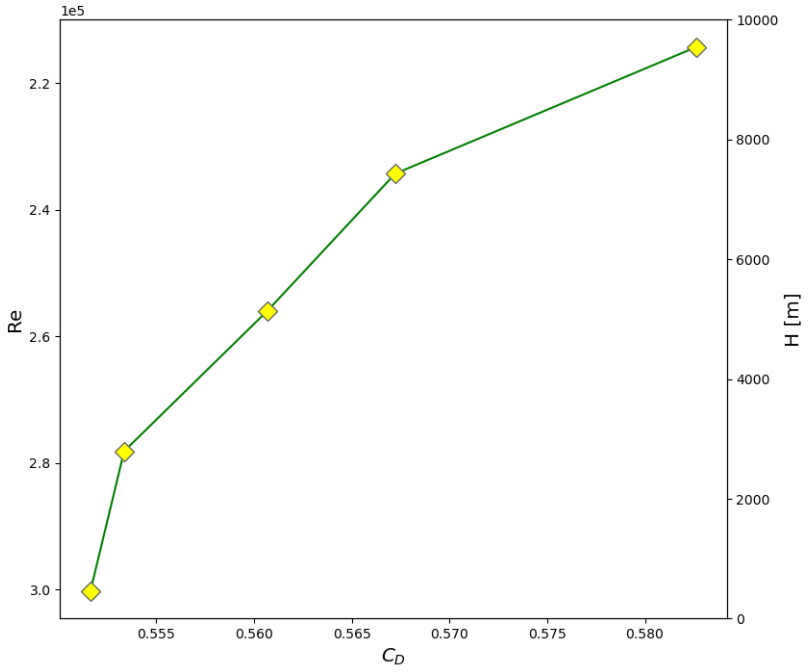

Figure 2.14: Variation of the mean coefficient of drag force with the altitude and corresponding flow Reynolds number.

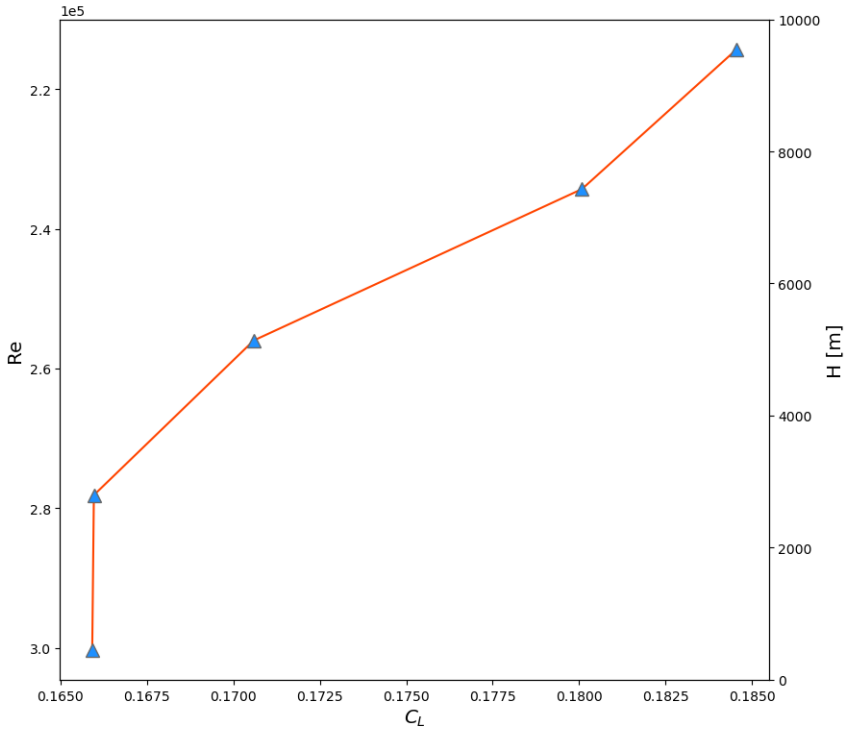

Figure 2.15: Variation of the mean coefficient of lift force with the altitude and corresponding flow Reynolds number.

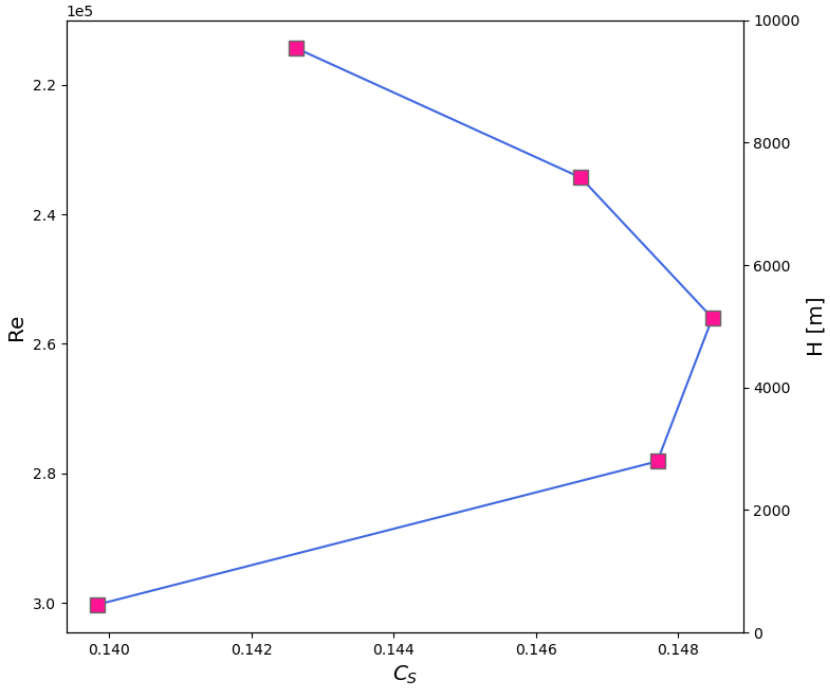

Figure 2.16: Variation of the mean coefficient of side force with the altitude and corresponding flow Reynolds number.

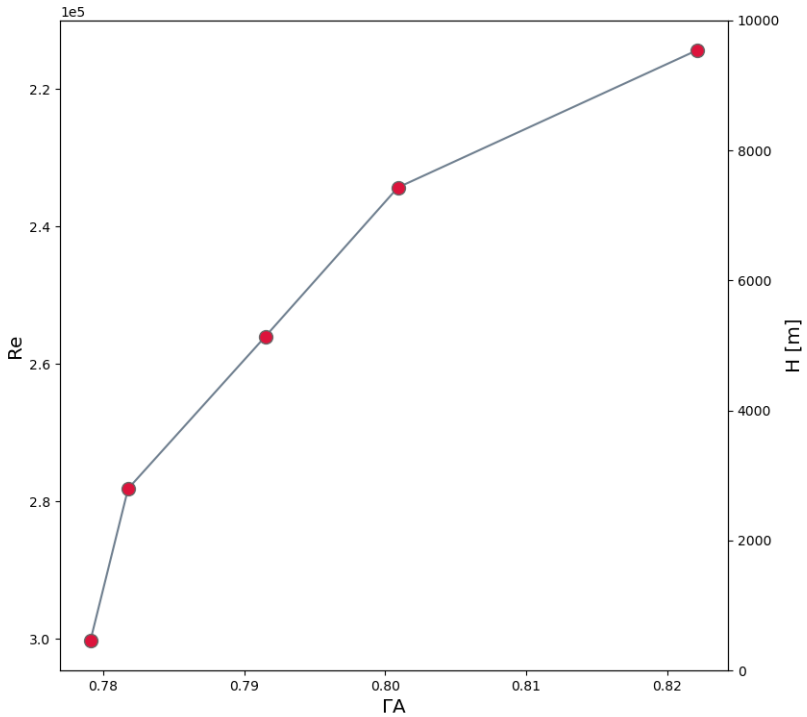

Figure 2.17: Variation of the mean value of ΓA of the meteorite with the altitude and corresponding flow Reynolds number.

Therefore, for a single meteorite, with varying altitude, the aerodynamic characteristics can be seen to vary. As a result, it can be inefficient to assume a single value for the entire body for varying altitude. Further studies can help to sketch the generic variation of these properties for a meteorite. The variation of each of these parameters with Reynolds number for all six faces is plotted in Fig. 2.18. It can be seen from the figure that the aerodynamic parameters during the free fall almost does not vary with the Reynolds number, except in few cases. which are discussed in detail below.

Coefficient of Drag force

Face 1 experiences lesser drag at higher Reynolds number (2.14×10^5 and 3×10^5) as shown in Fig. 2.18a compared with the lower Reynolds number in Fig. 2.10a. Therefore, at higher Reynolds number, the decrease in C_D might indicate that the dimple present in the meteorite is not influencing the flow around the meteorite, thus resulting in lesser drag. Interestingly, face 2 experiences more drag at higher Re and even comes closer to face as shown in 2.18a. The drag force measured for the faces 3,4, and 5 is little lesser at higher Re compared to lower flow velocities. Nevertheless, face 6 follows almost the same trend with the increase of Reynolds number. Consequently, it can be inferred that the faces with curved surfaces experience lesser drag with increasing Reynolds number. Similar trend can be observed in the variation of ΓA from Fig. 2.18d.

Coefficient of Lift force

From Fig. 2.18c it can be noticed that face 1 experiences more lift than the face 2, as opposed to the finding in Fig. 2.10b. This further supports the conjecture of absence of dimple effect with increasing Re, therefore, smoothing the flow at that point. Further investigations can be carried out using flow measurement and visualization techniques to peruse the effects of the dimple. Hence, similar to Fig. 2.10b, Faces 1 and 2 creates higher lift compared to other faces. Likewise, even with the increase in the Reynolds number face 5 faces the negative lift force. Faces 3,4, and 5 follow the similar trend and no significant variation was observed in the lift forces.

Coefficient of Side force

Face 3 and 4 still experience highest side force as shown in Fig. 2.18b similar to Fig. 2.10c due to the highly curved surface. However, the equal and opposite trend observed in three pairs in the lower Reynolds number was not noticed in higher Reynolds number, as face 1 experienced a constant side force in negative sense as observed from Fig. 2.18b.

In short, with the free fall analysis, it was observed that Face 1 behaves differently with increasing Reynolds number, this can be attributed to the smoothing of flow around the nose and can be further studied using the flow measurement techniques for better understanding. And finite amount of side and lift forces were observed from the experiments. Haack et al. (2019) argues that the oriented flight of the meteorite might have created a lateral acceleration that resulted in the deviation of the fragment of Ejby fall. Further, the effect of lateral velocities attained by the meteorite due to aerodynamic forces can be observed in the speculations of Borovička et al. (2019), Brown et al. (2019), and Spurný et al. (2014). This finding supports the speculated hypothesis regarding side and lift forces acting on the meteorite. Therefore, it can be clearly observed that there is a need to consider the aerodynamic forces during the meteorite dark flight.

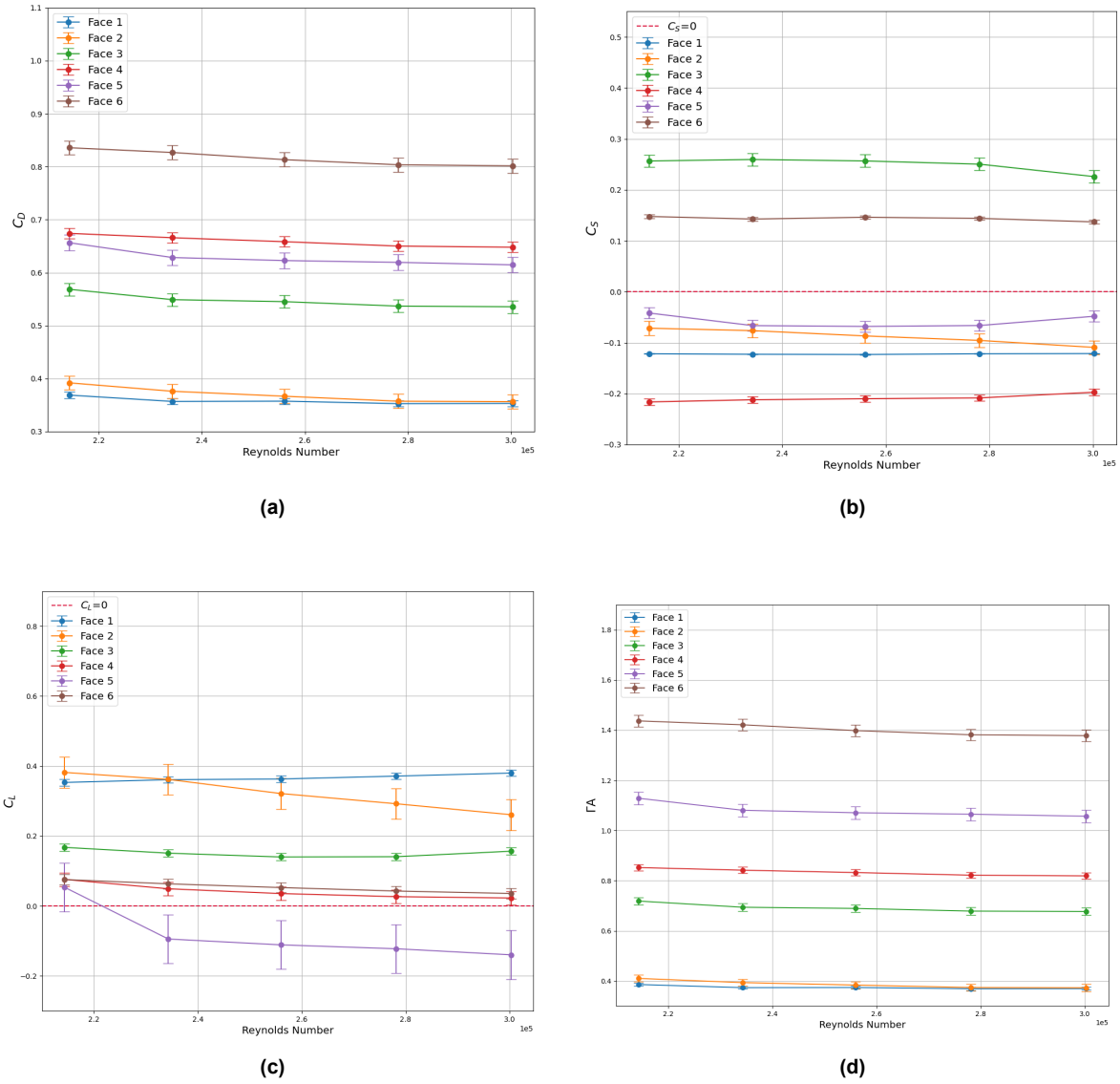

Figure 2.18: Variation of the aerodynamic parameters for six faces of the meteorite model with Reynolds number of the flow measured during the free fall analysis. (a) Variation of C_D; (b) Variation of C_S; (c) Variation of C_L; (d) Variation of ΓA.

2.4.3. Rotation of meteorite

Interesting findings such as the least side force and the negative lift force encountered by the meteorite along with its well-rounded edges provided the impetus to explore the rotational aspects of the meteorite model and the corresponding effects on its dynamics. With this, the meteorite model was mounted on a shaft in both vertical and horizontal orientations as explained in section 2.3.3. The setup in Fig. 2.5 presents the vertical orientation of the model, this makes face 5 to face the incoming flow generated by the wind tunnel. In a similar manner, when the model is oriented horizontally, face 1 faces against the incoming air flow. The setup and the flow over the meteorite in both orientations is graphically illustrated in Fig. 2.19.

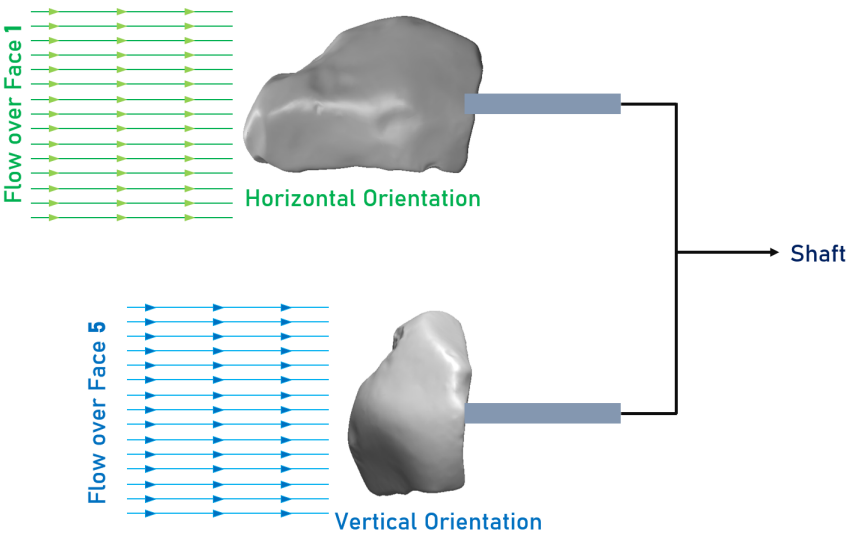

Figure 2.19: Flow over two orientations of the meteorite model mounted on a shaft. It can be observed that for the horizontal and vertical orientations, Faces 1 and 5 will be against the incoming flow.

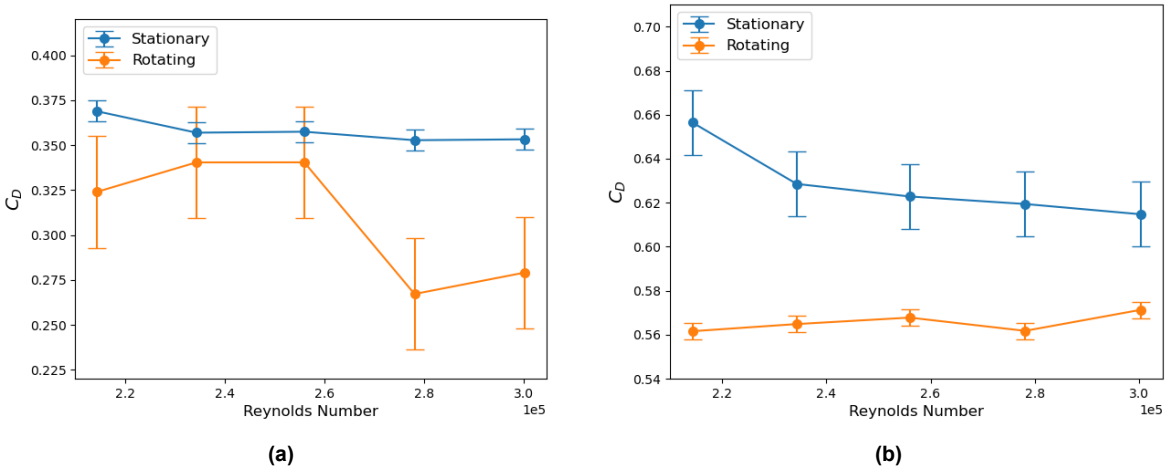

Figure 2.20: Variation of the drag force with Reynolds number of incoming flow for a rotating model. (a) Horizontal orientation with **face 1** facing the incoming flow. (b) Vertical orientation with **face 5** facing the incoming flow.

The scope of the current set of experiments explores the natural rotational ability of the meteorite. For this, no external or internal motor is used to rotate the model. The rotation of model is created by the motion of shaft fitted in the support structure when the air flows past the meteorite model. However, during the experiment the meteorite model did not rotate on its own. For this reason, to initiate the rotation, a minute perturbation is created by nudging the model assuming that wind gusts might create similar perturbations during the atmospheric flight. In case of vertically oriented model, with a little nudge, the model started to rotate naturally and smoothly until the end of the experiment. When the model was oriented horizontally, the model started rotating naturally, but whenever the motor speed of the wind tunnel is varied, the model ceased to rotate. For that, whenever the flow velocity is varied, little nudge is provided to horizontally oriented model to initiate rotation. In both cases, the incorrect alignment of the shaft with the COP is speculated to be the reason for the hindrance of rotation. However, with its

irregular shape of the meteorite made the estimation of COP complicated. Nevertheless, the experimental data is collected only after the consistent rotational motion was achieved, but not immediately after the perturbation. The results obtained from these experiments are presented in Fig. 2.20, 2.21 and 2.22. The results obtained from the horizontal orientation might not reflect the true nature of the rotational facets of the horizontally oriented model. Yet, in the current study, the results of horizontally oriented model is used to uphold the results of vertically oriented model.

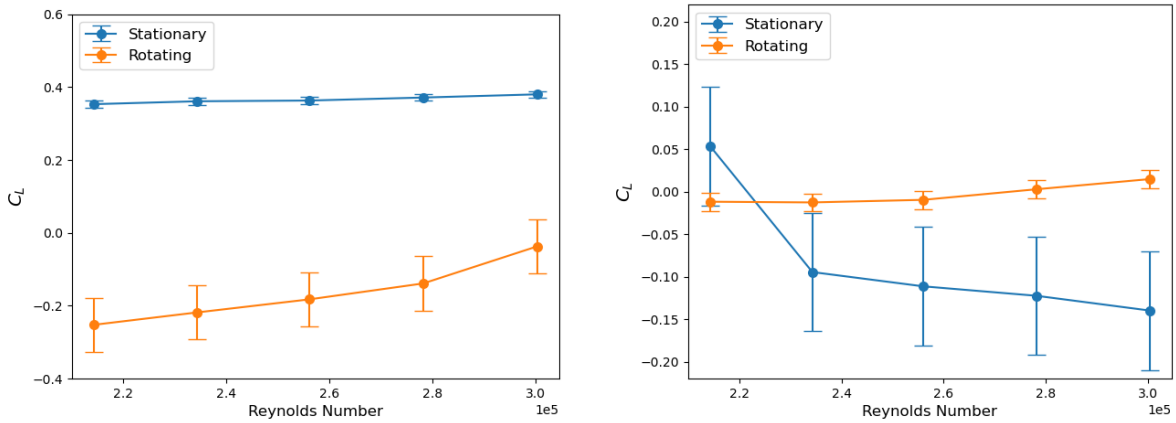

Figure 2.21: Variation of the lift force with Reynolds number of incoming flow for a rotating model. (a) Horizontal orientation with **face 1** facing the incoming flow. (b) Vertical orientation with **face 5** facing the incoming flow.

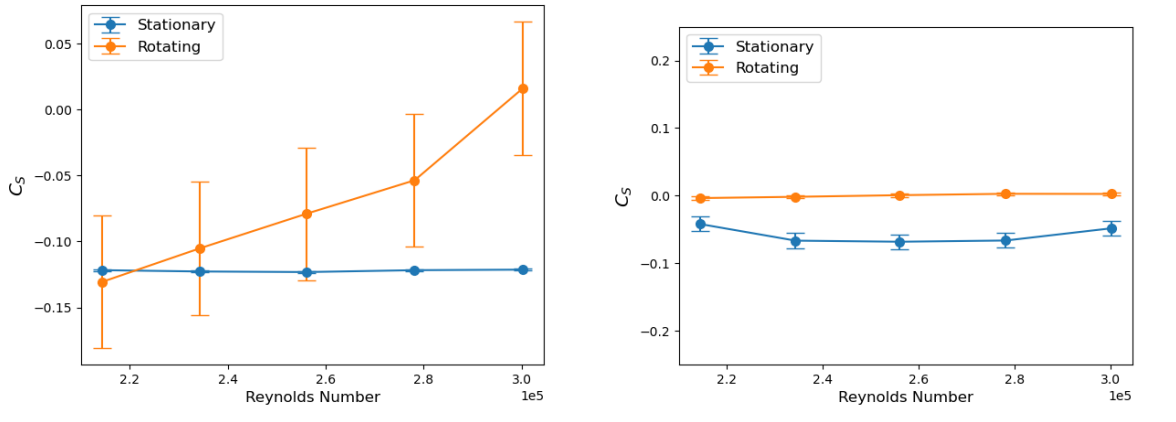

Figure 2.22: Variation of the side force with Reynolds number of incoming flow for a rotating model. (a) Horizontal orientation with **face 1** facing the incoming flow. (b) Vertical orientation with **face 5** facing the incoming flow.

For a rotating model, the drag force reduces, this trend can be seen for both the orientations as plotted in Fig. 2.20. In case of the vertical orientation, the drag reduces by almost 10% on average and maximum by 14%. For the horizontal orientation, a maximum decline of 25% was noticed. For the vertically oriented model, both the lift and side forces almost stays zero throughout the flow as shown in Fig. 2.21b and 2.22b. For the vertically oriented model, the lift and side forces both increased by 100% compared to the stationary model. Similarly, for

the horizontally oriented model, the lift and side forces approach zero value with increasing Reynolds number, with a variation of approximately 150% and 40% respectively compared to the stationary model. Thus, it can be inferred that the rotating meteorite generates positive lift and side forces compared to the stationary model in the same orientation. However, it cannot be inferred as 'Magnus Effect' because the flow direction with respect to the direction of rotation is different from the one observed in the Magnus effect. Nevertheless, prospective study can be conducted with a more optimised meteorite rotation mechanism to investigate the Magnus effects.

Therefore, from the above results for the rotating model, it can be inferred that for an oriented fall, the lift and side forces are significant enough to contribute to the atmospheric flight of meteorite. In such a case, the meteorite deviates from the predicted trajectory due to the lift and side forces. Conversely, for a rotating model, the side and lift forces become zero. Consequently, follows the predicted path. Nevertheless, most of the dark flight studies assume no rotation of meteorite and also assume the side and lift forces does not exist throughout the flight. But, based on the experimental analysis, both of the assumptions will not be valid. So, in case of non-rotating flight, the lift and side forces must be considered. Even though the placement of rotational shaft was not optimised for the current study, the results of the experiment were significant enough to pursue further studies to examine the rotational characteristics of the meteorites.

2.4.4. Implementation

As a further stride, to study the influence of the aerodynamic parameters on the impact points of a meteorite fall, the ablation and dark flight calculator (Bettonvil and Bettonvil, submitted) was utilised to simulate a meteorite dark flight. The input to this simulator includes wide range of variables including the meteorite properties such as initial mass, density, drag coefficient (C_D or Γ), shape factor (A) and trajectory properties such as the beginning and terminal locations and altitudes for both luminous and dark flight part. From the above experiments, different values were obtained for each face of the meteorite ranging between 0.35 to 0.82. However, in the literature, different values were used for the drag coefficient and shape factor for a spherical body. For example, Borovĭcka and Kalenda (2003) and Borovička et al. (2021) assumes Γ to be 0.7 and 0.5 respectively for the same shape factor of 1.21. Similarly, Borovička et al. (2019) assumes higher A of 1.4 for a Γ of 0.5. Therefore, in other case, Gritsevich (2008) assumed Γ and A of 1 and 1.209 for the same spherical body. Hence, the inconsistency in the assumptions for a single spherical body can be observed clearly. Therefore, the values of Γ and A obtained from the experimental results as well as the values from the aforementioned literature will be implemented in this code. The discrepancies caused by the inconsistency in the assumptions regarding the aerodynamic coefficients will be studied in this implementation.

Unfortunately, the fireball observations of the Broek in Waterland meteorite fall were not well documented and the only recorded observation is captured using a dashboard camera. Consequently, this data is insufficient to extract data regarding the luminous phase of the fall. Nevertheless, this study is focused on the importance of the aerodynamic aspects of the fall, which are well known and estimated from the current set of experiments. Besides, based on the volume and mass of the recovered meteorite, the density of the Broek in Waterland meteorite is estimated to be 3025 kgm^{-3}. Hence, remaining unknown input parameters were fed according to the relevant literature as well as according to the suggestions from one of the experts studying the fall (Bettonvil, *personal communication*) which was discussed in detail in section 3.3.

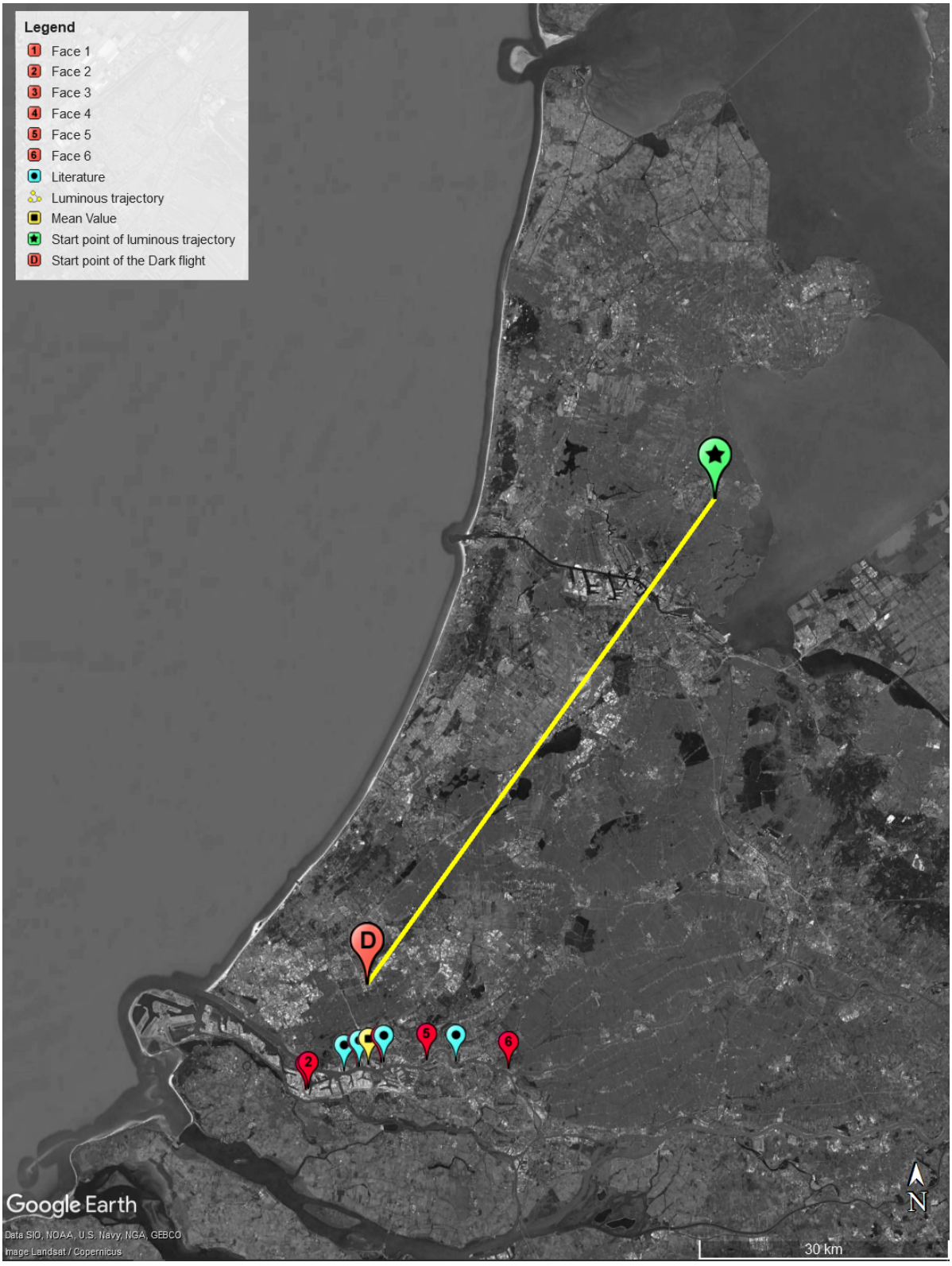

Figure 2.23: Illustration of dark flight simulation implemented as a part of study to verify the influence of the aerodynamics on the atmospheric flight. Yellow line illustrates the fictitious luminous trajectory of the meteorite which was assumed to enter the atmosphere at 50° near Broek in Waterland region. The dark flight was assumed to start at Delft University of Technology. The green marker with star label points the beginning point of luminous trajectory at $(52.50, 5.00)$ at an altitude of 85,000 m. The red marker labelled as 'D' denotes the beginning point of dark flight at $(51.99, 4.376)$ at an altitude of 25,000 m. The group of multi-coloured markers at the bottom represent the group of impact points estimated from the simulation.

Figure 2.24: Impact points calculated using a dark flight calculator for each face of the meteorite model. Fig. 2.23 is presented as Panel 'A' at the upper left corner of the image. Panel A illustrates the fictitious luminous trajectory of the meteorite which was assumed to enter the atmosphere at 50°, close to the Broek in Waterland region. The dark flight was assumed to start at Delft University of Technology. The dark yellow rectangular box in Panel A is zoomed in as Panel 'B' which consists of the fall points with the same legend from Fig. 2.23. The red markers denote the impact points for each face of the Broek in Waterland meteorite with the number denoting the meteorite face. The yellow marker denotes the impact point estimated using the mean value of all six faces ($\overline{\Gamma} = 0.563$ and $\overline{A} = 1.343$). The cyan markers represent the fall points that are estimated using the assumed values from the literature. The broad yellow line in Panel 'B' illustrates the separation of 24 km between the impact points of face 1 and 6 of the meteorite.

For the simulation, the fictitious luminous phase is used, starting roughly from Broek in Waterland and ending above Delft to illustrate the outcome of different aerodynamic assumptions. Therefore, the luminous trajectory is assumed to start at the geographical coordinates of $(52.50, 5.00)$ at an altitude of 85 km, presented as green marker with star symbol in Fig. 2.23. The meteoroid is assumed to enter the Earth's atmosphere at an angle of 50°, with a speed of 22 kms^{-1}. And this luminous trajectory is assumed to continue until the dark flight point, which is assumed to be $(51.99, 4.376)$ at 25 km, shown as red marker labelled as 'D' in Fig. 2.23 and the yellow line connecting these two points represents the luminous trajectory of the meteorite flight. And, similar to the experiments, no fragmentation was assumed during the flight. Consequently, under these input parameters, the dark flight code is executed for following cases,

- Γ and A for each of the six faces of meteorite estimated from the free fall analysis.
- Mean value of drag coefficient and shape factor ($\overline{\Gamma} = 0.563$ and $\overline{A} = 1.343$), averaged for six faces.
- Γ and A from the literature assumed for the dark flight studies.

The impact points obtained from the simulations are plotted below the marker 'D' as smaller markers of different colours. The Fig. 2.24 presents a focused view of these impact points in Panel 'B', with Fig. 2.23 as Panel 'A' for reference. The spread of the impact points due to the variation in Γ and A for each point can be seen clearly from the results. This further reinforces the significance of aerodynamic parameters on the atmospheric flight of the meteorite. From the results, the impact points of faces 1 and 6 are separated by 24 km as shown in Fig. 2.23 with the yellow line. Hence, a variation in the orientation of the meteorite can shift its impact point by a significant distance. And from the results, the impact points are noticed to shift rightwards (laterally) with increasing ΓA with lowest begin face 1 ($\Gamma A = 0.374$) and highest for face 6 ($\Gamma A = 1.403$). Based on the results from this implementation, in case of Broek in Waterland, the strewn field shift **laterally** with the increase in the shape factor. This might be subjected to the meteorite shape and direction of wind. Yet, the shift of impact points can be clearly seen for a single meteorite body. However, in case of multiple fragments, it can be inferred that larger fragments might travel eastward, and the more streamlined fragments travel south, or in the direction of the wind.

The values that are considered in the literature were used to check the proximity of the impact points to the values from the experimental results, as well as to study the inconsistency in the assumptions. And the impact points seem to fall within the estimated range. Interestingly, it can be noted that, the values used for Γ and A in the literature for a spherical body resulted in widespread impact points in the fall site. It can be clearly observed that the values from Borovička et al. (2019) and Borovĭcka and Kalenda (2003) is very close to the impact points of faces 3 and 4 respectively. It is interesting to note that, in the aforementioned literature, the values were assumed for a spherical shape. However, face 3 and 4 were non-spherical in nature, approximately resemble hemispherical shape. Therefore, this highlights the inconsistency of the Γ and A assumption for a single spherical body in the literature.

In brief, the aerodynamic characteristics of the meteorite can be seen to strongly influence the impact points of the meteorite fall and results in a significant spread between the fall points for various orientations. This supports the conclusion drawn from the rotational study, that in an oriented fall, the meteorite gets heavily influenced by the aerodynamic forces and as a consequence, it can deviate from the predicted trajectory.

2.5. Conclusions

The main goal of the present study was to experimentally investigate the aerodynamic forces acting on a meteorite during its dark flight. To achieve this, a 3D printed model of Broek in Waterland meteorite was used as the test model in the wind tunnel tests. The variation of aerodynamic forces was measured for each of the six faces of the meteorite and the results were analysed and discussed above, based on which the following conclusions are drawn for this study.

- Each of the six faces of the meteorite has a unique drag coefficient as expected. The range of Γ lies between 0.35 and 0.88 , for a single body. Therefore, assuming a single value for Γ during the dark flight studies can result in excluding the other possible impact points. Finite amount of lift and side forces were measured from the experiments. Also, the effects of the irregular meteorite shape on the lift and side forces were noticed. A dominant curved surface that strongly influences the direction of the side force acting on the meteorite was identified.
- In the free fall analysis carried out for the descent from 10 km to 100 m, variation in lift, drag and side forces with the decreasing altitude were observed. Face 5 was identified to be most stable orientation, in terms of the aerodynamic forces. As it is the only surface that experiences negative lift force along with least side force in the entire test flow regimes. This results in lesser deviation of the meteorite from the predicted path and the negative lift does not carry the meteorite farther away from the predicted path. The well-rounded surface of face 5 might suggest that meteorite may have ablated during its luminous phase facing the flow in this orientation, further upholding the hypothesis of stable orientation and infers an oriented flight during the fall.
- Rotating meteorite experienced lesser drag than the stationary model. Also, zero lift and side forces were experienced for a rotating meteorite, when face 5 faces the flow. Thus, it can be deduced that in case of oriented fall, aerodynamic forces are significant enough to turn the meteorite from the predicted path. Hence, if no rotation is assumed during the dark flight studies, then lift and side force must be accounted in the dynamics of the meteorite.
- Depending upon the variation of ΓA, the impact points are spread accordingly in the dark flight implementation. The impact points are separated by 24 km for a single body when the orientation of meteorite is changed from face 1 to 6, assuming an oriented flight. This supports the conclusion that in an oriented fall, the meteorite might deviate from its path due to the aerodynamic forces acting on it.

Based on this experimental study, it is clearly evident that aerodynamic forces significantly influence the dark flight of the meteorite, consequently, its impact points as seen from the simulations. Particularly, in case of non-rotating oriented fall for an irregular shaped meteorite, a range of aerodynamic coefficients exists for a single body, which needs to be accounted during the dark flight simulations. In such a way, by accounting for all possible ranges of Γ, A and including the lift and side forces in the meteorite dynamics can help one to estimate different possible strewn fields and by mapping out the common intersecting areas, thus indicating the impact sites with a higher probability. Modelling the variation of aerodynamic forces as a function of flow Reynolds number will make it suitable for different meteorite shapes.

Future work

Prospective studies include designing better models including the lift and side forces, experimental studies with flow visualization techniques and different flow regimes of complete understanding of meteorite aerodynamics such as Magnus forces, boundary layer effects during the hypersonic velocities. Prospective experimental studies also include using untethered 3D printed models in a vertical wind tunnel to understand the dynamics of free fall in a sophisticated way. With this, even dynamics of meteoroid fragments can also be studied. Thus, offering a wide scope of research in the field of meteoritics as well as aerodynamics.

3

Supplemental Material

This chapter provides the additional information regarding the underlying fundamental work that was carried out during the thesis project. Hence, this discussion provides further insight into the journal article that was presented in chapter 2. The content of this chapter includes a detailed discussion regarding the experimental setup instrumentation and data acquisition, flow similarity analysis of free fall flow regimes, and the information about the dark flight model that was implemented in the thesis project as discussed below.

3.1. Experimental data acquisition

The experiments of the current thesis study were performed in the W-Tunnel. It is a subsonic open jet wind tunnel with square test section. In this wind tunnel, three interchangeable contraction sections with exits of 40×40 cm^2, 50×50 cm^2 and 60×60 cm^2 can be used in this wind tunnel. With the varying test section, maximum achievable velocity will also vary accordingly. With increasing test section area, the maximum achievable velocity decrease. Therefore, the maximum velocity of 35 ms^{-1} can be attained for the 40×40 cm^2 test section. Nevertheless, if larger test model (scaled model) is placed in the test section, flow blockage will be created. In order to accommodate the larger model, accounting the flow blockage, then the maximum achievable velocity decreases. Also, with larger models, the printing time of the meteorite model also increases. Thus, a trade-off needs to be achieved in terms of maximum achievable velocity, test section area and scaling of the meteorite model. Considering these factors, a 1.75x model was considered for the free fall analysis.

A six-component balance was used in the current experimental study to measure the forces and moments in three perpendicular directions acting on the body (Alons, 2008). The test object can be mounted on an Aluminium plate present on the balance. With the help of the bolt holes, the test setup can be mounted on the Aluminium plate. The data acquisition of the forces and moments acting on the test model is carried out continuously using six load cells (or Wheatstone bridges). These load cells are connected in a 6-wire configuration with sensing in the Load Cells of the excitation, with an excitation voltage of 10 V. The balance was calibrated using a dead weight during its delivery to Delft University of Technology.

The six load cells are connected to a sensor measurement system using data cables. Using this system, both time averaged as well as instantaneous data can be acquired during the measurement time. A built-in LabVIEW program in the wind tunnel laboratory was used to read, display, and export the data acquired from the sensors. For the experiments, data was

acquired for a period of 45 seconds with a sampling frequency of approximately 1996 Hertz, thus giving 89,800 samples of instantaneous data. The instantaneous data and time averaged data can be stored in the system. In the current set of experiments, the data at zero wind velocity was measured at the beginning of each set of experiments. Then the experiment was conducted at the required wind velocities and the corresponding data was collected. The data at the zero velocity contains the bias present in the measurement system and hence it can be removed from the measured data. This can be achieved by subtracting the zero-velocity data from the data measured at other velocities. Finally, this data was used for the data analysis and interpretation.

3.2. Flow similarity analysis

The recovered mass of the Broek in Waterland meteorite was measured as 530 grams. The free fall was analysed at the altitudes 10 km with an interval of 2.5 km. However, this would bring the final altitude to be Mean Sea Level (0 km). Hence, the final altitude is considered to be 100 m. Therefore, the five altitudes considered are 10 km, 7.5 km, 5 km, 2.5 km, and 0.1 km. Since the free fall analysis is considered from an altitude of 10 km, by the time the meteorite reaches this altitude, it was assumed that the body attained terminal velocity due to its lower mass. Terminal velocity (V_t) of the meteorite at a given altitude (h) during its free fall is calculated as follows.

$$V_t = \sqrt{\frac{2mg}{\rho A C_D}} \tag{3.1}$$

The flow Reynolds number is given by

$$Re = \frac{\rho v D}{\mu} = \frac{vD}{\nu} \tag{3.2}$$

where the properties such as acceleration due to gravity (g), density of the atmosphere (ρ), kinematic and dynamic viscosity (μ, ν) are calculated as follows (Anderson, 2017)

$$\rho = \rho_0 \left(\frac{T}{T_0}\right)^{-[(g_0/(aR))+1]} \qquad T = T_0 + a(h - h_0) \qquad g = g_0 \left[\frac{R_E}{R_E + h}\right]^2 \tag{3.3}$$

The dynamic viscosity of air is calculated using the Sutherland's law (Roy and Blottner, 2006)

$$\mu = 1.458 \times 10^{-6} \left[\frac{T^{1.5}}{T + 110.4}\right] \tag{3.4}$$

Properties such as acceleration g, ρ, μ and ν are dependent on the altitude, whereas the mass (m), characteristic length (D), Projected area (A) and Drag coefficient (C_D) are attributes of the meteorite. Based on the experimental calculations, the mean value of the drag coefficient of the Broek in Waterland meteorite was measured as 0.62. Using SOLIDWORKS, the characteristic length and projected area of the meteorite were estimated to be 9 cm and 54.1 cm^2 when the face 5 faces the flow. Wind tunnel (W) operates at the sea level conditions at following flow properties

- Density, ρ_W = 1.225 kgm^{-3}
- Velocity, V_W = 30 ms^{-1}
- Dynamic Viscosity, μ_W = 1.7890$\times$10^{-5} Pa.s
- Kinetic Viscosity, ν_W = 1.4607$\times$10^{-5} m^{2}s^{-1}

Therefore, on the basis of flow similarity,

$$Re_W = Re_h \implies \frac{v_W D_W}{\nu_W} = \frac{v_h D_h}{\nu_h}$$

Where, V_h and ν_h are the terminal velocity (V_t) and kinematic viscosity at the given altitude 'h' km. And D_W, D_h are the characteristic lengths of the model in the wind tunnel and at considered altitude (h).

$$\mathbf{D_W} = \left[\frac{\nu_\mathbf{W}\mathbf{V_h}}{\nu_\mathbf{h}\mathbf{V_W}}\right] \times \mathbf{D_h} = \mathbf{K} \times \mathbf{D_h} \tag{3.5}$$

Where, **K** is 'Scaling factor' of the model. Therefore, D_h will be 9 cm as it is the original characteristic length of the meteorite during the fall. With the properties at certain altitude, the scaling factor can be estimated using equation (3.5). Nevertheless, this approach will result in different models with various characteristic lengths corresponding to various altitudes at a constant wind tunnel velocity.

Conversely, if the size of the test model used in the wind tunnel (D_W) is fixed, then the wind tunnel velocity can be varied to create similar flows over the body. However, two things need to be considered in this approach. (1) The limit of the wind tunnel velocity and (2) The blockage created by the model in the wind tunnel test section. In the current study, the blockage of the model was aimed not to cross 10 ± 0.5% and the estimated wind tunnel velocities should not exceed 30 ms^{-1}. The wind tunnel velocities corresponding to the terminal velocity at a given altitude is calculated as

$$\mathbf{V_W} = \left[\frac{\nu_\mathbf{W}\mathbf{D_h}}{\nu_\mathbf{h}\mathbf{D_W}}\right] \times \mathbf{V_h} = \mathbf{U} \times \mathbf{D_h} \tag{3.6}$$

Where, **U** is the velocity factor. In this approach, the logistics can be simply reduced to two models for horizontal and vertical orientations. Considering the trade-off requirements for the blockage and wind tunnel velocity, a **1.75x** scaled model is assumed in the current study. The wind tunnel velocities and flow Reynolds numbers corresponding to the five altitudes are presented below in table 3.1. This model would correspond to a blockage of 10.35% in the wind tunnel test section (40×40 cm^2), to which the corrections will be applied accordingly. It can also be observed from table 3.1 that the wind tunnel velocities did not exceed 30 ms^{-1}. Thus, the free fall analysis is conducted at these flow Reynolds numbers.

Table 3.1: Flow Reynolds number and corresponding wind tunnel velocities to create similar flows at five altitudes for the free fall analysis of a 1.75x scaled model of Broek in Waterland meteorite.

Altitude [m]	Terminal Velocity [ms^{-1}]	Reynolds number	Corresponding Wind tunnel velocities [ms^{-1}]
0	50.49	3×10^5	28.63
2500	56.84	2.78×10^5	26.54
5000	64.79	2.56×10^5	24.44
7500	74.49	2.35×10^5	22.40
10000	86.48	2.14×10^5	20.42

3.3. Implementation of the Dark flight model

To study the influence of the aerodynamic parameters on the impact points of a meteorite fall, a dark flight calculator is used. The code for the simulation of dark flight [1] was created by Bettonvil and Bettonvil (submitted). The input to this simulator includes wide range of variables including the meteorite properties such as initial mass, density, drag coefficient (C_D or Γ), shape factor (A) and trajectory properties such as the beginning and terminal locations and altitudes for both luminous and dark flight part.

Hence, in the current study, the results of Drag coefficient (Γ) and Shape factor (A) obtained from the experiments was implemented in this code to study their influence on the impact points. Each of the six faces of the meteorite as shown in Fig. 2.6 have unique Γ and A, thus creating six test cases. And mean of Γ and A for these six faces was also fed as test case to the simulator. Additionally, four test cases containing the values of Γ and A from the literature were also fed as the input. Thus, eleven test cases as presented in table 3.2 are fed into the simulator to obtain the fall locations for each case. Each of the input variable that was used in the test cases for this study is discussed elaborately below.

Due to the lack of the fireball observations for the Broek in Waterland meteorite, most of the input parameters are unknown. Other than Density, Drag coefficient and Shape Factor, other input parameters were fed according to the literature, default values provided in the code and upon the consultation with Felix Bettonvil (Bettonvil, *personal communication*). Hence, based on these, the values for each of the input parameter is presented below.

1. **Initial mass**: The value of entry mass for the Broek in Waterland meteorite is unknown. The dark flight calculator returns the value of the remnant mass after ablation during the simulation. The code was initially run with an arbitrary initial mass to check the remnant mass for a particular test case. Based on this, the initial mass value is iterated until the remnant mass of the meteorite reaches 0.53 ± 0.03 kg.
2. **Density**: Based on the recovered meteorite mass of 0.53 kg and its volume from the 3D analysis, the density of Broek in Waterland meteorite is 3025.153 kgm^{-3}.
3. **Entry speed & Zenith angle**: Based on the literature, the values for the meteorite entry speed and entry zenith angle were assumed to be 22 kms^{-1} and 50° respectively.
4. Γ **& A**: For each test case as mentioned above, different set of Γ and A. These values are presented in table 3.2.
5. **Luminous efficiency, Heat transfer coefficient & Ablation heat**: Default values of 0.001, 0.15 and 2×10^8 Jkg^{-1} were used for the luminous efficiency, heat transfer coefficient and ablation heat respectively.
6. **Fragmentation**: As mentioned before in chapter 2, fragmentation effects were not considered in the current study to avoid the complexity in the aerodynamic interactions. Nevertheless, in the current project, the aerodynamics of a single body was studied, thus making fragmentation less significant. Hence, no fragmentation was considered. Hence, the input value of fragmentation amount remains **1** with a blank value for the fragmentation altitude.
7. **Altitudes**: Considering the literature and the scope of the current study to analyse the free fall from an altitude of 10 km, the dark flight was assumed to start from an altitude of 25 km for the simulations. Thus, the input values for following input parameters were considered to be 25 km.

[1] https://github.com/dudaskule/AblationCalculatorPy

(a) Beginning height of dark flight calculation
(b) Height of End point luminous trajectory
(c) Terminal height luminous trajectory

8. **Coordinates of beginning & end points of luminous trajectory**: The coordinates of beginning and end point of luminous trajectory along with respective altitudes are usually obtained from the fireball observation data. These are used to compute the direction of the flight direction in the atmosphere. However, in the current case of fictitious simulation, following locations for luminous trajectory were arbitrarily considered for all test cases:

   - Beginning point: ($52°30'00.0"$N, $5°00'00.0"$E) at an altitude of 85 km.
   - End point: ($51°59'24.0"$N, $4°22'33.6"$E) at an altitude of 25 km.

Table 3.2: Value of input variables for different test cases for the dark flight implementation using dark flight calculator.

S.no	Test Case	Initial Mass [kg]	Drag Coefficient (Γ)	Shape factor (A)
1	Face 1	0.69	0.358	1.047
2	Face 2	0.68	0.370	1.047
3	Face 3	0.63	0.547	1.264
4	Face 4	0.61	0.659	1.264
5	Face 5	0.615	0.628	1.719
6	Face 6	0.595	0.816	1.719
7	Mean value	0.625	0.563	1.343
8	Borovĭcka and Kalenda, 2003	0.605	0.7	1.210
9	Borovička et al., 2019	0.64	0.5	1.400
10	Gritsevich, 2008	0.585	1	1.209
11	Borovička et al., 2021	0.64	0.5	1.21

With the following values for remaining input parameters for all the test cases presented in table 3.3

Table 3.3: Values for the remaining input parameters to the simulator common for all test cases

Input Parameter	Value
Density (kgm^{-3})	3025.153
Entry Speed	22
Zenith angle of entry	50
Luminous efficiency	0.001
Heat transfer coefficient	0.15
Heat of ablation (Jkg^{-1})	2×10^8
Fragmentation amount	1
Height of fragmentation (m)	–
Beginning height of dark flight calculation (m)	25000
Geographic latitude of End point luminous trajectory (deg)	51.99
Geographic longitude of End point luminous trajectory (deg)	4.376
Height of End point luminous trajectory	25000
Geographic latitude of Beginning point trajectory (deg)	52.5
Geographic longitude Beginning point trajectory (deg)	5.00
Terminal height luminous trajectory (m)	25000
Height of Beginning point luminous trajectory (m)	85000

4

Conclusions

In most of the dark flight studies, the aerodynamics of the meteorite is usually not considered in detail and its effect is overlooked with common assumptions regarding the meteorite shape, and by ignoring the aerodynamic forces acting on the meteorite model during its atmospheric flight. Also, the possibilities of an oriented fall or the meteorite rotation are also ignored. And, in few case studies of meteorite falls, the aerodynamic effects on the dark flight and the impact points were clearly observed, pointing out the significance of the meteorite shape, the aerodynamic forces acting on it, thus emphasizing the need to consider them in the dark flight. Hence, with this scientific gap as an impetus, following research question was formulated for this study

What are the aerodynamic characteristics of an irregularly shaped meteorite during the subsonic regime of its dark flight?

Hence, in this study, the aerodynamics of an irregular shaped meteorite in subsonic flow regime during its dark flight phase is experimentally investigated in wind tunnel. For this, a 3D printed model of Broek in Waterland meteorite was used as a test model, which fell in the Netherlands on 11th January 2017, making it one of the recent meteorites falls. In addition to this, the intact nature of the meteorite and the availability of its high-quality surface data recorded before it was cut for the scientific studies and its well-rounded surfaces with a flat back surface made this model particularly unique and therefore was considered as the meteorite model for this study. This study can be divided into four parts, as discussed below.

Firstly, using a 3D printed 1:1 model of the Broek in Waterland meteorite, accurate drag coefficient (C_D) is estimated. To estimate this, the variation of C_D is measured from 20 to 30 ms^{-1}, which corresponds to the flow Reynolds number 1.29×10^4 and 1.94×10^4. In addition to the drag force, the lift and side forces in this flow regime is also measured for a further understanding of meteorite dynamics. The study was conducted for the six faces of the meteorite model, to understand the effect of shape on the aerodynamic forces. From experiments, it was found out that each face has a unique drag coefficient as expected. And the estimated values of C_D in this flow regime lies between 0.45 to 0.88 for a single meteorite. On the other hand, single value within this range is usually assumed for the spherical shaped meteorite body. Hence, considering a single value for a meteorite can be inefficient for the strewn field estimation. In this flow regime, for the meteorite model, $\overline{C}_D = 0.625, \overline{C}_L = 0.143$ & $\overline{C}_S = 0.148$, indicating that there exists a finite amount of side and lift forces acting on the meteorite model. Apart from this, a surface with higher curvature was observed which strongly influences the

direction of the side force and was dominant in flow against each of the six faces during the experiment. In a similar way, a dimple shaped regmaglypt was noticed influencing the flow around the meteorite when face 1 was positioned against the air flow from the wind tunnel, thereby influencing the drag and lift forces acting on the meteorite model.

Subsequently, based on the estimated value of the drag coefficient for the meteorite, the free fall of the meteorite was simulated at altitudes 10 km, 7.5 km, 5 km, 2.5 km, and 100 m corresponding to the rise of Re from 2.14×10^5 at 10,000 m to 3×10^5 at 100 m. The scaling factor that could simulate the corresponding flow regimes in the wind tunnel is estimated to be 1.75, considering the trade-off between the wind tunnel velocities and the flow blockage in the test section of wind tunnel. This model is tested in the aforementioned flow regime to study the variation of the aerodynamic forces during the free fall. The flow measurements are corrected for the blockage caused by the 1.75x model in the test section. Based on the results, primarily, it was observed that for each face there a little reduction of drag coefficient in this flow regime, compared to the previous flow regime. This brought down the range of C_D to 0.358 - 0.816 in the flow Reynolds number 2.14×10^5 - 3×10^5. However, for each face the aerodynamic forces were not seen to vary very much with Reynolds number. Since each face experiences distinctive magnitude of aerodynamic forces, to study the body as whole, the properties of six faces were averaged. In that case, it was observed that with decreasing altitude, the force coefficients decrease a bit. The effect of the dimple was not observed in this flow regime, suggesting that the flow might have become smooth over the dimple at higher Re. Similar to the previous flow regime, face 5 with strongest curved surface, was the only orientation that experienced least side force and negative lift force. This might indicate that during the free fall of the meteorite with face 5 facing the flow, the least side force and negative lift force that thrusts down the model can make the model fall with least perturbations, thus making it most stable of all faces, in terms of aerodynamic forces. However, the stability aspects of the meteorite need further studies for better comprehension.

In order to study the feasibility of the rotation, the meteorite model was fitted to a shaft and was mounted against the flow, in both horizontal and vertical orientations such that face 1 and 5 would face the flow respectively. The rotational experiments were also conducted in the same flow regime of the free fall analysis. Natural rotation was observed in the vertical orientation when the body is perturbed slightly. However, intrinsic rotational capability was not observed in the horizontal orientation. For the rotating model in vertical orientation, the meteorite model experiences lesser drag compared to the stationary case for the same face. In addition to this, vertically rotating model generated zero lift and side forces throughout the flow regime, whereas the stationary model created finite amount of respective forces. Therefore, it can be concluded that, in case of a non-rotating oriented meteorite fall, finite amount of lift and side forces are experienced by the meteorite that can result in deviation of the body from the predicted trajectory. On the other hand, the zero lift and side forces generated by the rotating body can make the body follow the predicted trajectory. However, in the dark flight studies, both rotational and the aerodynamic forces are not considered together. Hence, based on these results, it can be observed that the aerodynamic forces must be considered during the simulation in case of non-rotating fall. This set of experiments produced significant result to propel the future studies in the dimension of meteorite rotation.

Finally, the experimentally calculated values of meteorite drag coefficient (Γ) and Shape factor (A) are implemented in a dark flight calculator to understand the influence of these parameters on the impact points. For this, a set of input values for Γ, A of six faces, whole body (mean

of six faces) and the values assumed in the literature were used to generate impact points for respective cases. Based on the simulation, it was concluded that meteorite fall has unique impact point for each face. Depending on the Γ and A of each orientation, the impact points are spread accordingly in the impact site. This further supports the notion that, in case of oriented fall, aerodynamic forces significantly affect the impact points of the meteorite fall. A separation of 24 km was calculated within the impact points for a single body, when the orientation of the meteorite is changed from face 1 to 6. Thus, the results from this simulation further reinforces the significance of the aerodynamics in the meteorite dark flight and the estimation of the strewn field.

In conclusion, based on this experimental study, it is clearly evident that aerodynamic forces significantly influence the dark flight of the meteorite, consequently its impact points as seen from the simulations. Particularly, in case of non-rotating oriented fall for an irregular shaped meteorite, a range of aerodynamic coefficients exists for a single body, which needs to be accounted during the dark flight simulations. In such a way, by accounting for all possible ranges of Γ, A and including the lift and side forces in the meteorite dynamics can help one to estimate different possible strewn fields and by mapping out the common intersecting areas, thus indicating the impact sites with a higher probability.

5

Recommendations

The present study can be considered as a first step towards a niche in meteoritics that has not been explored yet. Hence, this dimension of meteoritic aerodynamics has a potential to offer lot of prospective research opportunities. Based on the current study and the conclusions, few recommendations are made for the future work:

- Design studies can be conducted to construct vertical wind tunnel to simulate the free fall studies. Existing wind tunnels can also be modified to adapt to these studies. Using the vertical wind tunnel, untethered flights can be conducted with the meteorite models to simulate free fall studies and better comprehension of natural meteorite dynamics.
- The current study assumed no fragmentation during the meteorite dark flight. Using the vertical wind tunnel, the aspects of in-flight fragmentation, where the meteorite breaks up in flight can also be studied to comprehend the fragmentation effects such as Collimination effect. This can be achieved by simulating the separation of fragments during the experimental flight, when the model is placed is test section.
- The existing dark flight models can be modified such that it includes the variation of aerodynamic forces such as lift and side forces with the flow Reynolds number. If the size of the meteorite can be approximated from the fireball observation data, then a rough Reynolds number of the flow over the meteorite can be estimated.
- With the advancement in the additive manufacturing techniques, different materials such as metal can be used to 3D print the meteorite model that can be used to replicate the true mass as well as inertia around the rotation axis of the model that can be used to study of rotational dynamics.
- Estimation of center of pressure (COP) is a challenging task for an irregular object like meteorite, which is a crucial aspect of the stability studies. Using the force balance, the moments acting on the meteorite model can be measured. Using this data, the COP can be experimentally measured. Nevertheless, the model should be large enough such to measure the COP accurately. Also, using software such as ANSYS and COMSOL, extensive simulations can be made to compute the accurate location of COP. Consequently, the placement of shaft can be optimised, and the rotational dynamics of the meteorite can be studied in detail.
- The irregular shape of the meteorites makes the interaction of boundary layer with the air flow more complicated. Also, the surface roughness is another factor that influences that influence the boundary layer interaction. Hence, further research can be made into the boundary layer study using smoke visualization or PIV techniques.

- The study of meteorite aerodynamics in other flow regimes such as transonic to hypersonic regimes can help to map the properties in a larger picture and can offer interesting insights into the aerodynamics. In these flow regimes, in addition to the dynamics, the boundary layer interaction with the flow also becomes more complicated.

References

Alons, H. (2008). *OJF External Balance Documentation*. National Aerospace Laboratory NLR.

Anderson, J. D. (2017). *Fundamentals of Aerodynamics, Sixth Edition*.

Anderson, S., Towner, M., Bland, P., Haikings, C., Volante, W., Sansom, E., Devillepoix, H., Shober, P., Hartig, B., Cupak, M., Jansen-Sturgeon, T., Howie, R., Benedix, G., & Deacon, G. (2020). Machine learning for semi-automated meteorite recovery. *Meteoritics and Planetary Science*, *55*(11), 2461–2471. https://doi.org/10.1111/maps.13593

Andreic, Z. (2011). Dark Flight calculations: how accurate can they be? *WGN, Journal of the International Meteor Organization*.

Artemieva, N., & Pierazzo, E. (2009). The canyon diablo impact event: Projectile motion through the atmosphere. *Meteoritics & Planetary Science*, *44*, 25–42. https://doi.org/10.1111/J.1945-5100.2009.TB00715.X

Bettonvil, F., & Bettonvil, D. (submitted). Tests with a basic ablation and dark flight calculator. *WGN, Journal of the International Meteor Organization*.

Bland, P. A., Towner, M., Spurny, P., Bevan, A., & Smith, T. (2004). The desert fireball network. *Astronomy and Geophysics*, *45*, 5.20–5.23. https://doi.org/10.1046/J.1468-4004.2003.45520.X

Borovĭcka, J., & Kalenda, P. (2003). The Moŕavka meteorite fall: 4. Meteoroid dynamics and fragmentation in the atmosphere. *Meteoritics and Planetary Science*, *38*(7), 1023–1043. https://doi.org/10.1111/j.1945-5100.2003.tb00296.x

Borovička, J., Spurný, P., Kalenda, P., & Tagliaferri, E. (2003). The morávka meteorite fall: 1. description of the events and determination of the fireball trajectory and orbit from video records. *Meteoritics & Planetary Science*, *38*(7), 975–987. https://doi.org/https://doi.org/10.1111/j.1945-5100.2003.tb00293.x

Borovička, J., Bettonvil, F., Baumgarten, G., Strunk, J., Hankey, M., Spurný, P., & Heinlein, D. (2021). Trajectory and orbit of the unique carbonaceous meteorite Flensburg. *Meteoritics and Planetary Science*, 1–19. https://doi.org/10.1111/maps.13628

Borovička, J., Popova, O., & Spurný, P. (2019). The Maribo CM2 meteorite fall—Survival of weak material at high entry speed. *Meteoritics and Planetary Science*, *54*(5), 1024–1041. https://doi.org/10.1111/maps.13259

Borovička, J., Tóth, J., Igaz, A., Spurný, P., Kalenda, P., Haloda, J., Svoreň, J., Kornoš, L., Silber, E., Brown, P., & Husárik, M. (2013). The Košice meteorite fall: Atmospheric trajectory, fragmentation, and orbit. *Meteoritics and Planetary Science*, *48*(10), 1757–1779. https://doi.org/10.1111/maps.12078

Bronshten, V. A. (2012). *Physics of meteoric phenomena* (Vol. 22). Springer Science & Business Media.

Brown, P., Mccausland, P. J., Fries, M., Silber, E., Edwards, W. N., Wong, D. K., Weryk, R. J., Fries, J., & Krzeminski, Z. (2011). The fall of the Grimsby meteorite-I: Fireball dynamics and orbit from radar, video, and infrasound records. *Meteoritics and Planetary Science*, *46*(3), 339–363. https://doi.org/10.1111/j.1945-5100.2010.01167.x

Brown, P. G., Vida, D., Moser, D. E., Granvik, M., Koshak, W. J., Chu, D., Steckloff, J., Licata, A., Hariri, S., Mason, J., Mazur, M., Cooke, W., & Krzeminski, Z. (2019). The Hamburg meteorite fall: Fireball trajectory, orbit, and dynamics. *Meteoritics and Planetary Science*, *54*(9), 2027–2045. https://doi.org/10.1111/maps.13368

Brown, P., Hildebrand, A. R., Green, D. W., Pagé, D., Jacobs, C., Revelle, D., Tagliaferri, E., Wacker, J., & Wetmiller, B. (1996). The fall of the st-robert meteorite. *Meteoritics & Planetary Science*, *31*, 502–517. https://doi.org/10.1111/J.1945-5100.1996.TB02092.X

Campbell-Brown, M. (2007). The meteoroid environment: Shower and sporadic meteors. *Dust in Planetary Systems*, *643*, 11–21.

Carter, R., Jandir, P., & Kress, M. (2009). Estimating the drag coefficients of meteorites for all mach number regimes. *Lunar and Planetary Science Conference*, 2059.

Carter, R., Jandir, P., & Kress, M. (2011). Constraining the drag coefficients of meteors in dark flight. *Meteoroids: The Smallest Solar System Bodies*, 243. https://ntrs.nasa.gov/api/citations/20110016582/downloads/20110016582.pdf#page=255

Ceplecha, Z., Spalding, E., Jacobs, C., Revelle, D., Tagliaferri, E., & Brown, P. (1999). Superbolides. *Meteroids 1998*, 37.

Ceplecha, Z. (1966). Classification of meteor orbits. *Bulletin of the Astronomical Institutes of Czechoslovakia*, *17*, 96.

Ceplecha, Z. (1987). Geometric, dynamic, orbital and photometric data on meteoroids from photographic fireball networks. *Bulletin of the Astronomical Institutes of Czechoslovakia*, *38*, 222–234.

Ceplecha, Z., & McCrosky, R. E. (1997). Prairie network fireballs: Data on height, distance and brightness for each measured time-mar. *Meteoritics & Planetary Science*, *32*, A157–A158. https://doi.org/10.1111/J.1945-5100.1997.TB01594.X

Ceplecha, Z., Borovička, J., Elford, W. G., ReVelle, D. O., Hawkes, R. L., Porubčan, V., & Šimek, M. (1998). Meteor phenomena and bodies. *Space Science Reviews*, *84*(3-4), 327–471.

Colas, F., Zanda, B., Bouley, S., Jeanne, S., Malgoyre, A., Birlan, M., Blanpain, C., Gattacceca, J., Jorda, L., Lecubin, J., Marmo, C., Rault, J. L., Vaubaillon, J., Vernazza, P., Yohia, C., Gardiol, D., Nedelcu, A., Poppe, B., Rowe, J., … Zollo, A. (2020). Fripon: A worldwide network to track incoming meteoroids. *A&A*, *644*, A53. https://doi.org/10.1051/0004-6361/202038649

Devillepoix, H. A., Sansom, E. K., Bland, P. A., Towner, M. C., Cupák, M., Howie, R. M., Jansen-Sturgeon, T., Cox, M. A., Hartig, B. A., Benedix, G. K., & Paxman, J. P. (2018). The Dingle Dell meteorite: A Halloween treat from the Main Belt. *Meteoritics and Planetary Science*, *53*(10), 2212–2227. https://doi.org/10.1111/maps.13142

Gardiol, D., Cellino, A., & Di Martino, M. (2016). Prisma, italian network for meteors and atmospheric studies.

Gritsevich, M. I. (2008). Estimating the terminal mass of large meteoroids. *Doklady Physics*, *53*(11), 588–594. https://doi.org/10.1134/S1028335808110098

Gritsevich, M. I. (2009). Determination of parameters of meteor bodies based on flight observational data. *Advances in Space Research*, *44*, 323–334. https://doi.org/10.1016/J.ASR.2009.03.030

Haack, H., Sørensen, A. N., Bischoff, A., Patzek, M., Barrat, J. A., Midtskogen, S., Stempels, E., Laubenstein, M., Greenwood, R., Schmitt-Kopplin, P., Busemann, H., Maden, C.,

Bauer, K., Morino, P., Schönbächler, M., Voss, P., & Dahl-Jensen, T. (2019). Ejby—A new H5/6 ordinary chondrite fall in Copenhagen, Denmark. *Meteoritics and Planetary Science*, *54*(8), 1853–1869. https://doi.org/10.1111/maps.13344

Hankey, M., Perlerin, V., & Meisel, D. (2020). The all-sky-6 and the video meteor archive system of the ams ltd. *Planetary and Space Science*, *190*, 105005. https://doi.org/https://doi.org/10.1016/j.pss.2020.105005

Hansen, C. F., Field, M., & Washington, C. (1957). The erosion of meteors and high-speed vehicles in the upper atmosphere.

IAU. (2021). Meteors & meteorites: The IAU definitions of meteor terms [Accessed: 2021-12-21]. https://www.iau.org/public/themes/meteors_and_meteorites/

IMO. (2021). Glossary | IMO [Accessed: 2021-12-21]. https://www.imo.net/resources/glossary/#m

Jenniskens, P., Shaddad, M. H., Numan, D., Elsir, S., Kudoda, A. M., Zolensky, M. E., Le, L., Robinson, G. A., Friedrich, J. M., Rumble, D., Steele, A., Chesley, S. R., Fitzsimmons, A., Duddy, S., Hsieh, H. H., Ramsay, G., Brown, P. G., Edwards, W. N., Tagliaferri, E., … Worden, S. P. (2009). The impact and recovery of asteroid 2008 tc3. *Nature 2009 458:7237*, *458*, 485–488. https://doi.org/10.1038/nature07920

Jenniskens, P., & Jenniskens, P. M. M. (2006). *Meteor showers and their parent comets*. Cambridge University Press.

Kljuno, E., & Catovic, A. (2019). Estimation of projected surface area of irregularly shaped fragments. *Defence Technology*, *15*(2), 198–209. https://doi.org/10.1016/j.dt.2018.08.012

Konovalova, N., Madiedo, J., & Trigo-Rodriguez, J. (2011). The trajectory, orbit and preliminary fall data of the june bootid superbolide of july 23, 2008. *Meteoroids: The Smallest Solar System Bodies*, 251. https://ntrs.nasa.gov/api/citations/20110016582/downloads/20110016582.pdf#page=263

Lissauer, J. J., & De Pater, I. (2013). *Fundamental planetary science: Physics, chemistry and habitability*. Cambridge University Press.

McCrosky, R. E., Posen, A., Schwartz, G., & Shao, C.-Y. (1971). Lost City meteorite-Its recovery and a comparison with other fireballs. *Journal of Geophysical Research*, *76*(17), 4090–4108. https://doi.org/10.1029/jb076i017p04090

McKinley, D. W. R. (1961). Meteor science and engineering. *New York*.

Moilanen, J., Gritsevich, M., & Lyytinen, E. (2021). Determination of strewn fields for meteorite falls. *Monthly Notices of the Royal Astronomical Society*, *503*, 3337–3350. https://doi.org/10.1093/MNRAS/STAB586

Nguyen, S., Corey, M., Chan, W., Greenhalgh, E. S., & Graham, J. M. (2019). Experimental determination of the aerodynamic coefficients of spinning bodies. *Aeronautical Journal*, *123*(1263), 678–705. https://doi.org/10.1017/aer.2019.15

Oberst, J., Heinlein, D., Köhler, U., & Spurnỳ, P. (2004). The multiple meteorite fall of neuschwanstein: Circumstances of the event and meteorite search campaigns. *Meteoritics & Planetary Science*, *39*(10), 1627–1641. https://doi.org/https://doi.org/10.1111/j.1945-5100.2004.tb00062.x

Oberst, J., Molau, S., Heinlein, D., Gritzner, C., Schindler, M., Spurny, P., Ceplecha, Z., Rendtel, J., & Betlem, H. (1998). The “european fireball network”: Current status and future prospects. *Meteoritics & Planetary Science*, *33*, 49–56. https://doi.org/10.1111/J.1945-5100.1998.TB01606.X

Olech, A., Zoładek, P., Tymiński, Z., Stolarz, M., Wiśniewski, M., B□ben, M., Lewandowski, T., Polak, K., Raj, A., & Zar□ba, P. (2017). PF120916 Piecki fireball and Reszel meteorite fall. *Contributions of the Astronomical Observatory Skalnate Pleso*, *47*(1), 19–28.

Opik, E. J. (2004). *Physics of meteor flight in the atmosphere*. Courier Corporation.

Öpik, E. J., & Singer, S. (1959). Physics of meteor flight in the atmosphere. *Physics Today*, *12*(11), 54.

Pecina, P., & Ceplecha, Z. (1983). New aspects in single-body meteor physics. *Bulletin of the Astronomical Institutes of Czechoslovakia*, *34*, 102–121.

Riddell, F. R., & Winkler, H. B. (1962). Meteorites and re-entry of space vehicles at meteor velocities. *ARS Journal*, *32*, 1523–1530. https://doi.org/10.2514/8.6324

Rodríguez, J. M., Borovička, J., Llorca, J., Madiedo, J. M., Zamorano, J., & Izquierdo, J. (2009a). Puerto lápice eucrite fall: Strewn field, physical description, probable fireball trajectory, and orbit. *Meteoritics & Planetary Science*, *44*(2), 175–186. https://doi.org/https://doi.org/10.1111/j.1945-5100.2009.tb00726.x

Rodríguez, J. M., Borovička, J., Llorca, J., Madiedo, J. M., Zamorano, J., & Izquierdo, J. (2009b). Puerto Lápice eucrite fall: Strewn field, physical description, probable fireball trajectory, and orbit. *Meteoritics and Planetary Science*, *44*(2), 175–186. https://doi.org/10.1111/j.1945-5100.2009.tb00726.x

Rogers, L., Hill, K., & Hawkes, R. (2005). Mass loss due to sputtering and thermal processes in meteoroid ablation. *Planetary and Space Science*, *53*(13), 1341–1354. https://doi.org/https://doi.org/10.1016/j.pss.2005.07.002

Roy, C. J., & Blottner, F. G. (2006). Review and assessment of turbulence models for hypersonic flows. *Progress in Aerospace Sciences*, *42*(7), 469–530. https://doi.org/https://doi.org/10.1016/j.paerosci.2006.12.002

Sansom, E. K., Jansen-Sturgeon, T., Rutten, M. G., Devillepoix, H. A., Bland, P. A., Howie, R. M., Cox, M. A., Towner, M. C., Cupák, M., & Hartig, B. A. (2019). 3D meteoroid trajectories. *Icarus*, *321*(September 2017), 388–406. https://doi.org/10.1016/j.icarus.2018.09.026

Sansom, E. K., Bland, P., Paxman, J., & Towner, M. (2015). A novel approach to fireball modeling: The observable and the calculated. *Meteoritics and Planetary Science*, *50*(8), 1423–1435. https://doi.org/10.1111/maps.12478

Silber, E. A., Boslough, M., Hocking, W. K., Gritsevich, M., & Whitaker, R. W. (2018). Physics of meteor generated shock waves in the Earth's atmosphere – A review. *Advances in Space Research*, *62*(3), 489–532. https://doi.org/10.1016/j.asr.2018.05.010

Spurny, P. (1997). Photographic monitoring of fireballs in Central Europe. In F. A. Allahdadi, E. K. Casani, T. D. Maclay, F. A. Allahdadi, & T. D. Maclay (Eds.), *Small spacecraft, space environments, and instrumentation technologies* (pp. 144–155). SPIE. https://doi.org/10.1117/12.293337

Spurny, P., Heinlein, D., & Oberst, J. (2002). The atmospheric trajectory and heliocentric orbit of the neuschwanstein meteorite fall on april 6, 2002. *Asteroids, Comets, and Meteors: ACM 2002*, *500*, 137–140.

Spurný, P., Bland, P. A., Shrbený, L., Borovička, J., Ceplecha, Z., Singelton, A., Bevan, A. W., Vaughan, D., Towner, M. C., Mcclafferty, T. P., Toumi, R., & Deacon, G. (2012). The Bunburra Rockhole meteorite fall in SW Australia: Fireball trajectory, luminosity, dynamics, orbit, and impact position from photographic and photoelectric records. *Mete-*

oritics and Planetary Science, *47*(2), 163–185. https://doi.org/10.1111/j.1945-5100.2011.01321.x

Spurný, P., Borovička, J., & Shrbený, L. (2020). The žďár nad sázavou meteorite fall: Fireball trajectory, photometry, dynamics, fragmentation, orbit, and meteorite recovery. *Meteoritics & Planetary Science*, *55*(2), 376–401. https://doi.org/https://doi.org/10.1111/maps.13444

Spurný, P., Haloda, J., Borovička, J., Shrbený, L., & Halodová, P. (2014). Reanalysis of the Benešov bolide and recovery of polymict breccia meteorites - Old mystery solved after 20 years. *Astronomy and Astrophysics*, *570*, 1–14. https://doi.org/10.1051/0004-6361/201424308

Stempels, E., & Kero, J. (2016). The Swedish Allsky Meteor Network : first results. (3), 288–290.

Trigo-Rodríguez, J. M., Llorca, J., Castro-Tirado, A. J., Ortiz, J. L., Docobo, J. A., & Fabregat, J. (2006). The spanish fireball network. *Astronomy & Geophysics*, *47*, 6.26–6.28. https://doi.org/10.1111/J.1468-4004.2006.47626.X

Trigo-RodrÍguez, J. M., Llorca, J., Madiedo, J. M., Tancredi, G., Edwards, W. N., Rubin, A. E., & Weber, P. (2010). The Berduc L6 chondrite fall: Meteorite characterization, trajectory, and orbital elements. *Meteoritics and Planetary Science*, *45*(3), 383–393. https://doi.org/10.1111/j.1945-5100.2010.01029.x

Vida, D., Brown, P. G., Campbell-Brown, M., Wiegert, P., & Gural, P. S. (2019). Estimating trajectories of meteors: An observational monte carlo approach-ii. results. *MNRAS*, *000*, 1–17. http://sonotaco.jp/

Vida, D., Gural, P. S., Brown, P. G., Campbell-Brown, M., & Wiegert, P. (2019). Estimating trajectories of meteors: An observational monte carlo approach-i. theory.

Vida, D., Šegon, D., Gural, P. S., Brown, P. G., McIntyre, M. J. M., Dijkema, T. J., Pavletić, L., Kukić, P., Mazur, M. J., Eschman, P., & et al. (2021). The global meteor network – methodology and first results. *Monthly Notices of the Royal Astronomical Society*, *506*(4), 5046–5074. https://doi.org/10.1093/mnras/stab2008

Vinnikov, V., Gritsevich, M., & Turchak, L. (2017). Numerical simulation for dark flight stage of meteoroid fragments. *European Planetary Science Congress*, EPSC2017–926.

Vinnikov, V. V., Gritsevich, M. I., & Turchak, L. I. (2016). Mathematical model for estimation of meteoroid dark flight trajectory. *AIP Conference Proceedings*, *1773*. https://doi.org/10.1063/1.4965020

Vlasek, J. (1963). Multiple fall of príbram meteorites photographed. vi. some results of aerodynamic measurements. *Bulletin of the Astronomical Institutes of Czechoslovakia*, *14*, 222.

Zhdan, I. A., Stulov, V. P., Stulov, P. V., & Turchak, L. I. (2007). Drag coefficients for bodies of meteorite-like shapes. *Solar System Research*, *41*(6), 505–508. https://doi.org/10.1134/S0038094607060068

Zurita, M., Marreira, R. D. A., Agustoni, J. S., Di Pietro, C. B., Domingues, M., Trindade, L., Souza, J. J. d., Lima, A. R., Silva, G. G., Mourão, D. C., et al. (2020). A bright fireball over the state of rio grande do sul. *4*, 1–4. http://repositorio.ufba.br/ri/handle/ri/31932

A

Conversion of STL file into SLDPRT format

The high-quality surface data of the Broek in Waterland meteorite that was captured using photogrammetry will be stored in an STL (STereoLithography) format. However, editing the design of the model and analysis will be complex and sometimes not possible using SOLIDWORKS. Hence, the format of the data file was converted into SLDPRT format, native file format of SOLIDWORKS part file. With this, any design additions, such as threaded holes, cylindrical cavities required for mounting the meteorite model in the wind tunnel test section can be created. After this conversion, the 3D model can be edited just as a usual SOLIDWORKS part file. The process of this conversion is presented below.

1. Run the 'SOLIDWORKS 2020 (Student Edition)' application. Once opened, go to 'Options' in the toolbar present at the top of the window. Then, click **Add-ins** present in the options to check the add-ins that are present in the system as shown in Fig. A.1.

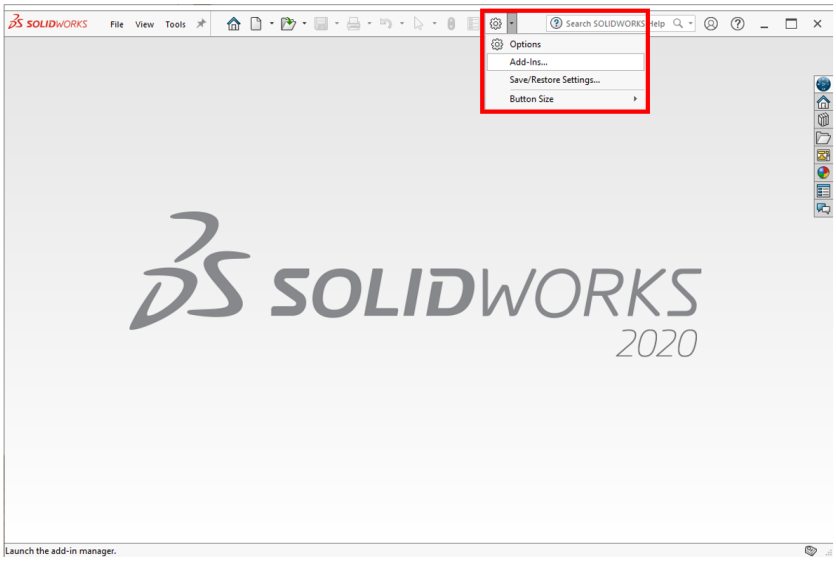

Figure A.1: STEP 1: Click Add-ins in the 'Options' to check the existing Add-ins.

2. Once clicked, a window is prompted which shows the existing add-ins present in the system. Select the **ScanTo3D** add-in as shown in Fig. A.2 and then click **OK**.

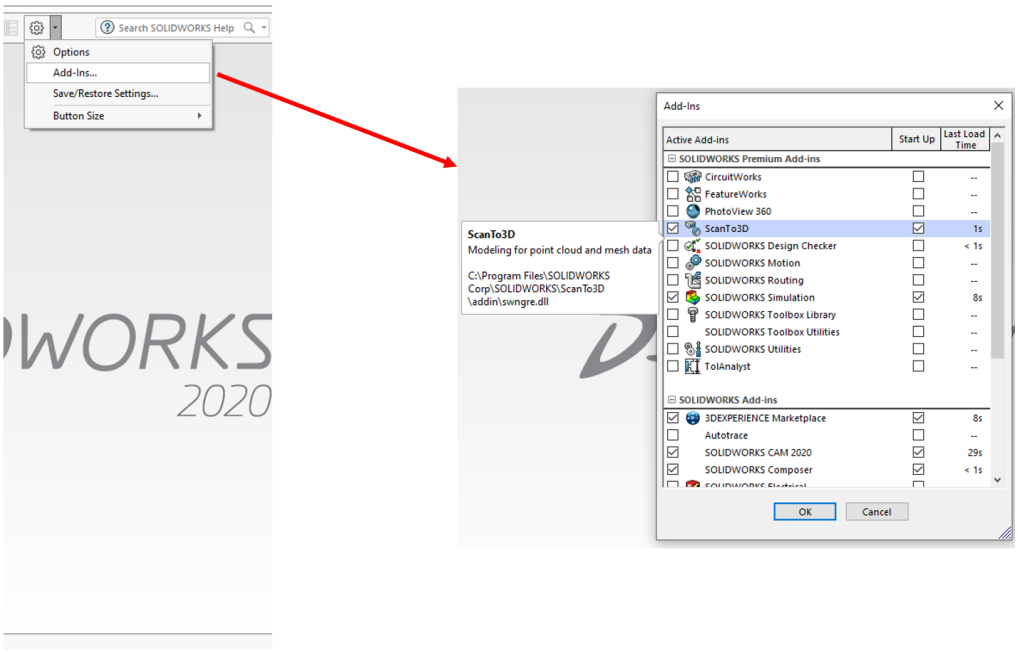

Figure A.2: STEP 2: Select ScanTo3D in the add-ins window

3. Click **Open** option in the toolbar. Once the open window is prompted, go to the location where the STL file is stored. Before selecting the file, change the file format in the bottom right corner in the 'Open file' window as shown in Fig. A.3. Change the file format to **ScanTo3D Mesh Files (*.3ds;*.obj;*.stl...)**.

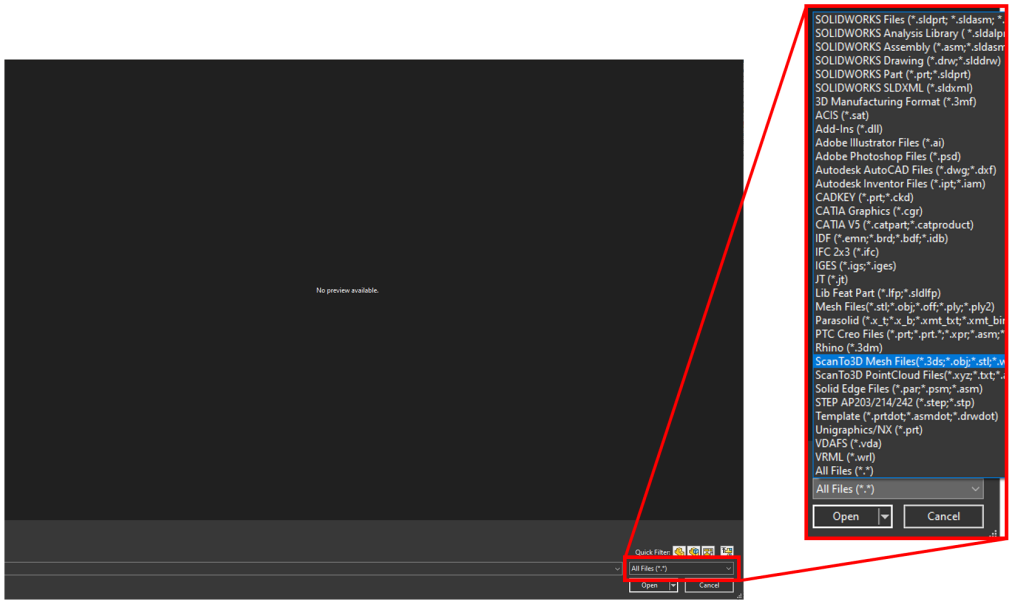

Figure A.3: STEP 3: Change the file format to ScanTo3D Mesh Files in the 'Open file' window.

4. Then, select the required STL file and click **Options** in the 'Open file' window. A 'System Options' window will be prompted as shown in Fig. A.4. Select the 'Import as' option to be **Solid Body**. This option allows the SOLIDWORKS to read the mesh data of the STL file as a complete body with faces. And then click **OK** and click **Open**.

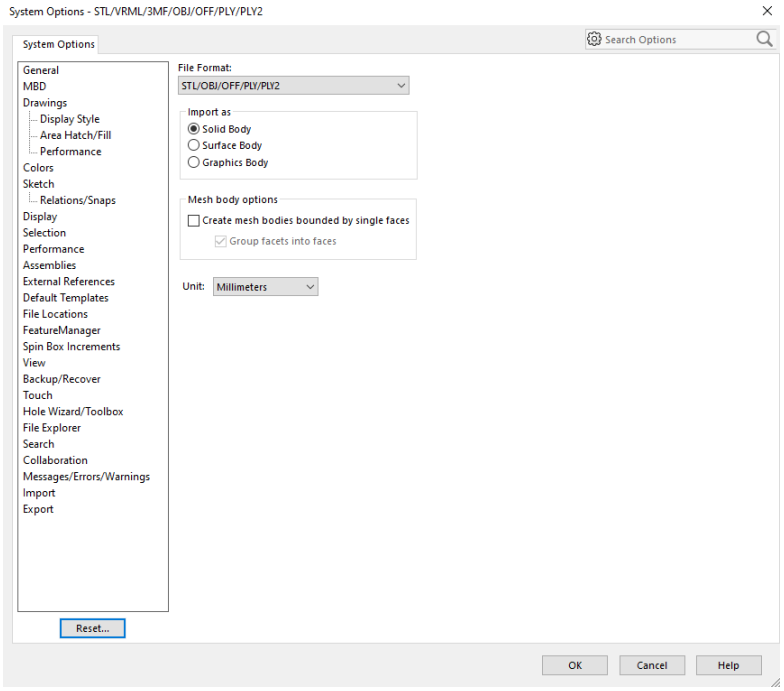

Figure A.4: STEP 4: Select 'Options' in the 'Open file' window before opening the required STL file, to import the 3D mesh data as a Solid Body.

5. The mesh data from the STL file will be imported into SOLIDWORKS, and this can take some time depending upon the system processing power. Once the mesh is imported, it will appear as shown in Fig. A.5 with a tree of various options on the upper left pane. The imported mesh is displayed in the option pane as 'Mesh1'. Right click on Mesh1 and select the **Mesh Prep Wizard** option.

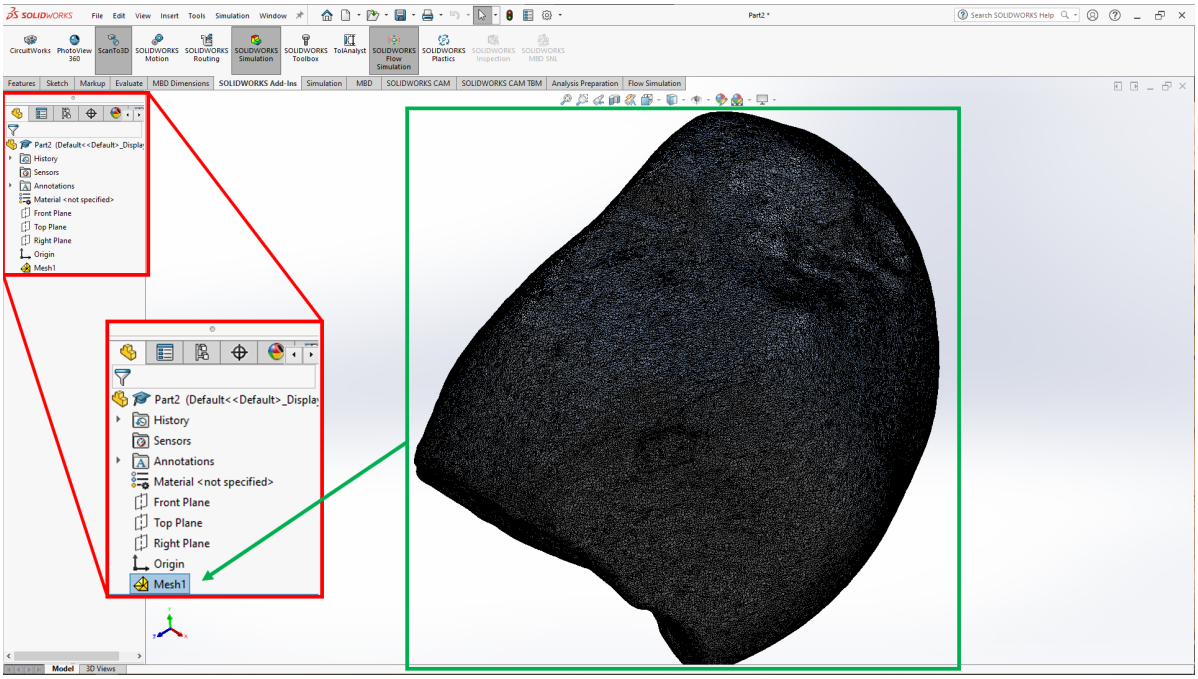

Figure A.5: STEP 5: View of the high-quality mesh imported into SOLIDWORKS as 'Mesh1'.

6. Mesh Prep Wizard will be prompted in the upper left pane with the number of faces present in the mesh. Click the Right arrow to proceed to next step. If any specific orientation it is not required, then select the 'Automatic' option. If needed, then click the **Select references** for a specific orientation of the model. Select points manually to select the any two of the three perpendicular axes. Then, proceed to the next step.

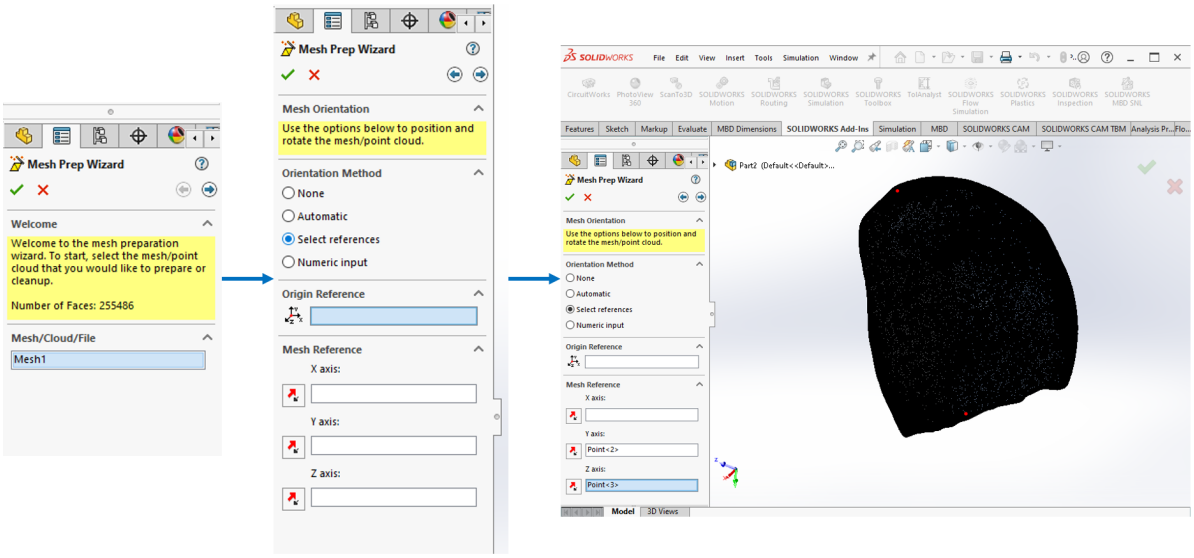

Figure A.6: STEP 6: After launching Mesh Prep Wizard, select the 'Orientation Method' based on the requirement, The red dots present in the mesh, represents the manually selected points for Y and Z axes.

7. Proceed to the 'Simplification' step where the mesh will be simplified based on the percentage of the **Reduction amount**. In the current case, the mesh was not simplified to preserve the irregular surface data. Hence, the Reduction amount is fed as 0%. The simplification can also be achieved by varying the 'Target mesh size' of the simplified model. The 0% reduction can be seen in Fig. A.7. Then, proceed to the next step.

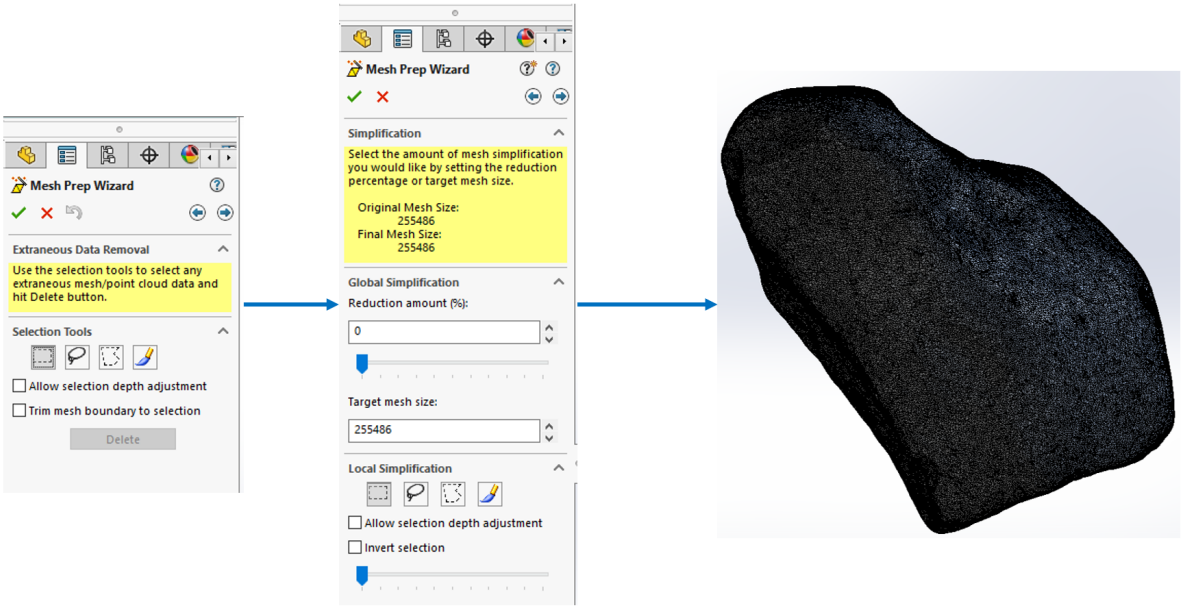

Figure A.7: STEP 7: Simplification of the mesh size based on feeding the required 'Reduction amount' of the surface quality.

8. Similarly, the smoothness of the surface can also be varied globally and locally using the slider bar as shown in Fig. A.8. In the current study, the highest quality of the smoothness was chosen. And proceed to the next step to complete the mesh creation. Then, based on the requirement, Automatic or Guided creation can be chosen. In the current study, the mesh was created using **Automatic creation**.

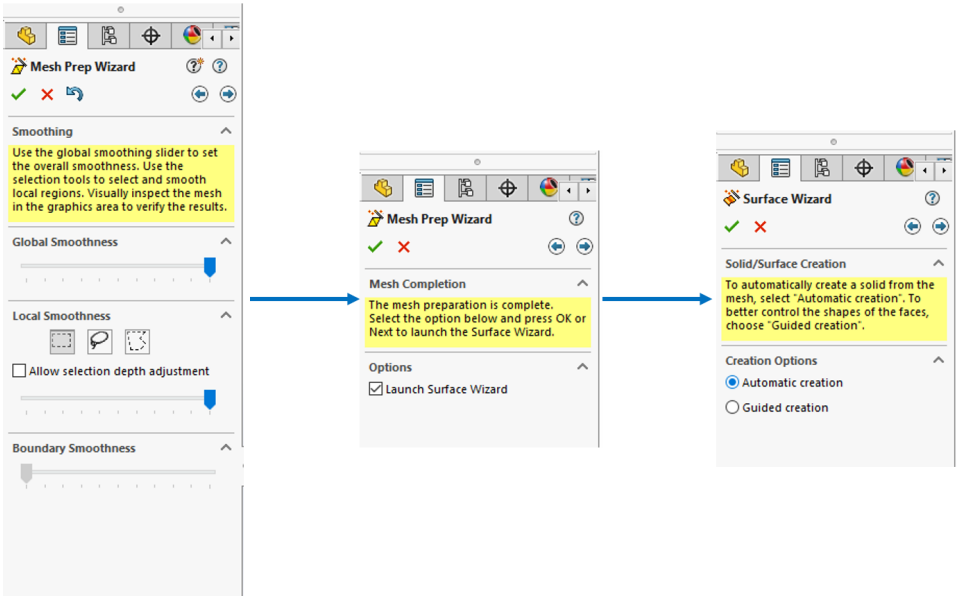

Figure A.8: STEP 8: Choose the quality of smoothness and then create the body using either automatic or guided creation.

9. In the next step, the 'Surface Detail' can be varied similar to previous step by using a slider bar. After choosing the required Surface Detail, click on the **Update Preview** to see the preview of mesh with the resultant surface errors as shown in Fig. A.9 and displayed on mesh in Fig. A.10a. The surface errors can be rectified, if necessary, by clicking on each error. In the current study, the mesh size is too large and relatively, the surface errors were not significant enough to correct. Hence, the surface errors were not considered. Proceed to next step and final number of faces present in the converted solid body will be displayed.

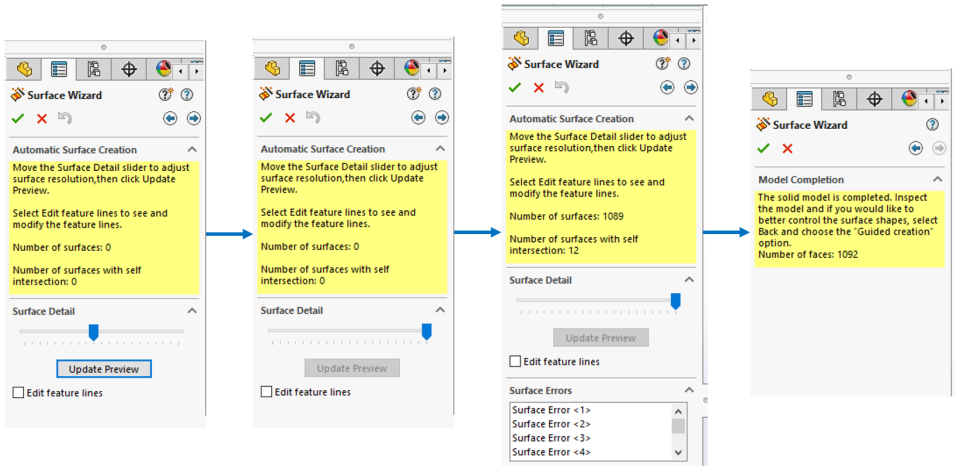

Figure A.9: STEP 9: Choose the required 'Surface Detail' to see the preview of the model with the resultant surface errors.

10. Finally, click the green tick option to finish the creation of solid model. The final solid model will be similar to Fig. A.10b with the resultant faces. Now, this can be saved as a SLDPRT file and can be worked as a usual SOLIDWORKS part file. The regmaglypts (surface indentations) can be observed in the final sold body clearly, thus indicating the preservation of surface detail quality.

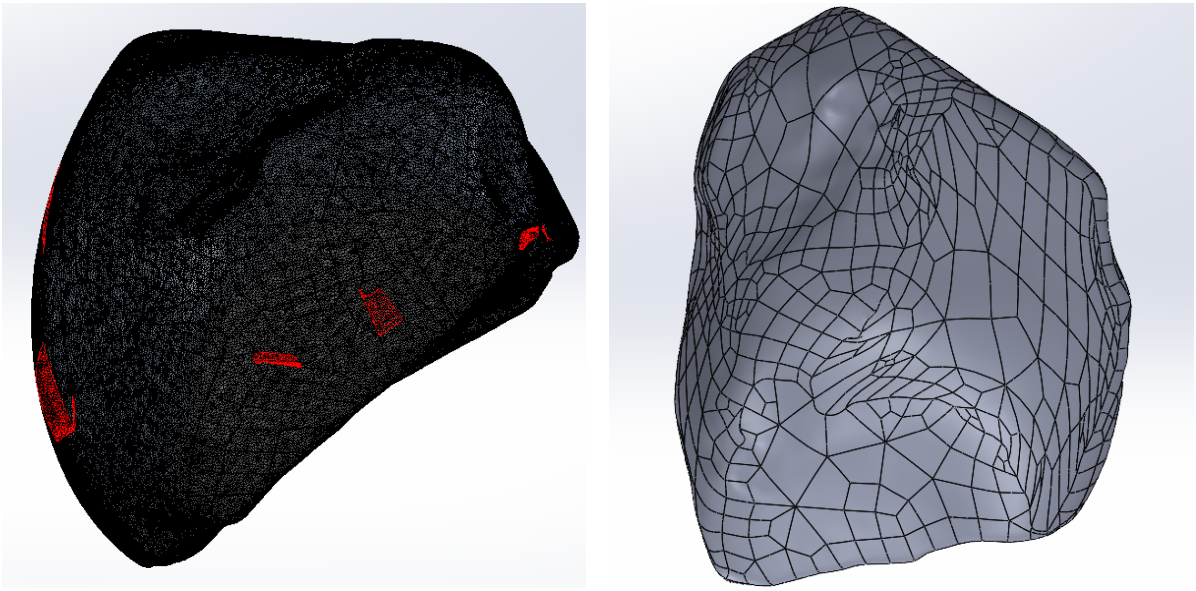

(a) (b)

Figure A.10: 3D model of the Broek in Waterland meteorite.
(a) Preview of the surface details with the resultant surface errors. (b) Final solid model created from the imported mesh data.

After necessary modifications were made on the solid body, the body then can be saved as an STL file again for final 3D printing.